NATIONAL ENERGY TECHNOLOGY LABORATORY
OIL & GAS

**DOE Award No.: DE-FE0010160**

# Final Technical Report (Period Ending 03/31/2016) Advanced Gas Hydrate Reservoir Modeling Using Rock Physics Techniques

**Project Period (10/1/2012-3/31/2016)**


Submitted by:
Dan McConnell

Signature

Fugro GeoConsulting, Inc., dba Fugro Marine Geoservices, Inc.
DUNS #:118972301
6100 Hillcroft
Houston, Texas 77081
Email: dmcconnell@fugro.com
Phone number: (713) 778-6801


Prepared for:
United States Department of Energy
National Energy Technology Laboratory

December 30, 2017

U.S. DEPARTMENT OF ENERGY | NATIONAL ENERGY TECHNOLOGY LABORATORY

**Office of Fossil Energy**

## DISCLAIMER



## ABSTRACT

Prospecting for high saturation gas hydrate deposits can be greatly aided with improved approaches to seismic interpretation and especially if sets of seismic attributes can be shown as diagnostic or direct hydrocarbon indicators for high saturation gas hydrates in sands that would be of most interest for gas hydrate production.

A large 3D seismic data set in the deep water Eastern Gulf of Mexico was screened for gas hydrates using a set of techniques and seismic signatures that were developed and proven in the Central deepwater Gulf of Mexico in the DOE Gulf of Mexico Joint Industry Project JIP Leg II in 2009 and recently confirmed with coring in 2017.

A large gas hydrate deposit is interpreted in the data where gas has migrated from one of the few deep seated faults plumbing the Jurassic hydrocarbon source into the gas hydrate stability zone. The gas hydrate deposit lies within a flat-lying within Pliocene Mississippi Fan channel that was deposited outboard in a deep abyssal environment. The uniform architecture of the channel aided the evaluation of a set of seismic attributes that relate to attenuation and thin-bed energy that could be diagnostic of gas hydrates. Frequency attributes derived from spectral decomposition also proved to be direct hydrocarbon indicators by pseudo-thickness that could be only be reconciled by substituting gas hydrate in the pore space. The study emphasizes that gas hydrate exploration and reservoir characterization benefits from a seismic thin bed approach.

## TABLE OF CONTENTS

## LIST OF TABLES



## LIST OF FIGURES

## LIST OF ACRONYMS AND ABBREVIATIONS

| | |
|---|---|
| AVO | Amplitude Versus Offset |
| BSR | Bottom Simulating Reflector |
| DHI | Direct Hydrocarbon Indicator |
| DOE | Department of Energy |
| DSDP | Deep Sea Drilling Project |
| Ft | Foot/Feet |
| GC955 | Green Canyon Block 955 |
| GoM | Gulf of Mexico |
| GH | Gas Hydrate |
| GHSZ | Gas Hydrate Stability Zone |
| Ip | Compressional Wave Impedance |
| Is | Shear Wave Impedance |
| IODP | Integrated Ocean Drilling Program |
| JIP | Joint Industry Project |
| JIP Leg II | 2009 DOE Supported Gulf of Mexico Gas Hydrate Drilling Program. Operated by Chevron with Industry Partners |
| JMPG | Journal of Marine and Petroleum Geology |
| LL511 | Lloyd Ridge Block 511 |
| LWD | Logging While Drilling |
| M | Meter/Meters |
| MCAVLU | (Not an acronym or abbreviation, but appears to be one). A Miocene submarine fan in the Eastern Gulf of Mexico |
| MTD | Mass Transport Deposit |
| M/V | Motor Vessel |
| NETL | National Energy Technical Laboratory |
| OCS | Outer Continental Shelf |
| ODP | Ocean Drilling Program |
| RC | Reflection Coefficient |
| RGB | Red Green Blue Color Blend |
| Sgh | Saturation of Gas Hydrate |
| SWF | Shallow Water Flow |
| UBGH1 | The First Ulleung Basin Gas Hydrate Drilling Expedition- Korean National Gas Hydrate Program |
| UBGH2 | The Second Ulleung Basin Gas Hydrate Drilling Expedition- Korean National Gas Hydrate Program |
| US | United States |
| USGS | United States Geological Survey |
| Vp | Compressional Wave Velocity |
| Vs | Shear Wave Velocity |
| WR313 | Walker Ridge Block 313 |

## 1. EXECUTIVE SUMMARY

The purpose of this project was to find additional ways to find gas hydrate sands in conventional 3D seismic data using rock physics theory, amplitude analysis, and spectral decomposition.

Natural gas hydrates are an underexplored component of the hydrocarbon system. At cold temperatures and high pressures that are found on the continental margins natural gas and water can concentrate in a clathrate form that resembles ice. Gas hydrates represent an additional unexploited source of clean hydrocarbon energy relative to coal and oil.

When this project was proposed, it was expected that we would be able to use the 3D seismic data that was made available to the 2009 Department of Energy (DOE) Gulf of Mexico Gas Hydrate JIP Leg II Logging-While-Drilling expedition (DOE project DE-FC26-01NT41330). These data would have been ideal because the logging while drilling data confirmed high saturation gas hydrate sands. Instead, we had to look for other suitable data. After a long delay, we secured the use of a large 3D seismic data set from the Eastern Gulf of Mexico that included deepwater areas with conditions for not disclosing specific location information. The seismic data were post-stack only which limited the gas hydrate detection techniques that could be applied. These U.S. Federal areas on the Outer Continental Shelf have been off-limits for oil and gas exploration so there are very few well penetrations.

Nevertheless, the data were suitable for identification of gas hydrate saturated sands because thick buried Mississippi Fan sediments that were deposited about 2 to 3 Million years ago intersect with the lower part of the gas hydrate stability zone. A large gas hydrate deposit was interpreted at the base of gas hydrate stability corresponding to a zone of gas migration from the basin sediments below.

Studying the sediments at the base of gas hydrate stability is ideal for determining the seismic response of gas hydrate saturation. First, this zone is more likely to have concentrated gas hydrate because it encompasses the zone in which upward moving buoyant gas transitions to form immobile gas hydrate deposits. Second, this zone is interesting because these areas have the potential to encounter a hydrate filled zone and a gas filled zone within the same sediments. Third, the fundamental measurement within seismic data is impedance between layers as a function of velocity density contrasts between the layers. High saturation gas hydrates and free gas inhabit opposite ends of these measurements making the study of this zone ideal for investigating the seismic characteristics of gas hydrate and, hence, the investigation of other seismic attributes that change with gas hydrate fill.

The Eastern Gulf of Mexico seismic data were screened for the seismic signatures for gas hydrates. A large seismic high amplitude anomaly with impedance characteristics consistent with gas hydrate deposit was found at a depth consistent with the predicted base of gas hydrate stability for the area. The amplitude anomaly encompasses NW-SE oriented channel sediments, interpreted to be sandy, within abyssal fan deposits. Cross sections over the amplitude anomaly show a polarity reversal- a high amplitude “leading peak” on the western side that transitions to high amplitude “leading trough” on the eastern side. The combined gas hydrate-gas amplitude anomaly covers an area of ~9 sq. km.

One of the hypotheses of this research was that since simple seismic amplitude can be diagnostic for gas hydrate in certain settings, then other seismic attributes may prove useful for gas hydrate detection. Other post stack seismic attributes from the seismic volume were generated including geometric, amplitude, and frequency attributes. Geometric attributes can help define the sediment architecture and lithologies. Amplitude attributes can indicate impedance, fluid content, lithology contrasts, cementation, among others. Frequency attributes can show energy loss, absorption, attenuation, among others. Time-frequency attributes using spectral decomposition were used to identify channel geometries and for gas hydrate imaging. Instantaneous Q attributes indicated attenuation from both the gas hydrate and gas deposits. Derivatives of the amplitude envelope corroborated the time-frequency attributes associated with interpreted gas hydrate deposits. One of the research goals was to explore spectral (frequency) decomposition- a time frequency attribute for utility in identifying gas hydrate deposits.

Spectral decomposition, a process of transposing the seismic bandwidth in the seismic data in time (or depth) into separate frequency domain components is widely used for visualizing seismic architectural components within seismic facies such as channel systems. Spectral decomposition is also used to identify hydrocarbon reservoirs in a manner below the resolution limit of other direct hydrocarbon indication methods. Originally spectral decomposition was a method to address the thin layer problem in seismic data. The events that cause the impedance contrasts in actual geologic sections are thinner than the corresponding impedance layers resolvable in seismic data. Using the principles of tuning interference between layers, spectral decomposition methods allowed the thickness of impedance events below the resolution of the seismic data to be estimated.

In addition to frequency attributes to determine gas hydrate fill, seismic attributes related to attenuation, thin-bed stacked high energy layer that are associated with gas hydrates were tested on the gas hydrate deposits. All provided multiple lines of evidence of being useful for direct hydrocarbon indicators for gas hydrate and were consistent with saturation model derived from acoustic impedance.

It is hoped that ideas such as are presented in this research are can be tested by drilling and sampling in future gas hydrate field research expeditions.

## 2. INTRODUCTION

### 2.1 Research Goals

The primary goal of this research is to develop analytical techniques capable of quantitatively evaluating the nature of methane hydrate reservoir systems through modeling of their acoustic response using techniques that integrate rock physics theory, amplitude analysis, and spectral decomposition.

Past efforts under the DOE-supported Gulf of Mexico Joint Industry Project included the selection of well locations utilizing prospectivity analysis based primarily on a petroleum systems approach for gas hydrate using 3-D exploration seismic data and derivative analyses that produced predicted gas hydrate saturation volumes. Logging–while-drilling at those locations confirmed the presence of high saturation gas hydrate reservoirs at two boreholes in Green Canyon Block 955 (GC955) and two boreholes in Walker Ridge Block 313 (WR313) in the Gulf of Mexico. The success of the four wells was a significant achievement and legitimized the conceptual approach taken to prospect for potential producible methane hydrate reservoirs in deepwater that could be exploited with modifications to present-day technology.

The success of future hydrate research wells and, eventually, resource exploration wells, will depend on the continued evolution of the techniques employed to select successful drilling locations. Geophysical prospecting techniques will need to be developed to both identify potential gas hydrate accumulations and better delineate and characterize these potentially complex systems and reservoirs.

### 2.2 Modified Research Goals

When Fugro proposed this research project we anticipated being able to use the seismic data sets used by DOE-Chevron Gulf of Mexico Gas Hydrate JIP Leg II. Despite many entreaties, the seismic data owners of these well publicized data with respect to gas hydrate deposits denied our requests to use those data for this research project. Because of the lack of suitable data, this research project was delayed for several years. Two no-cost time extensions to complete the research were granted. Late in the project timeline, permission to use a seismic data set in the Eastern Gulf of Mexico that was owned by Fugro was secured. Although the use of this data would seem straightforward, it wasn't. Fugro had previously sold the marine exploration seismic acquisition business, among others to competitor, CGG in 2012. Although Fugro owned the data, the right to market and sell the data was given to CGG which complicated our ability to receive, interpret, and use the data. Shortly after securing permission to use the Florida 3D seismic data for this project, Fugro sold all rights to the data to Spectrum Geo. Spectrum Geo graciously allowed us to use the data for this research project with conditions. The goals for the research project had to be modified because of the lack of confirmed gas hydrate deposits and data use conditions proscribed by the data owners.

# 3. MARINE GAS HYDRATE CHARACTERIZATION FROM SEISMIC DATA – EXISTING AND DEVELOPING TECHNIQUES

## 3.1 Introduction

Gas hydrates are a solid form of natural gas and water that forms where gas is in excess of solubility within a range of high pressure and/or low temperature conditions. Such conditions occur in marine sediments on continental margins with water depths greater than ~350 m and primarily where there is secondary migration of gassy hydrocarbons into the gas hydrate stability zone. Gas hydrates have been inferred from seismic data, geophysical logs, and confirmed by cores or pressurized cores across a wide range of depths and host sediments on continental margins. The thickness of the gas hydrate stability zone is controlled by hydrostatic pressure in the sediments and the geothermal gradient. All the world's continental margins have areas where gas hydrates can form in the marine sediments. The distribution of gas hydrates within the gas hydrate stability zone is, however, highly variable.

Beginning in 1995 with Ocean Drilling Program (ODP) Leg 164 on the Blake Ridge off the SE US coast, there have been approximately 20 major marine hydrate-focused field expeditions. A common thread through many programs was the objective to confirm the presence of gas hydrate and to understand geologic controls on gas hydrate formation and distribution in the study areas. All used some form of geophysical data to determine where gas hydrates would be encountered. Early gas hydrate field programs, using the state of knowledge at the time were guided by overly simplistic interpretations of BSRs (bottom simulating reflectors) and their relationship to gas hydrate distribution and saturation. The field programs in the GOM and elsewhere, (e.g. Japan, India, Korea, China) have shown that factors controlling the distribution of hydrates are more complicated.

A concept of a gas hydrate petroleum system began to emerge with the establishment of a set of criteria analogous to those used in conventional petroleum exploration. Testing the petroleum systems approach to gas hydrate prospecting was one of the principal objectives of the JIP Leg II field program. The good agreement of the LWD data acquired during this program with pre-drill predictions marked an important milestone in gas hydrate exploration.

### 3.1.1 Existing Techniques

Gas hydrate targets, whether shallow, middle or deep are all relative to the thickness of the gas hydrate stability zone. The shallowest gas hydrates in the system are those on the seafloor and associated with near seafloor vents (Brooks et al., 1985). These are typically associated with carbonate hardgrounds and chemosynthetic communities and are commonly recovered in marine geochemical programs that target natural hydrocarbon seepage but have also been sampled to support gas hydrate programs (Kojima, 2002).

Gas chimneys within the gas hydrate stability zone also contain gas hydrates (Matsumoto and Sato, 2011). Shallow and mid depth hydrates in clays or, in sands intersected by the gas chimney are targets of interest in some gas hydrate systems. The two Korean field programs (UBGH 1 and UBGH 2) and JIP Leg I targeted these types of deposits (Park et al., 2008). Strata-bound gas hydrates in clays (JIP Leg II), high amplitudes in strata along faults or on structures offer targets (ODP Leg 204), and areas exhibiting amplitude blanking

(ODP Leg 164), also present within the middle of the gas hydrate stability zone (McConnell et al, 2009 a). The deepest targets for gas hydrate are associated with gas charged sands at, or near, the base of gas hydrate stability (JIP Leg II) and continuous BSRs (ODP Leg 164 & Nankai Trough). It should also be noted that a common finding of all the field programs is only a small subset of sediments within the gas hydrate stability zone host gas hydrate.

A summary of these findings for gas hydrate occurrence is tabulated according to energy resource potential in Figure 3.1 (modified from Boswell et al., 2015). Representative gas hydrate saturations are superimposed on five stylized wells. The GC955 and WR313 locations are shown on this figure as type sections. The GC955 gas hydrate deposits are represented on the far left of the figure as the most prospective targets and, next to them and also prospective, are the primary targets at the WR313 sites. The strata-bound fracture-fill gas hydrates found at the WR313 locations are stylized on the right side of the diagram, as the least prospective targets. A range of interpretation techniques were used to identify the various emplacement styles for gas hydrate. This study focuses on the detection of high saturation gas hydrate sands. It is worth reviewing, in this report the main techniques to identify gas hydrates. First, these screening methods used in this study to narrow and located the gas hydrate deposit to which additional techniques were tried. Second, some of the classic seismic attributes such as BSRs, seismic blanking, and enhanced reflectors can each be better understood when considering these additional techniques for identifying gas hydrate direct hydrocarbon indicators (DHIs).

#### 3.1.1.1 Bottom Simulating Reflectors or BSRs

The first and most important attribute used to identify gas hydrates was the bottom simulating reflector. The bottom simulating reflector was identified as marking the base of gas hydrate stability by Shipley et al., (1979). The base of gas hydrate stability is the pressure-temperature boundary above which, excess gas and water can form gas hydrate and below which the excess gas is free gas. The BSR is an anomalous reflection that cross-cuts stratigraphy at depths consistent with the pressure and local basin temperatures that correlate with gas hydrate to gas phase boundary. The cause of the reflector was widely postulated to mark the impedance change for an abrupt lowering of velocity caused by free gas (Bangs et al., 1993). Others postulated that the impedance change was caused primarily by cemented gas hydrate over non-cemented sediments (Hyndman and Davis, 1992) or some combination of both (Dillon and Paull, 1983). Early scientific drilling supported the hypothesis that the BSR was caused by the thin low-velocity layer. It does not require high concentrations of gas to produce a BSR. Free gas concentrations of less than 5% have been found to be sufficient to generate a BSR (MacKay et al., 1994).

In the early phase of natural gas hydrate studies, say between 1980 and 2000, the BSR and gas hydrate distribution was very closely linked by most gas hydrate researchers. Almost all discussions of geophysical evidence for gas hydrate including the presence of, absence of, exploration for, evidence for, and volumes of, and more, were dominated by discussions of the BSR. It was, in fact, the discovery of extensive BSRs off the East Coast of Japan, off India, and elsewhere that launched and inspired several national gas hydrate research programs.

Scientific drilling at key locations that tested hypotheses relating the BSR to the distribution concentration of gas hydrate showed that the relationships were not straightforward. Drilling along the BSR profile at the Blake Ridge (ODP Leg 164) confirmed gas hydrate in the sediments above the BSR but not with a consistent distribution. The control hole (994) where there was no BSR was hypothesized to be free of gas hydrate but drilling confirmed distributions of gas hydrate were similar to where the BSR was present (Paull et al., 2000). Drilling results in other area, such as in the Nankai trough and elsewhere, also confirmed that the presence and character of a BSR was not a good indicator of gas hydrate deposit distribution within the gas hydrate stability zone.

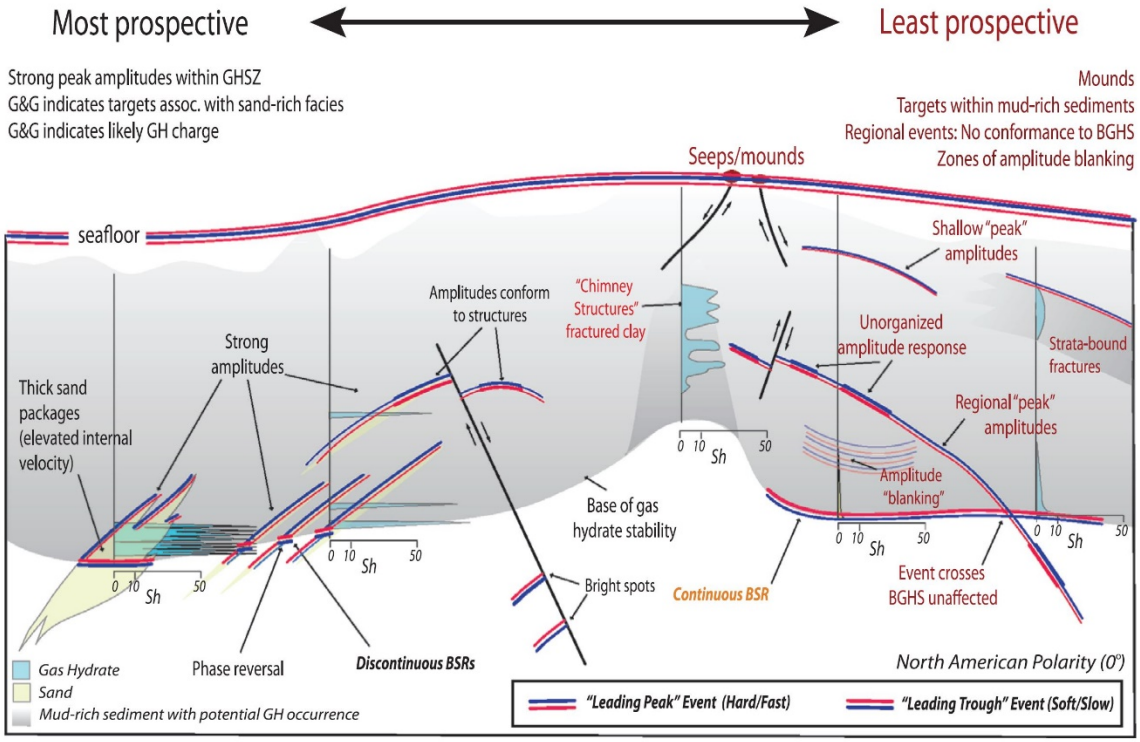


**Figure 3.1 Simplified schematic showing "type sections" for gas hydrate accumulations and associated geophysical indications. From Boswell, et al., 2016.**

### 3.1.1.2 Gas Proxy

A method developed by the author, and likely others, for identifying the base of gas hydrate stability is to use the gas proxy method in which, in a leaky hydrocarbon basin, a screening for the shallowest free gas anomalies is used a first approximation of the base of gas hydrate stability. The Gulf of Mexico basin in which many of the hydrocarbon plays are closely associated with traps caused by salt buoyancy and tectonics is a leaky petroleum system. Seismic bright spots within the upper 1000 m of sediment are ubiquitous across the Central and Western Gulf of Mexico. The "shallow gas" anomalies are typically, patchy, discrete, thin bed high amplitude trough-over-peak seismic responses in the North American polarity and seismic display convention. These trough over peak gas amplitude anomalies, are often, as a rule of thumb, at least 5 times background amplitude for the same reflector without the gas fluid effect. The interpretation of these bright spots is that the strong impedance contrast is caused by the low velocity of some amount of free gas over 5% saturation.

The gas proxy method for determining the base of gas hydrate stability uses the principle that free gas bright spots tend to not be present within the gas hydrate stability zone and that an imaginary surface connecting the top-most free gas anomalies will be the first-order estimation of the base of gas hydrate stability and assumes that the gases are methane and assumes that the geothermal gradient is, unless the geology suggests otherwise, more similar that different over the local area (McConnell and Kendall, 2002).

Gas amplitudes can be higher within the gas hydrate stability but need supporting explanation of why they are there. Usually these exceptions are along conduits of rapid transport of heat and fluids.

Because the method also encompasses, in part, seismic interpretation techniques for locating hydrocarbon migration areas, zones of secondary or tertiary gas migration to the gas hydrate stability zone where gas hydrate deposits can form can often be identified.

#### 3.1.1.3 Polarity Reversals

Polarity reversals (also known as a phase change and in this report, they are used interchangeably) have been long recognized as a direct hydrocarbon indicator for conventional oil and gas deposits (Brown, 1996). With deeper burial and age than is found in the gas hydrate stability zone, sands often have a higher impedance than the bounding shales. When filled with hydrocarbon the acoustic impedance of the sands will reduce. A polarity reversal occurs when the impedance of the hydrocarbon bearing sand is less than the bounding shale. Without hydrocarbon fill the sand would have higher impedance than the bounding shale. Polarity reversals can also be a direct gas hydrate hydrocarbon indicator. Polarity reversals as a gas hydrate indicator is discussed in the key early paper on bottom simulating reflectors (Shipley, 1979). In the context of recognizing the significance and geophysical cause of the bottom simulating reflector, they showed that the two strong reflections, the seafloor reflection and the BSR reflection, were opposite in polarity. “The BSR- a strong reflector, *opposite in polarity*, cross-cutting stratigraphy and mimicking the seafloor” became a diagnostic descriptor for identifying gas hydrate systems.

A polarity reversal indicating gas hydrate fill relates to changes in relative impedance of shallow buried marine clays and sands and is a different from the continuous reflector caused by small amounts of gas at the BSR. The seismic polarity convention of sediments within the gas hydrate stability differs from older more compacted sediments that are more deeply buried, as a rule. In the gas hydrate stability zone, the clays are not yet shale and the sands are not yet rock. At shallow burial, the clays dewater and compact faster than the sandy sediments which results in the normal relative impedance convention of the sands being lower impedance than the bounding clays. Practitioners of shallow gas mapping in deepwater clastic environments recognize that shallow gas anomalies are in low impedance layers that, when filled with some gas, are high-amplitude low impedance reflectors. The polarity reversal as a direct hydrocarbon indicator for gas hydrate occurs where the shallow sand has a higher impedance than the bounding clay. The gas hydrate system at Walker Ridge 313 clearly shows polarity reversal where gas hydrate filled sediments create high impedance reflectors in what would have been, without gas hydrate fill, a low impedance reflector as shown in Figure 3.3 (McConnell and Zhang, 2005).

#### 3.1.1.4 Blanking

Seismic blanking refers to the absence of reflections in seismic data. Blanking can be caused by attenuation or scattering of seismic energy cause by fluid migration, faults, and dispersed gassy sediments. The physical cause of the dim and blank zones in gassy fine-grained sediments, however, is less understood but is thought to be some combination of p-wave scattering, attenuation, and velocity reduction or homogenization. Higher frequencies are especially inhibited by attenuation within gassy sediments, and is controlled, in part, by gas bubble resonance (Toth et al. 2015). Blanking as an indicator of gas hydrates was identified on the Outer Blake Ridge where the widespread amplitude loss is coincident with the BSR (Shipley, 1979). Acoustic blanking is also an attribute positively associated with gas chimneys and gas hydrate occurrence (Matsumoto and Sato, 2011).

Areas that may have gas hydrate concentrated within fine grained sediments near gas vents can be easily delineated but not quantified with high resolution and conventional seismic data (see comparison of Figures 5.2 and 6.1). The same seismic signal (dim or near zero amplitude) in fine-grained sediments will likely be associated with both low-to-no concentrations of gas hydrate and high concentrations of gas hydrate.

A stage of amplitude blanking is, however, predicted by rock physics models of gas hydrate saturation in sands. A plot of gas hydrate saturation against reflection coefficient based on well logs from the gas hydrate LWD data from GC955 shows, in the topmost curve, a weak trough sand reflector reducing in amplitude to a blanking condition near the zero crossing with 20% to 30% gas hydrate saturation. Amplitude increases with increasing gas hydrate saturation (Figure 3.2). A zero crossing (blanking) is a logical step between low impedance wet sand to high impedance gas hydrate sand.

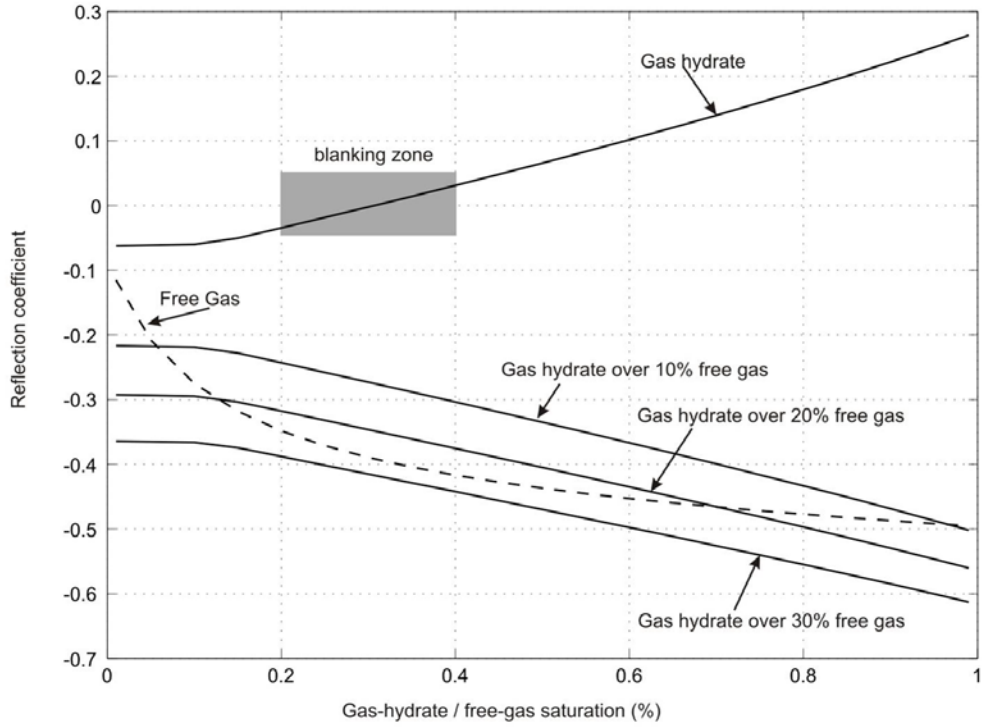


**Figure 3.2 Reflection coefficients of gas hydrate and coupled free-gas saturations. Zhang, personal communication, 2010.**

### 3.1.1.5 Acoustic Inversion

In an inversion for gas hydrate, the extent of the high velocity gas hydrate pore fill and gas hydrate saturation can be delineated. The gas hydrate and gas contact will also be more accurately mapped. An acoustic inversion or acoustic impedance data displays velocity * density layers instead of relative velocity * density reflections. Seismic date is band limited. It is missing both the low frequencies and high frequencies. In order to derive an accurate model of impedance layers through the part of the earth imaged in seismic data, a trend line to represent gradual velocity density trends with depth. The missing high frequencies are usually brought into an acoustic impedance model by relevant well logs that contain high resolution velocity and density information. The advantage of a good model for acoustic impedance data is that it provides a starting basis for understanding layer reservoir properties. One critical impediments for an inversion in the gas hydrate stability zone is that there are usually no sonic or density well logs. In practice, these logs are acquired after the surface casings are set for oil and gas wells and these be towards the base or below the base of gas hydrate stability. Many wells do not have well logs within the gas hydrate stability zone. Cook et al., identified 788 industry wells out of 2700 or 29% in the U.S. Gulf of Mexico with at least 15 m of well log data within the gas hydrate stability zone (Cook and Majumdar, 2016). These logs, however are almost entirely gamma and resistivity logs which have limited value in inversion work. A portion of resistivity logs may be present, but usually other substitutes for the high frequency trend are needed. Mud-line compaction models can be employed as substitutes for sonic and density logs. Direct lithology and density

measurements from geotechnical cores could also substitute, but the scope of measurements from a geotechnical boring would need to be increased and regularized to be useful for inversion.

McConnell and Zhang (2005) used mud-line compaction model to invert for gas hydrate identification and saturation at WR 313. The inversion was useful to clearly identify the phase reversal of the gas hydrate filled sand/silt vs the gas and water wet condition and the extent of gas hydrate deposition into the gas hydrate stability zone along dipping, permeable basin sheet sands/silts at WR313. Saturations predicted from acoustic inversion in the WR 313 gas hydrate system were 60% and were consistent with predrill gas hydrate predictions using full waveform inversion that were confirmed by LWD in the GoM JIP Leg II gas hydrate drilling expedition (McConnell et al., 2009 a).

Isolated gas hydrate deposits and sheets of gas hydrate were identified in the Green Canyon area of the U. S. Gulf of Mexico by acoustic inversion and a rock-physics transform that related acoustic impedance ratios to gas hydrate saturation (Zhang et al., 2011).

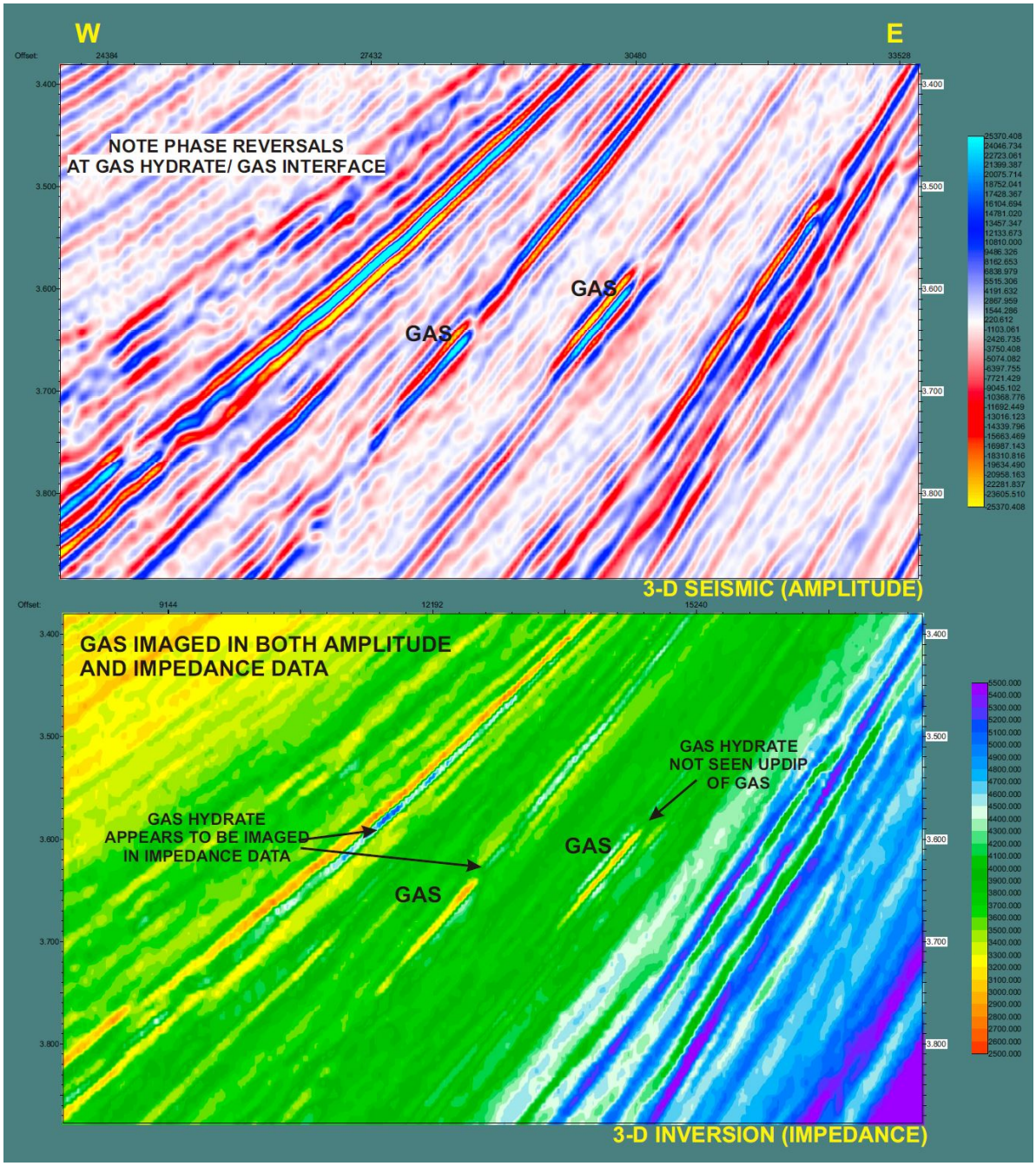


**Figure 3.3 Amplitude and inversion showing phase reversals where dipping sands cross the base of gas hydrate stability. From McConnell and Zhang 2005.**

### 3.1.1.6 Full Wave-Form Inversion

The output of an elastic or full waveform inversion is also an impedance section from which gas hydrate saturation can be predicted. As with acoustic impedance the missing low frequencies and high frequencies

need to be brought into the model. What is different is that full waveform or elastic inversion methods use prestack data to generate both P (compressional) impedance and S (shear) impedance. The low frequency model is derived from the seismic gathers by iteratively computing P and S velocities and density profiles into an optimal solution. The lack of high frequency velocity and density data (no or sub-optimal well logs) within the gas hydrate stability zone is also a problem. Approaches to solve this include computationally intensive high-resolution velocity modeling and the derivation of pseudo-sonic, shear, and density logs through prestack waveform inversion. The advantage of an elastic impedance model is that compressional and shear impedances help constrain the gas hydrate saturation model. The gas hydrate saturation model employed in JIP Leg II used a sophisticated model-constrained Bayesian inversion (Shelander et al., 2010 and Shelander et al., 2012).

### 3.1.2 Developing Techniques

As seismic response models for gas hydrate become incrementally clearer with each completion of a dedicated gas hydrate drilling program, the techniques for identifying gas hydrate can be expanded. Techniques that use AVO, spectral decomposition, and seismic attributes can be applied to gas hydrate identification. AVO is a powerful pre-stack technique used for oil and gas exploration. It can also be used to identify gas hydrate and may be especially powerful for identifying whether a gas hydrate sand overlies free gas or not. Spectral decomposition is mostly used to reveal sedimentary architecture and structure. It has been used as a DHI for oil and gas exploration but mostly in an empirical manner. For application to gas hydrates the wide range of velocities that can be within a single sedimentary feature might be exploited with spectral frequencies. The number of seismic attribute that can be calculated is large. Ascribing a geologic meaning to any seismic attribute can be a challenge, but there are likely some attributes that can help confirm and delineate gas hydrate deposits. AVO analysis of thin bed gas hydrate is discussed in the next section but because no pre-stack data was available, it was not applied to the Eastern GoM dataset. Spectral decomposition and select seismic attributes were generated and analyzed for this project to determine how they might be applied to identify gas hydrate deposits.

#### 3.1.2.1 AVO

Amplitude versus offset (AVO) is a method in which angle dependent reflection coefficients can be used to make predictions about rock properties, lithology, and fluid content. AVO methods have been widely used for direct hydrocarbon indication (DHI) since the 1980s for identification of clastic hydrocarbon-bearing sands and especially for gas sands. In addition to being used to help identify deep commercial gas deposits, AVO have also been used to detect shallow gas sands in marine environment. AVO for deepwater shallow gas is more robust than attempting AVO for shallow gas in shallow water marine survey data because of the much narrower range of offsets in shallow water surveys. When AVO is performed in deep water clastics where the sand has lower impedance than the shale, gas sands will plot as Class III AVO with absolute amplitude increasing with offset. Gas hydrates at high concentrations exhibit strong AVO behavior. The Class III gas sand, if it were a polarity reversed gas hydrate sand will exhibit the opposite AVO behavior within the trough event associated with the thin-bed gas hydrate (Figure 3.4).

AVO techniques can be used to determine gas hydrate concentrations in deposits that are bounded by wet sand and clays that not in contact with gas. A 25% concentration of gas hydrate is flat and may not be detectable because it will plot in the blanking zone. At 50% concentration of gas hydrate in a sand, amplitude will decrease (in absolute amplitude) with offset. High concentrations of gas hydrate 75% in sand will show high amplitude with a marked decrease in absolute amplitude with offset (Figure 3.4).

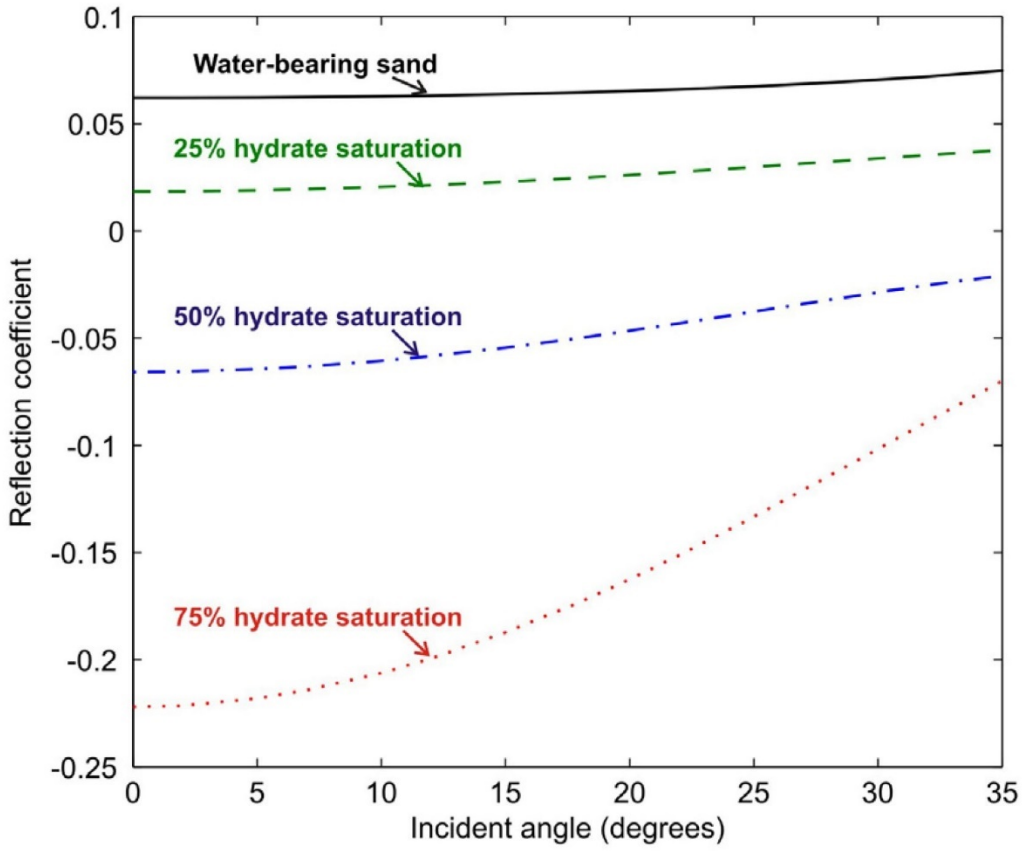


**Figure 3.4 AVO behavior of gas hydrate sand. Note that the AVO behavior is extracted from the thin bed "base" reflector which is a high amplitude low impedance trough. From Zhang et al., 2011.**

AVO can also be used to determine gas hydrate concentrations in cases where the gas hydrate overlies gas. At 25% hydrate saturation over 30% free gas, the reflection coefficient (RC) is high and the absolute amplitude increases with offset. At 50% saturation over free gas, the RC has a higher negative value, but absolute amplitude decreases with offset. At 75% saturation gas hydrate sand over free gas, the RC plots as a higher negative value and absolute amplitude sharply decreases with offset (Figure 3.5).

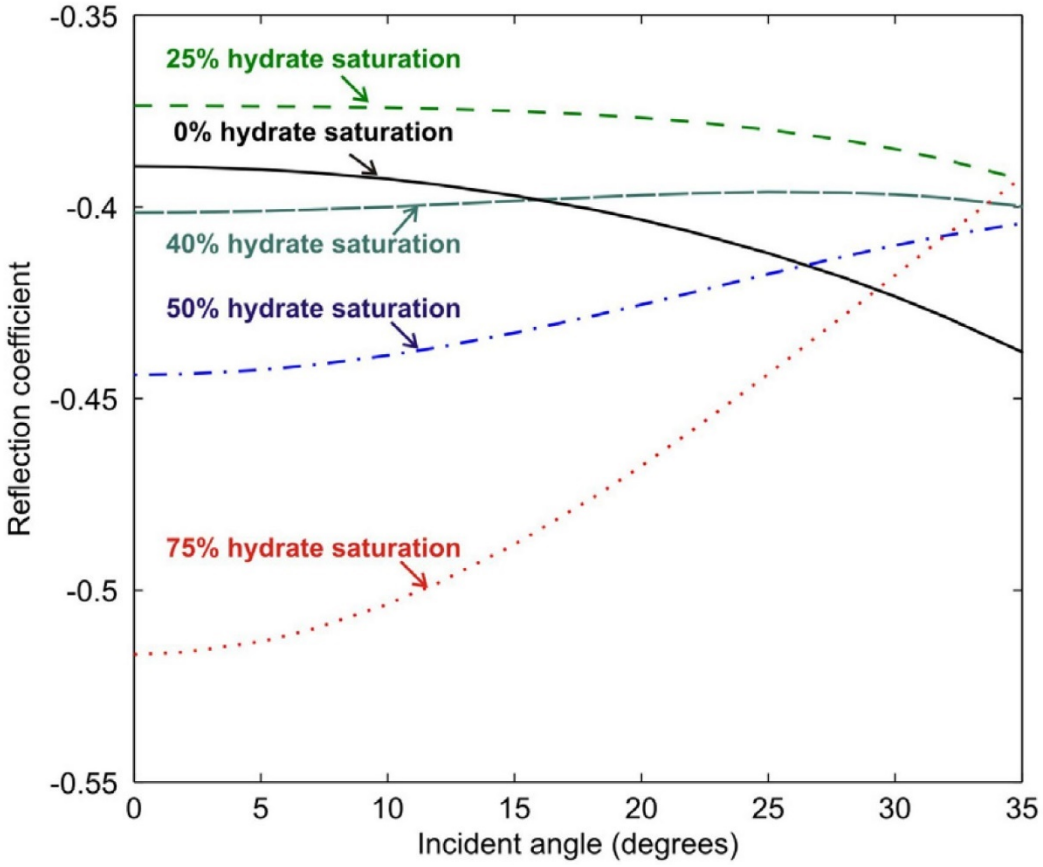


**Figure 3.5 AVO behavior of gas hydrate sand over 30% saturation gas. Note that the AVO behavior is extracted from the thin bed "base" reflector which is a high amplitude low impedance trough. From Zhang et al., 2011.**

### 3.1.2.2 Spectral Decomposition

Seismic data contain a wide range of frequencies within the bandwidth and these frequencies vary with travel time and depth. Isolating different frequencies from a seismic data set is called spectral (or frequency) decomposition. Methods for frequency mapping in time are non-unique, in part, because time windows, the model wavelet, and number and slope of frequency bands are among the input conditions used to produce spectral decompositions.

The utility of the method in seismic data interpretation is that different frequencies in the data contain different information. For instance, regional structural information can be seen in the lower frequencies and smaller detailed information relating to faulting and fractures can be seen in the higher frequencies. Additionally, different lithologies tune at different frequencies depending on the composition and thickness.

For example, a commonly used spectral decomposition method is the short-time Fourier transform in which a time-frequency spectrum is produced by taking the Fourier transform over a set time window. The data are convolved with wavelets of a constant filter length and a constant bandwidth to create frequency limited volumes.

Figure 3.6 is an illustration of a seismic spectrum in the frequency domain. In this example the spectrum is divided into equal frequency bands to cover the entire spectrum with the same bandwidth and filter length in each frequency. Spectral decomposition is used as an effective interpretation tool by combining the magnitude of different frequencies, typically a low frequency, mid-frequency, and a high frequency band into an RGB blend. Subsurface interpretation insights can be gained by seeing which subsurface features illuminate at which individual or combinations of frequencies. Figure 3.7 shows a blending of low frequency in red, mid frequency in green, and high frequency in blue applied to a map view of seismic data in which different geologic events can be seen.

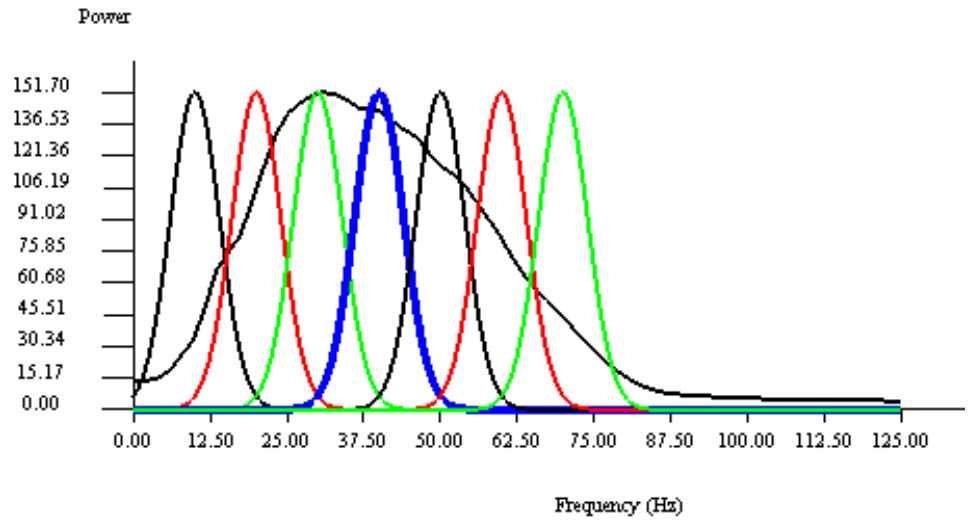


**Figure 3.6 Seismic spectrum divided into equal frequency bands through short-time Fourier transform. Image courtesy Geoteric.**

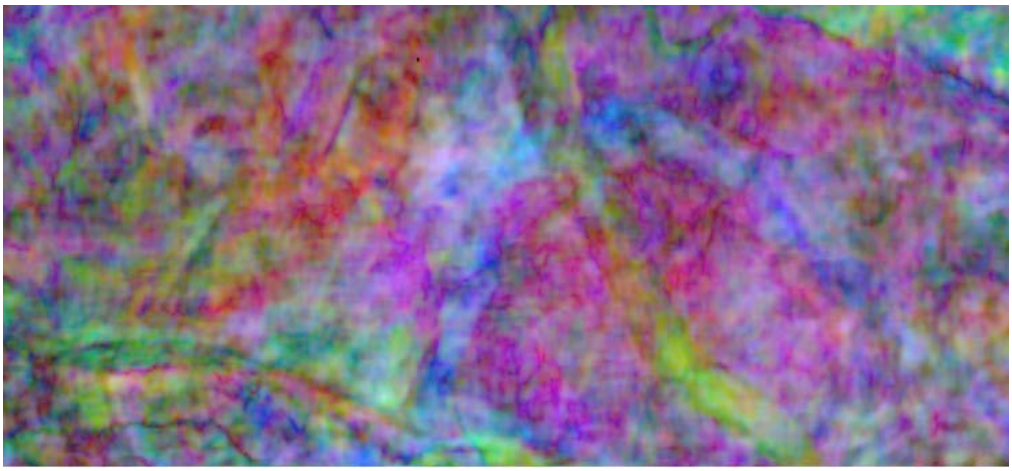

**Figure 3.7 Time slice through the frequency decomposition showing several channels in the data. Image courtesy Geoteric.**

One of the original uses for spectral decomposition was for thin-bed analysis and quantification. In wedge models, spectral amplitudes will cycle as the inverse of temporal thickness. Thus, amplitude and phase components in spectral decomposition can quantify thin bed interference and detect subtle discontinuities (Partyka, 1999).

Spectral decomposition has also been investigated for potential as a direct hydrocarbon indicator or DHI. Castagna and Siegfried (2003) showed that spectral analysis is effective to distinguish between gas sand and brine sands in Tertiary clastics offshore NW Australia. High energy low-frequency shadows beneath sands illuminated in the 10 Hz spectra and high energy within the 30 Hz spectral section illuminated gas sands and did not illuminate the brine sands. These special isolation and correlation techniques in which existing reservoirs were shown to illuminate with high energy at certain frequencies to find additional oil in fields off Nigeria (Fahmy et al., 2008).

3.1.2.3 Other Seismic Attributes

Seismic amplitude is the fundamental seismic attribute. Almost all other attributes are related to, or are components of, seismic amplitude. There are broad classes of seismic attributes derived from amplitude, wave shape, frequency, time, energy, and attenuation, from which numerous pre-stack and post-stack seismic attributes can be derived (Taner and Sheriff, 1977; Chen and Sidney, 1997; Taner, 2003). Modern seismic acquisition, processing, and interpretation software allow for calculation and easy visualization of many measurements derived from seismic data. Seismic attributes can aid in the interpretation of seismic data by revealing features or patterns not seen in seismic amplitude sections and slices. Attributes can be generated that aid in the interpretation of faults, unconformities, thin layers, lithology, pinch outs, and as direct hydrocarbon indicators (DHI).

There are several schemas for categorizing seismic attributes such as in Figure 3.8 from the Society of Exploration Geophysicists.

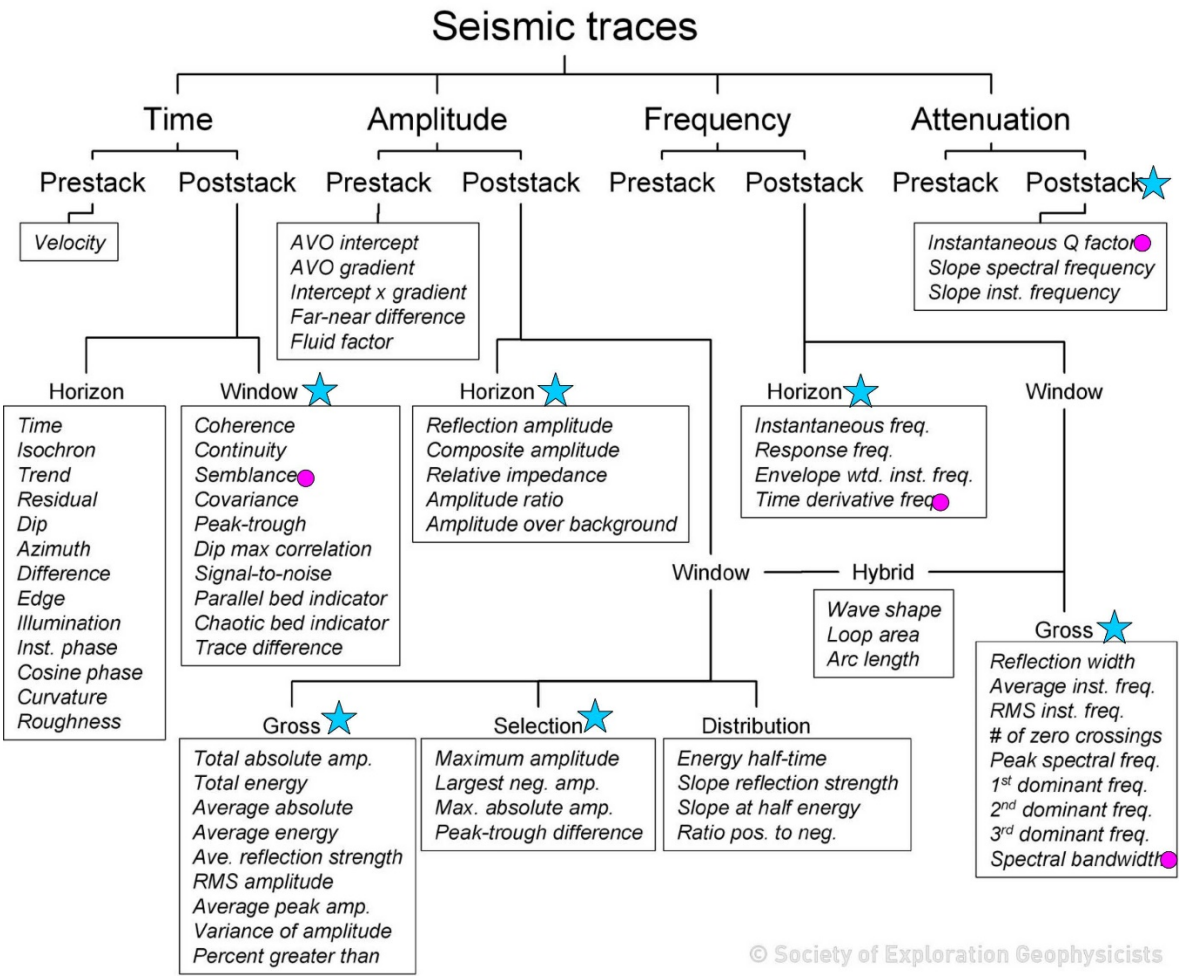


**Figure 3.8 List of seismic attributes by type by Society of Exploration Geophysicists. Categories of attributes considered in this study marked be stars. Circle mark selected attributes used in this study.**

Barnes (2016) advises that the best use of seismic attributes is to use them as filters that quantify properties that have useful meaning. This study selected attributes that might be useful to identify or add a level of interpretive confirmation to high saturation gas hydrate sands in channels.

## 3.2 Insights from JIP Leg II

One of the key hypotheses that was tested during exploration drilling in JIP Leg II, was whether a simple reading of a seismic response was a direct hydrocarbon indicator for gas hydrate saturated sands. LWD drilling at WR313 and GC955 confirmed that specific thin bed seismic responses (although they were not fully recognized as such), within a framework of the gas hydrate petroleum system can be direct gas hydrate indicators.

The main drilling targets at WR313 and GC955 were polarity reversed bright spots. At WR313 these were a series of bright spots within individual units at the base of gas hydrate stability (McConnell and Kendall, 2002; McConnell et al. 2009a). At GC955 patchy high velocity phase reversals within an uplifted and faulted channel sand levee complex outboard of the Sigsbee Escarpment were targeted (McConnell et al., 2009b).

### 3.2.1 Polarity Reversal

Rock physics modeling for what the seismic response of a gas hydrate sand indicated that as gas hydrate deposited in the pore space in sands, the velocity of the sands would increase with gas hydrate saturation (Nur and Dvorkin, 2008). In the context of under-consolidated deepwater GoM sands in the gas hydrate stability zone a wet sand would change from low impedance relative to bounding clays to high impedance when gas hydrate saturations exceeded a threshold of about 40%. At WR313 the gas hydrate petroleum system was described in detail by McConnell and Kendall (2002) where a series of discontinuous dipping gas bright spots defined the base of gas hydrate stability. Acoustic inversion revealed these gas bright spots to phase reverse across the base of gas hydrate stability and that the high amplitude phase reversed thin bed response indicated high saturation of gas hydrate (McConnell and Zhang, 2005) that was confirmed by LWD drilling (McConnell et al., 2009).

### 3.2.2 Leading Peak Anomaly

The same prospecting philosophy was applied at GC955 to patchy discrete "leading peak" anomalies in sands at the base of gas hydrate stability. These leading peak anomalies were drilled, and logs showed high saturation gas hydrate correlated tightly with the high amplitude thin-bed seismic response (Figures 3.9 and 3.10). X-rays of pressure cores taken at the anomaly confirmed layered high saturation gas hydrate in the silty sands (Flemings, 2017).

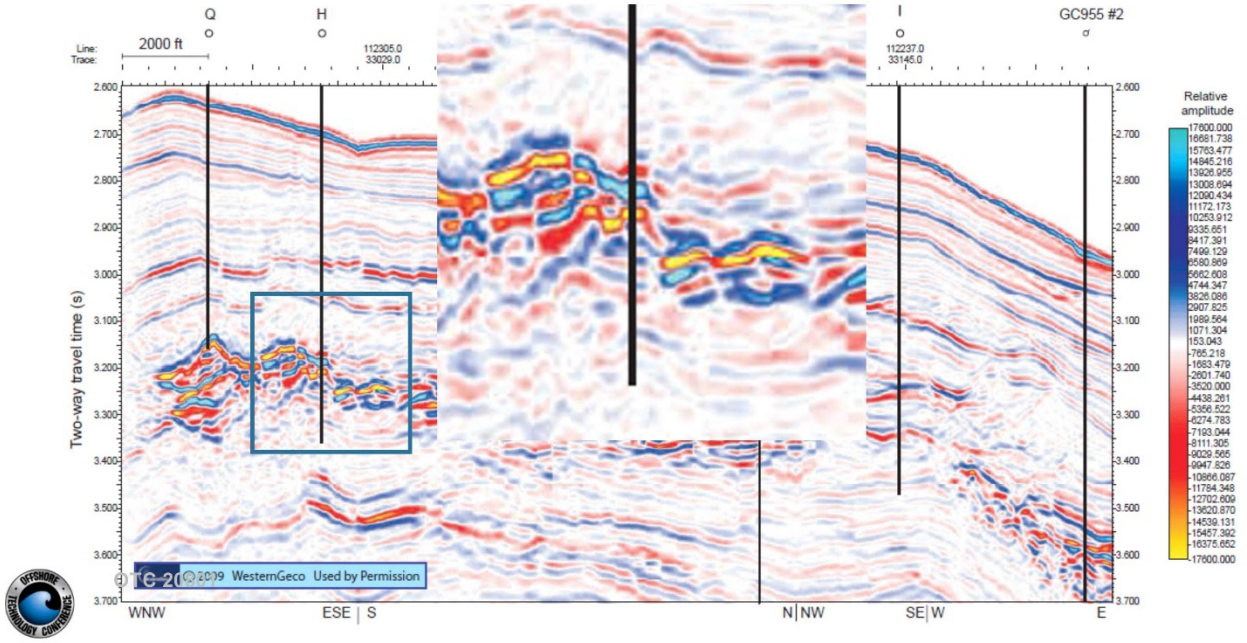


**Figure 3.9 Green Canyon 955 (GC955) H showing polarity reversal at "leading peak" seismic anomaly that tightly correlates to high saturation gas hydrate confirmed by well logs and pressure cores. Inset shows magnified view of area in blue box.**

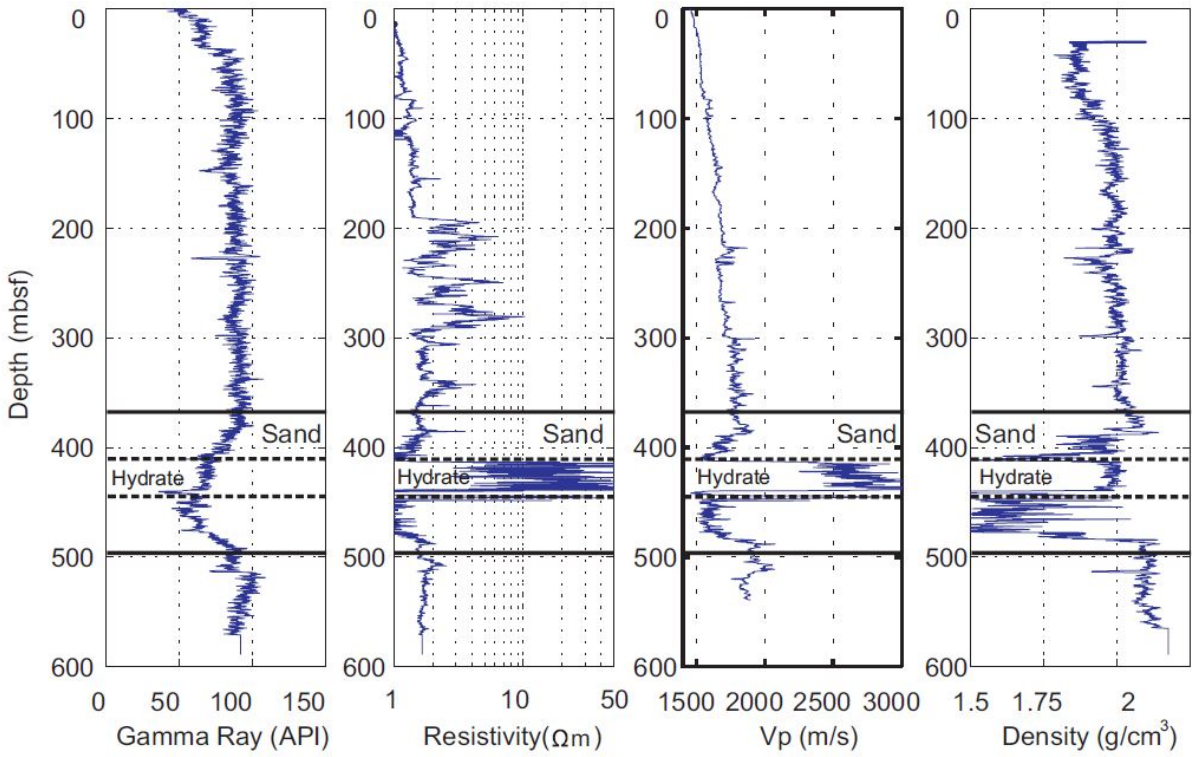


**Figure 3.10 Gamma ray, resistivity, compressional-wave (Vp) acoustic, and density logs from well GC955-H, showing high concentrated gas hydrate within a thick sand. The low-density values in the non-hydrate bearing portion of sand-rich section are probably produced by borehole washout (Guerin et al., 2009). From Zhang et al., 2012 b.**

### 3.2.3 Simplified Framework for Prospecting for High Saturation Gas Hydrate Sands

After the success of the gas hydrate direct hydrocarbon indicators for high saturation gas hydrates in sands, Boswell and others (2016), assembled “type” sections from gas hydrate field programs from around the world and ranked them by the types of deposits more prospective for energy resource and those less prospective (Figure 3.1). Most gas hydrates are in low permeability marine clays, either pore filling such as found in a Mahandi basin off India (Collett, et al., 2008) and Blake Ridge (Matsumoto) or grain displacive in chimney structures (Matusmoto, Ryu). Coring and drilling programs have investigated these types of gas hydrate deposits guided by the geophysical indicators associated, but not uniquely associated, with these deposits- BSRs and blanking in pore filling clays, and chimney structures in vein-fill grain-displacive clays. Low concentrations of gas hydrate, often less than 10% saturation of the low permeability clays were typical. Higher concentrations of hydrate, up to 40% of pore space, in both disseminated or massive habit have been found in the chimney structures, but the geophysical signature (acoustic blanking) is not tightly correlative to discrete deposits, but rather delimit an area in which these grain displacive gas hydrate in clays can be found. These type deposits on right, are considered less prospective than gas hydrate deposits in sands near the base of gas hydrate stability on left (Figure 3.1).

Furthermore, drilling results at the discrete thin bed phase reversals in sands at the base of gas hydrate stability indicated that amplitude could be diagnostic of gas hydrate saturation in contrast to the thin bed gas response in which amplitude is insensitive to gas saturation (Figure 3.11). Seismic amplitude appears to be a more robust DHI for gas hydrate than it is for gas in that it not only can indicate the presence but also the saturation at the saturation threshold of interest for economic gas hydrate deposits.

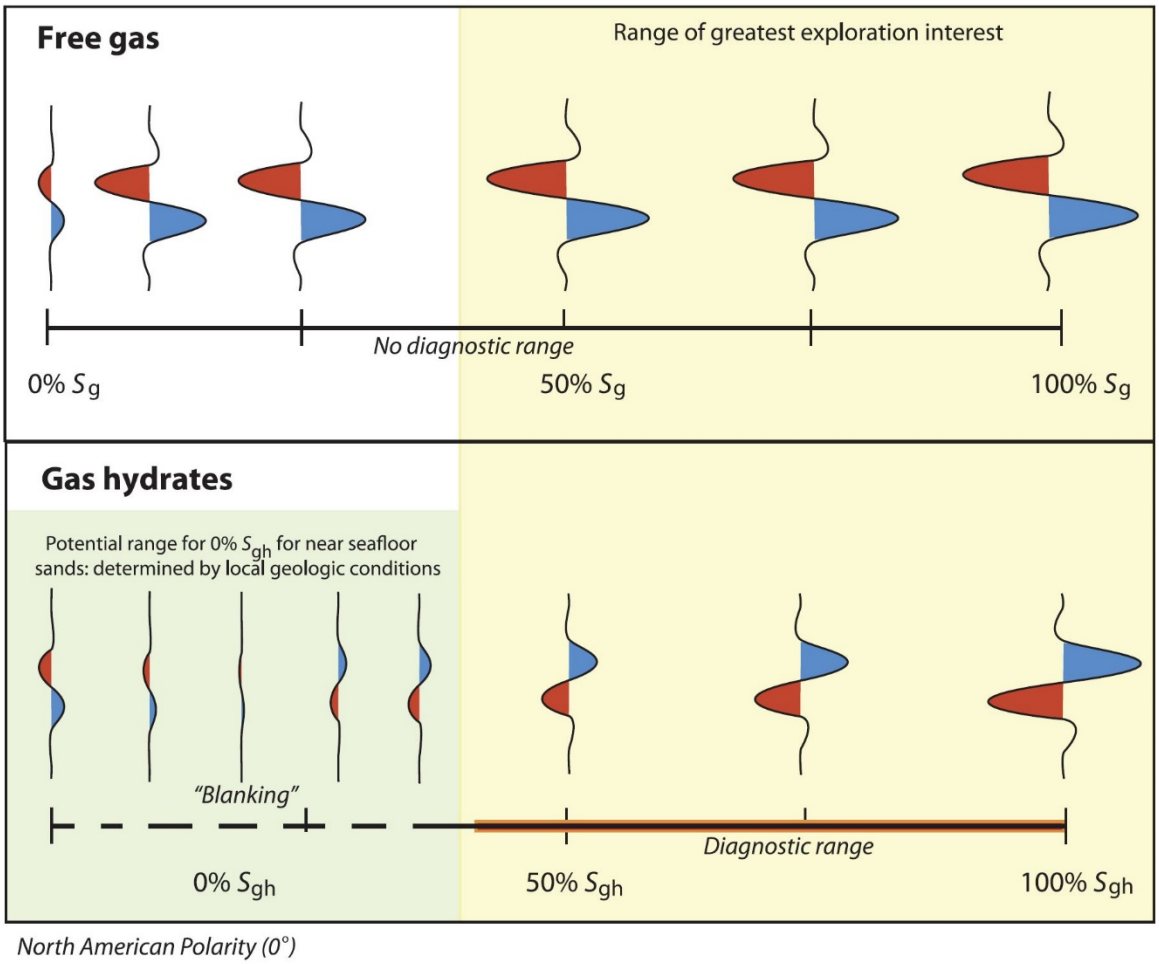


**Figure 3.11 Simplified thin bed response for free gas and gas hydrates. Assumes under-consolidated sands in which a wet sand is less dense than bounding clays such as in deepwater settings. From Boswell et al., 2016.**

# 4. GEOLOGIC SETTING AND PETROLEUM SYSTEMS IN THE EASTERN GULF OF MEXICO

The Eastern portion of the deepwater Gulf of Mexico is much less explored than the Central and Western regions because of the moratorium on hydrocarbon exploration that has been in place prior to deepwater exploration in the Central and Western portions of the United States federal waters.

The Eastern Gulf of Mexico, here, refers to the area bounded on the west by approximately longitude 88.25 projecting south from where the modern distal Mississippi River discharge, on the north by the North American continental shelfs off Mississippi, Alabama, and Florida, to the east by the carbonate reef comprising the Florida escarpment, and the Yucatan shelf and the Straits of Florida to the south and southeast, respectively (Figure 4.1).

In contrast to the Western and Central regions, where the subsurface geology is strongly influenced by thick sediment loading onto Jurassic salt, the Eastern region is less characterized by salt tectonics and instead by simpler thick up to 15 km of Cenozoic sedimentation overlying Cretaceous sediments deposited on the rifted Jurassic section. Salt does play an important role in trapping hydrocarbon and gravitational movement of salt is important for the development of the deepwater Norphlet play, for example.
These thick clastic sediments were deposited in abyssal fans both mud and sand rich from the Eastern and Central Mississippi River Deltas. The MCAVLU (named for the Mississippi Canyon, Atwater Valley, and Lund protractions areas) is a sand rich Miocene submarine fan that deposits up to 1km thick into the Eastern GoM. Late Pliocene slope bypass deposits were followed by an approximately 1 km thick sand rich Pleistocene Mississippi fan and Eastern Mississippi fan deposits. The modern deepwater Mississippi fan comprises the modern seafloor over the Eastern GoM (Galloway et al., 2000).

As a result, the Eastern GoM has an unusually thick section of sandy channel and potential sandy reservoirs. Thick sandy facies spanning the base of gas hydrate stability in the study area correspond to late Pliocene and Pleistocene basin floor fan deposits.

## 4.1 Data Availability and Description

**Table 4.1 Available data**

| *Data* | *Description* | *Notes* |
|---|---|---|
| *Florida 3D Exploration Seismic Data Volumes* | *a) Final Pre-Stack Depth Migration*<br><br>*b) Final PSDM in time*<br><br>*c) Pre-Stack Depth Migration Velocity*<br><br>*d) Final Reverse Time Migration Stack* | *Data agreement had conditions that generally preclude reporting of precise locations and depths. Only Post-Stack data provided.* |
| *DSDP Leg 96* | *Publicly available field and summary reports* | |
| *Well Logs from LL511 #1* | *Publicly available paper records of logs* | *Digital versions of the logs requested from Murphy Oil Corporation* |

### 4.1.1 Florida 3D

The Florida 3D survey was shot as a multi-client data in anticipation of the opening of the Eastern Gulf of Mexico by the US federal government to oil and gas exploration prior to the Deepwater Horizon accident. The data were acquired by Fugro in 2011 and 2012 in the Eastern GoM in two phases using the M/V Geo Caspian and M/V Geo Caribbean with both vessels using same acquisition parameters. It is a narrow-azimuth 3D seismic covering 510 OCS block with a total area of ~ 12,750 km2 (Each OCS Block is 9 sq miles or ~25 sq km in area) in water depths ranging from 280 m to 3268 m. The data are in the Lloyd Ridge and The Elbow protraction areas (Fugro, 2013) (Figure 4.2).

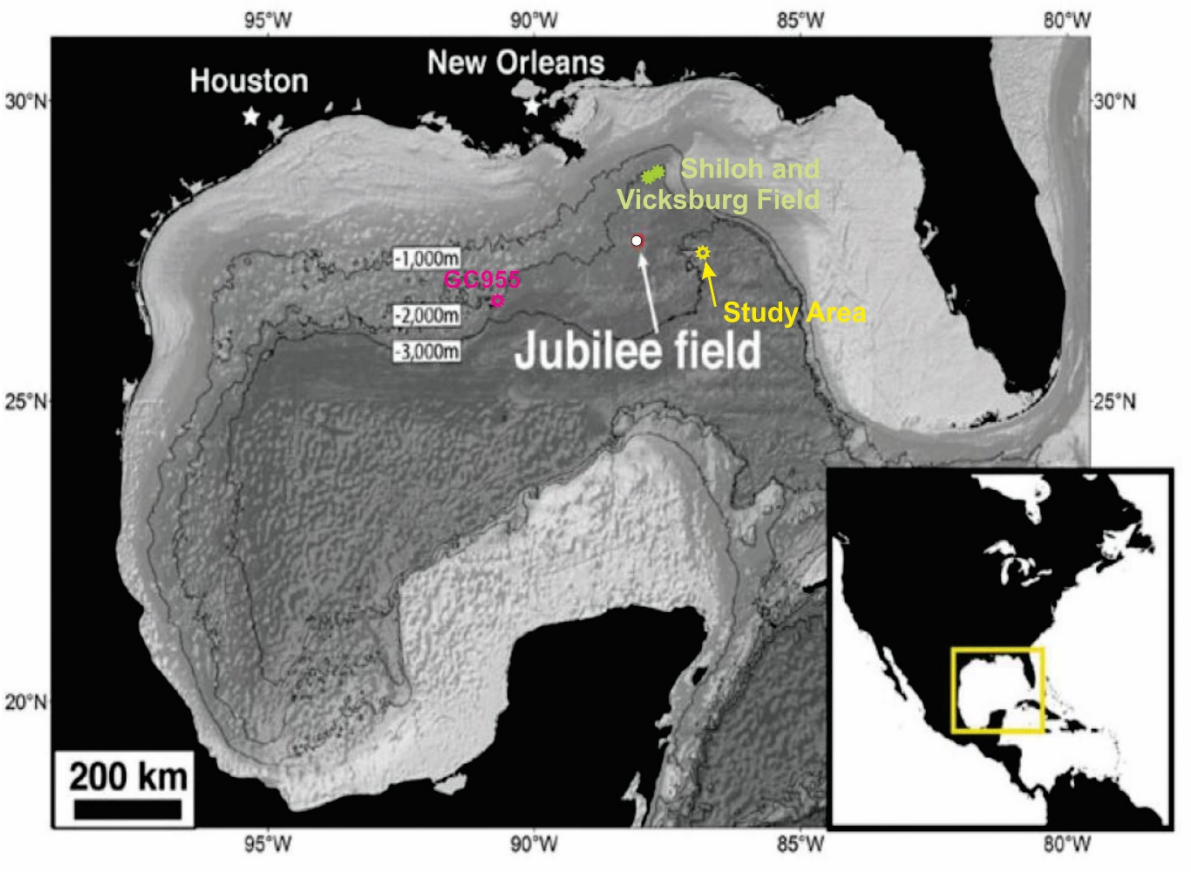


**Figure 4.1 Location map showing study area and nearby hydrocarbon finds – Jubilee Miocene (gas) and Shiloh and Vicksburg Jurassic (oil). Also shown is GC955 gas hydrate discovery.**

The data were shot with ten 9 km steamers towed at 9.0 m. The streamer group interval was 12.5 m. The processing grid is 30.0 m in the inline and 25.0 m in the crossline direction with a coverage fold of 60. The data were processed record length of approximately 10 seconds or15,000 m. A tomographic depth model was built from the principal horizons, seafloor, salt in the shallow water part of the survey and, a salt weld horizon and a Jurassic horizon in the deep water areas of the survey. The flat lying nature of the sediments in deep water allowed the tomographic velocity model to isolate and image slow velocities related to fluid migration in the deep water areas (CGG, 2014).

The data volumes that were provided are listed in Table 1. Only post-stack data volumes were provided. This limited the range of interpretation techniques. Important interpretation techniques such as amplitude vs offset (AVO) could not be performed.

The reverse time migration showed the clearest imaging of faults, but the downside is that the processing sequence shifted to lower frequencies, greatly reducing the resolution within the section of interest at the base of gas hydrate stability. Work was done using the depth migration and the converted depth migration in time. It was easier to use some of the software in time. Reported depths, when allowed by the data

owners refer to the final depth migration. Thicknesses computed from frequency decomposition are computed from time. A cross section is shown as Figure 4.3.

## 4.2 Gas Hydrate Petroleum (Hydrocarbon) Systems in the Eastern GoM

The gas hydrate petroleum or hydrocarbon system is simply an extension of the conventional oil and gas petroleum system with only few differences. The petroleum system approach is a framework that integrates the component elements and processes that result in oil and gas accumulations and is used as a guide understanding and exploring for conventional oil and gas. The fundamental concepts involved in the analysis of a conventional hydrocarbon system, such as source, reservoir, and seal along with generation, migration, and accumulation also apply to the gas hydrate system. For example, a fundamental objective for conventional oil and gas exploration is to understand and determine where secondary and tertiary migration of oil and gas hydrocarbons can accumulate in traps that can be produced economically. Further up-section, a key gas hydrate component of the overall petroleum system includes where the secondary and tertiary migration of gas extends into and through the gas hydrate stability zone where pressure and temperature conditions exist that allows gas and water in the sediment pore spaces to form gas hydrates. The only mechanism for gas hydrate emplacement that is significantly different from that of a conventional oil and gas petroleum system are gas hydrates that form in-situ by methanogenesis within the gas hydrate stability zone

.

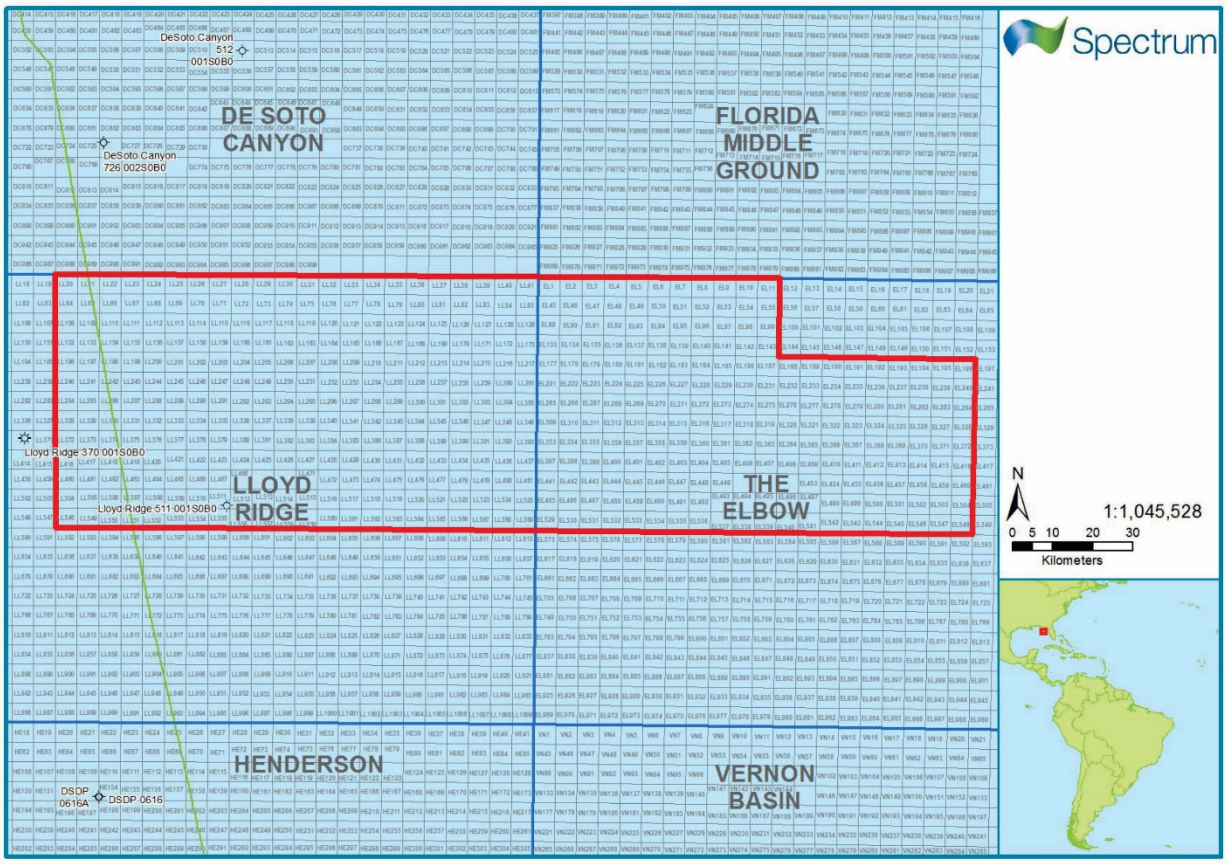


**Figure 4.2 Outline of Florida 3D shown in red. Named areas such as Lloyd Ridge are names of protraction areas in the US Federal Outer Continental Shelf.**

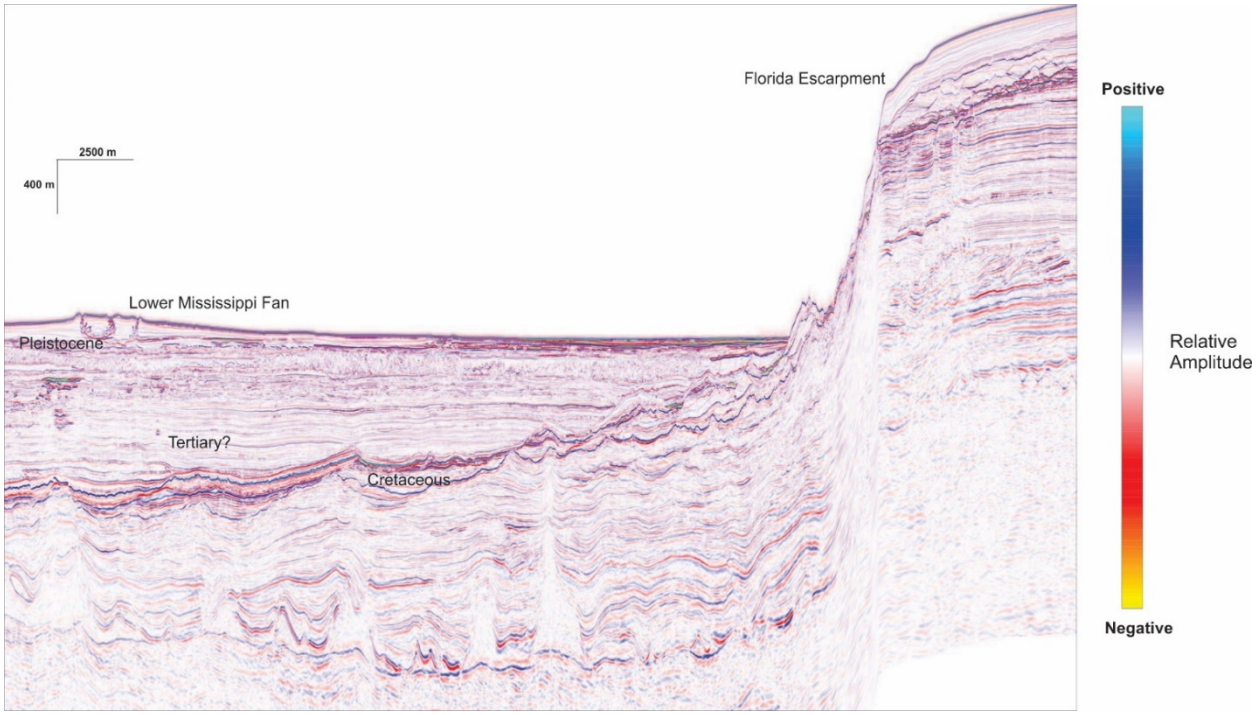


**Figure 4.3 Seismic cross section across Florida 3D. Ages are inferred from other sources.**

The gas hydrate hydrocarbon system in the Eastern GoM is thought to be like that which has been studied in the Central GoM. In the Central GoM, gas hydrates have accumulated in sands at the base of gas hydrate stability from secondary and tertiary migration of gas into the gas hydrate stability zone. These gas hydrate accumulations were discovered in the absence of BSRs.

### 4.2.1 Source and Migration

Source rocks for hydrocarbon generation in the Eastern GoM are thought to be Jurassic and Cretaceous. Jurassic (Tithonian) calcareous marine shales are world-class source rocks that generate most of the conventional hydrocarbons in the Central and Western GoM (Salvador, 1991). In the Eastern Gulf of Mexico, Jurassic Norphlet dune oil reservoirs approximately 5500 m below the seafloor (7600 m below sea surface) are being produced. These large oil discoveries are approximately 50 km to the NNW of the study area, above which, lies the thick Jurassic gas-rich Hayneville source rock. Mapping of these of these well-known source rocks into the study area is out of the scope of this study but it is likely that these widespread Jurassic and Cretaceous source rocks are present in the study area. Thick sections (over 2000 m) of Smackover, Haynesville, and Cotton Valley are present in the northern part of the Desoto Canyon protraction area (Pashin et al., 2017). Norphlet sands and associated petroleum generation facies are projected to extend into the northern portion of the Lloyd's Ridge protraction area (Smith, 2015).

In the central Gulf of Mexico, the mobilization of salt through the younger sediments is arguably, the most important mechanism for hydrocarbon migration. Louann salt deposits were likely deposited in the study area but maps show the southeast margins of the deposits in the area (Salvador, 1991; Smith, 2015). Some

salt extrusions are seen in the in the Eastern GoM data. Salt movement in the study area is implied from regional interpretation and the identification of “salt weld” and “Jurassic” horizons that were used as primary controls in the velocity tomography used for the pre-stack depth migration (CGG, 2014). Salt welds allow for the migration of hydrocarbons across what had been a salt seal. The timing of the salt movement that allows for hydrocarbon migration from hydrocarbon generating sediments below are all critical components with first order implications for migration and accumulation in the gas hydrate stability zone.

### 4.2.2 Reservoir

#### 4.2.2.1 Channel Deposits and Reservoir Characterization

In the study area, deepwater clastic deposition begins with the widespread early Miocene sandy basin floor apron deposits Central Mississippi delta system that extends across most of the Gulf of Mexico basin in the Early Miocene 25-18 Ma. Galloway, et al., (2000) shows the sandy abyssal facies extending across the southwestern half of the Lloyd Ridge protraction area with a starved basin setting in the northeastern half. In the Middle Miocene, the MCAVLU fan deposits sand-rich sediments across the southwestern half of the study area. The study area was sediment starved despite proximity to deposition into the Central Gulf of Mexico until thick sandy basin floor sediments were deposited in the late Pliocene and Pleistocene (2- 0.1 Ma) (Galloway et al., 2000) (Figure 4.4).

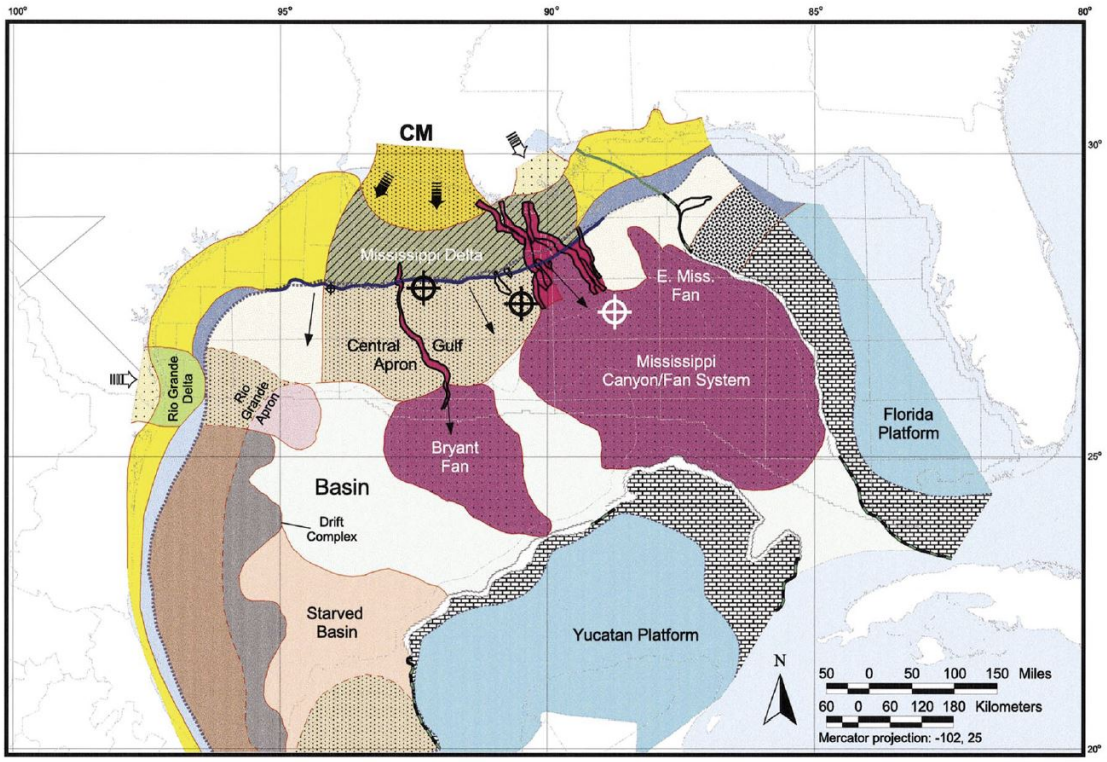


**Figure 4.4 Late Pliocene depocenters in Gulf of Mexico. Study area labeled E. Miss. Fan. From Galloway et al., 2000.**

#### 4.2.2.2 Well Penetrations

DSDP drilling into the modern Mississippi fan in the Eastern Gulf confirmed thick sand deposits 400 km from the source. Seismic data show thick repeating sections of channel and channel lobe deposits continuing past the shallow penetration of the DSDP hole to at least 600 m below the seafloor.

Lloyd Ridge 551 #1 was drilled by Murphy in August 2008, within the Area of Restriction in the Eastern Planning Area within 15 km of the area of interest in this study. The well logs from the Murphy well in LL 551, like the DSDP well, indicate thick sandy facies as thick as 100 m in the upper portion of the well within the gas hydrate stability zone (Figure 4.5).

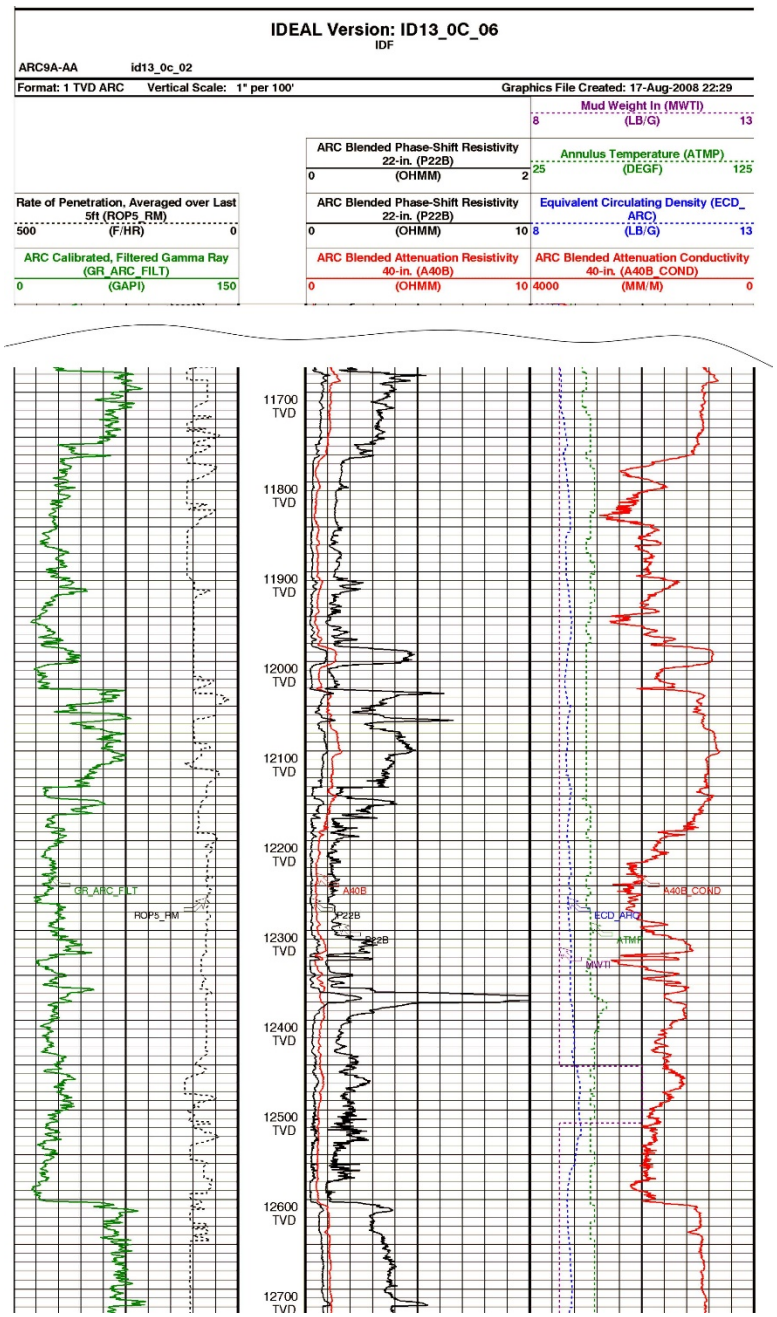


**Figure 4.5 Well logs from LL511 within 15 km of study area showing thick Pliocene sands (low gamma ray, green) within the gas hydrate stability zone**

### 4.2.2.3 Pleistocene Abyssal Fan Channels

Pleistocene abyssal fan sediments in the study area are composed of multiple levels of channel deposits. Channel exhibit high sinuosity and have low profiles suggestive of lower sand/mud ratios. Point bars are

common, as are braided channels within the same channel run. Channel are, in general, uniform in size. Narrow channels are 0.5 km across and 50 m thick. Larger, main, channels are 1 to 1.5 km across and 90 m thick.

# 5. METHODS APPLIED

## 5.1 Data Screening

The Florida 3D is large data set encompassing the Florida Shelf, Florida Escarpment, and deepwater with respective water depths range from 280 m to 3268 m. The petroleum systems surmised for this part of the Eastern Gulf of Mexico include, on the Florida Platform, Cretaceous shelf edge reefs and fans, and inner platform plays. In the deepwater area potential hydrocarbon play are speculated to have potential in Jurassic horst-graben buried hill structures, traps associated with Jurassic and Cretaceous salt tectonics, and traps within the Oligocene and Miocene clastic section (Roberts and Finstad, 2006).

The data were scanned for BSRs and for the trend of the shallowest gas anomalies (gas proxy). Initial interpretation involved screening the data for shallow gas amplitudes. Some interpreters working this project focused on sediments within the Florida Escarpment where the gas-gas hydrate interface where cross cutting reflectors (BSRs) could be more easily seen. Other interpreters focused on the flat lying deepwater section for indications of possible gas-gas hydrate interfaces.

While other potential gas hydrate anomalies were found across the data such as along the basin margin slopes, the potential gas hydrate deposits selected for this study are found the western half of the data where particularly well-channelized deposits from Plio-Pleistocene sandy basin floor sediments are positioned above a fluid migration pathway.

## 5.2 Identification of Gas Hydrate Deposit

The research project was fortunate to be able to screen a large area (over 12,500 sq. km) because the Eastern GoM is much less leaky than the Central and Western GoM. Very few faults offset into the gas hydrate stability zone. The cross section through the gas hydrate deposit shows two of the few long-reach buried faults in this area of the Eastern GoM (Figure 4.3). No conduits for hydrocarbon seepage to the seafloor were identified.

As mentioned, a gas hydrate petroleum system requires a flux of gassy fluids to the gas hydrate stability zone. The Central GoM is a complex leaky system that allows for gassy fluids to move through the gas hydrate stability zone and to seeps at the seafloor from cross-strata migration and fault conduits caused by mobile salt. Sediments in the Eastern GoM are much less disrupted by salt. Salt in the Eastern GoM tends to be deeper, autochthonous or rooted to autochthonous stocks. This difference manifests as an area characterized by regional deep structures overlain by succession of thick Miocene and Plio-Pleistocene deepwater abyssal fan deposits.

A gas hydrate deposit was identified along the long-reach buried faults trend and is shown on Figure 5.1. The deposit has the geophysical signature of a high velocity gas hydrate filled sand. The seismic character is like the proven gas hydrate deposit at GC955 in the Central GoM. The amplitude at the interpreted gas hydrate deposit is a strong peak over trough reflector at the predicted base of gas hydrate stability above a deep seated fault. The deposit was unique in that given the facies and fault trends, more gas hydrate deposits would be expected. None with similar characteristics, however, were identified.

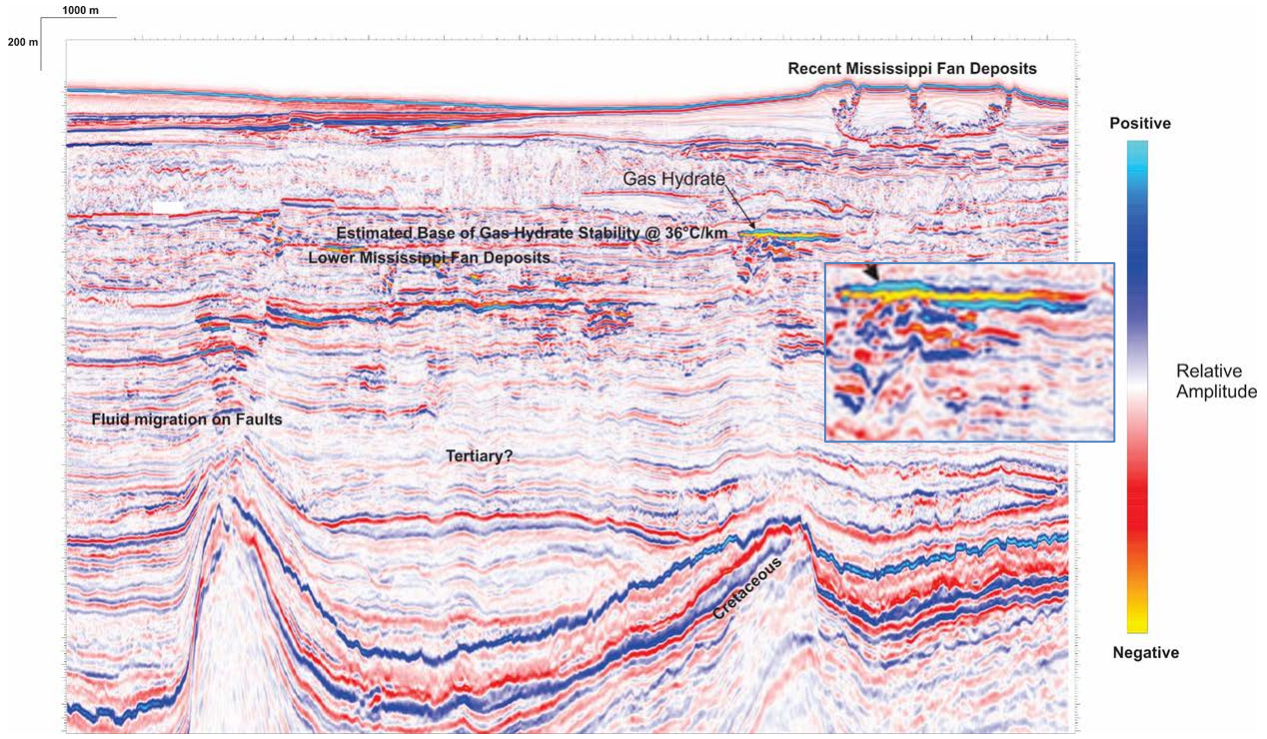


**Figure 5.1 Seismic cross section (amplitude, full spectrum) showing deep fluid migration to gas hydrate stability zone with gas hydrate deposit shown as inset.**

### 5.2.1 Source, Migration, and Reservoir

Oil is being produced from the deepwater Eastern Gulf of Mexico Jurassic Norphlet play 50 km north of the study area. Vicksburg and Shiloh fields in the Desoto Canyon protraction area are examples (Figure 5.2). The thick Jurassic and Cretaceous source rocks in Desoto Canyon are also present in Lloyd Ridge and the study area (Figure 5.1).

In addition to the deep Jurassic oil play there is a Miocene gas play. The Jubilee gas field, approximately 100 km ENE produces from upper Miocene high density turbidites and frontal splay channels with a mass transport complex top seal (NOIA, 2014).

Few faults offset the thick Cenozoic section in the study area. The area lack lacks complex salt structures that pierce the Cenozoic section in the Central Gulf of Mexico. In the Eastern Gulf of Mexico, salt, even though autochthonous is more closely rooted to, or confined within, the Jurassic sediments in which they were deposited. In large part, because of this, there are fewer migration pathways for hydrocarbon to and through the gas hydrate stability zone in the study area.

Hydrocarbon seepage to the seafloor is used to establish a working petroleum system for conventional hydrocarbon exploration (McConnell et al., 2008). Evidence of seepage is more important to establishing a gas hydrate petroleum system because of the requirement of a flux of gas fluids flux to at least the base of

gas hydrate stability. The geologic mechanisms, faults, diapirs, carrier bed for gas emplacement to the base of gas hydrate stability are classes of features that also may intersect the seafloor. Evidence of hydrocarbon migration to the seafloor can confirm a working petroleum (or gas hydrate) system, but the absence of seafloor seepage does not indicate that there is no working petroleum (or gas hydrate) system. The seismic section shown over the Vicksburg and Shiloh oil producing fields, for instance, does not suggest that the hydrocarbon system extends into the Plio-Pleistocene sediments.

The few faults that do offset the Cenozoic section are SW of the study area includes faults at the crest of an interpreted salt diapir (Figure 5.1). One of these faults extends to the near seafloor sediments, but, given the limitations of 3D seismic, the data don't suggest the presence of seeps. Nevertheless, there is amplitude brightening, in the sediments above this fault, like the apparent hydrocarbon target for the Murphy exploration well. The fault does offset the Plio-Pleistocene sandy channel and potential lateral hydrocarbon migration.

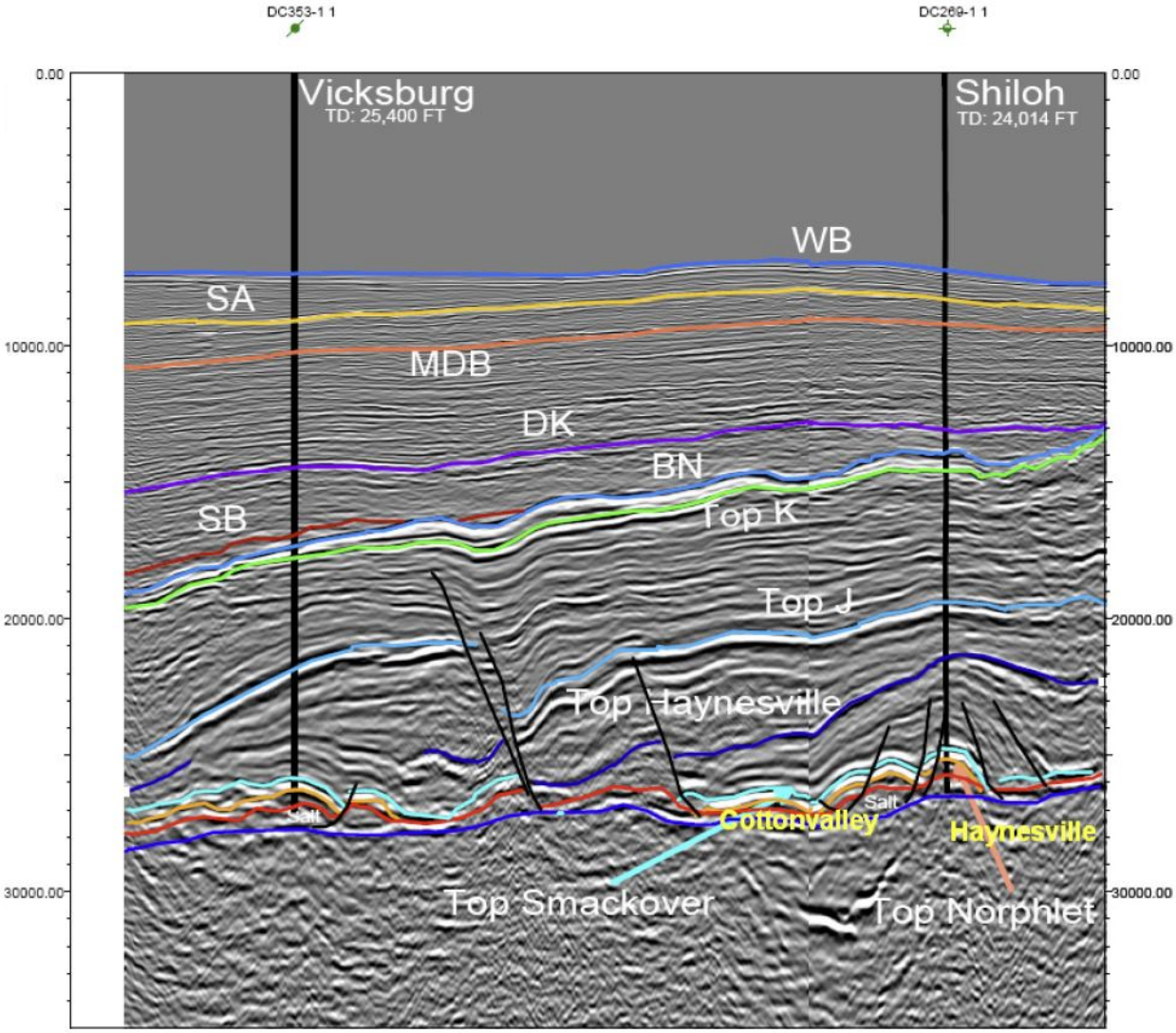


**Figure 5.2 Vicksburg and Shiloh oil fields producing from the Jurassic Norphlet and Smackover play. Note thick Jurassic and Cretaceous source rocks and deep salt remnants. From Chowdhury, 2009.**

### 5.2.2 Gas Hydrate Stability Conditions and Geothermal Gradient

The pressure and temperature conditions for gas hydrate to form have an upper bound at approximately 450 m in the Gulf of Mexico, where typical water bottom temperatures can be 7 to 8 °C. The gas hydrate stability zone expands in thickness as pressure increases with water depth. Regional geothermal gradients define the thickness of the gas hydrate stability zone for a given pressure. Geothermal gradients vary across the deepwater Gulf of Mexico, with cool geothermal gradients typically 15 °C/km in the Walker Ridge protraction area to 20 °C/km in Mississippi Canyon using well temperature data only (Forrest et al., 2005). A more sophisticated method for calculating geothermal gradients using additional well log data show a similar wide range of geothermal gradients from 15 °C/km in Atwater Valley protraction area to 34 °C/km in Alaminos Canyon. (Jones, 2003). Note that local geothermal anomalies are included in the database since many well have targeted prospects near allochthonous salt. Both investigators report a wide range of

geothermal gradients are in all deepwater areas with the method by Jones showing more convergence. Because of the lack of oil and gas wells, no similar data exist for reporting regional geothermal gradients in the Eastern Gulf of Mexico.

Numerous authors have used BSRs or equivalent seismic indications of the base of gas hydrate stability to estimate geothermal gradients (examples: Uyeda et al., 1982; Lee, 1995; Rastogi and Deka, 2001; Vanneste, et al., 2005). In the Gulf of Mexico examples include McConnell and Kendall (2002) and McConnell et al., (2009). Estimates of geothermal gradients from BSRs are consistent with measurements taken by other means. For example, the geothermal gradient of 27 °C/km estimated from the apparent base of gas hydrate stability GC 955 (McConnell et al., 2009) matches the 26.9 °C/km geothermal gradient derived from well data from GC 955 #1 (Jones, 2003).

#### 5.2.2.1 Heat Flow Measurements in the Eastern GoM

A heat flow measurement of 41 mW/m2 that can correspond to a shallow geothermal gradient of approximately 36 °C/km was taken within ~20 km southwest of the seafloor above the gas hydrate target (Langseth, 1970). Other nearby heat flow measurements in the database (Hutnak, personal communication) are 39 mW/m2 (~34°C/km) and 19 mW/m2 (~16.5 °C /km) are within 40 km. Heat flow measurements by TDI Brooks in the northern deepwater area of Lloyd Ridge fall in the range of 35-45 mW/m2 (Jones, 2003) The thermal conductivity used to compute the geothermal gradient from heat flow is 1.15 W/m-K, which is higher than the 0.84 W/m-K measured at the site. It is, however, normal for raw thermal conductivity measurements to be adjusted to estimate basin heat flow. Lee (1995) used an average depth dependent thermal conductivity of 1.146 W/m-K for thermal modeling of thick sections of silts and clays on the Carolina continental rise.

#### 5.2.2.2 Geothermal Gradient in the Study Area

The average thermal conductivity value of 1.15 W/m-K that was chosen to correspond with the heat flow measurement of 41 mW/m2 proved to be serendipitous since the predicted base of gas hydrate stability directly matches the depth of the interpreted gas hydrate deposit for 100% methane and seawater (Figure 5.3). The thermal conductivity could, of course, be different. No bottom hole temperatures accompanied the public well logs at the nearest well, LL511. Given the intersection between the large gas hydrate-gas seismic anomaly and the predicted base of gas hydrate stability, the geothermal gradient is not likely to be colder than 36 °C/km.

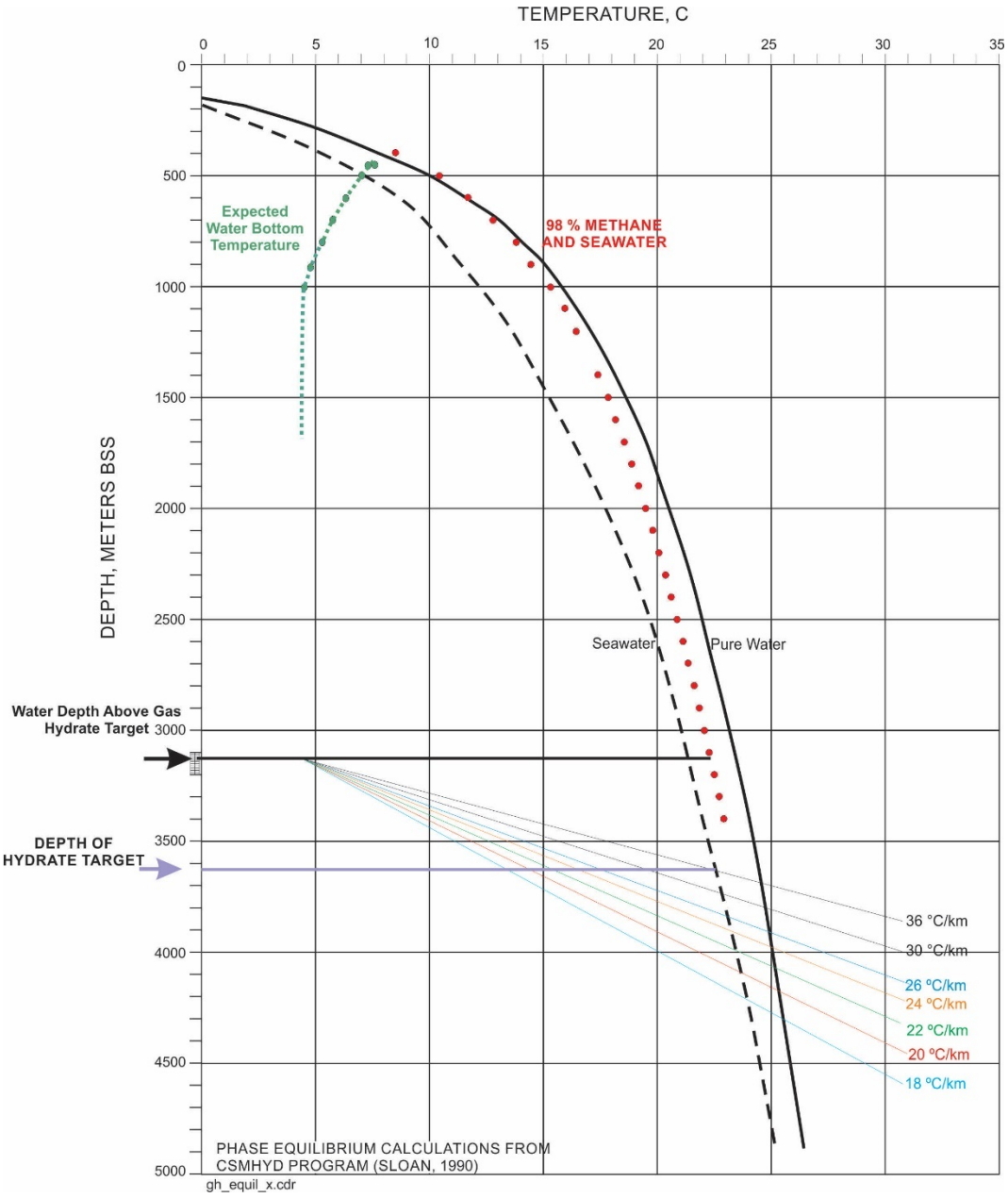


**Figure 5.3 Phase equilibrium for 100% methane, pure water, and seawater showing depth of gas hydrate target below seafloor and geothermal gradient intersect**

### 5.2.3 Seismic Character of the Interpreted Gas Hydrate Deposit

Amplitude interpretation suggests a gas hydrate bearing sand at the base of gas hydrate stability where a deep-seated fault has been a conduit for gas migration. In the west and northwest, the channel sand has the characteristics of gas hydrate fill. In the east and southeast, the channel sand has the characteristics of gas fill. The channel sands are flat-lying with a very gentle dip to the southeast. The channel deposits are having high sinuosity with an overall depositional trend west-northwest to east-southeast. The gas hydrate deposits are delineated by a high amplitude anomaly caused by fluid migration along and up the buried fault. The sediments are interpreted to be Pliocene sands. The strong seismic anomaly is caused by the high velocity of gas hydrate fill with a likely contribution from the low velocity of gas. The seismic signature

implies that saturations are likely to be greater than 40%. The gas hydrate seismic amplitude can be interpreted as a polarity reversal of a gas sand. Several techniques are applied to support and expand the interpretation of the gas hydrate deposit in this report.

The characteristics of this interpreted gas hydrate deposit, flat lying, within channels with continuous dimensions of thickness and width at the base of gas hydrate stability is an ideal setting to test gas hydrate direct hydrocarbon indicators.

The amplitude is “leading peak” gas hydrate signature in the west-northwest. It transitions to a “leading trough” gas signature in the east-southeast as the hydrocarbon filled sand crosses the base of gas hydrate stability. A time slice across the deposit is shown in Figure 5.4. The topmost cyan-blue reflector is interpreted as gas hydrate and the yellow-orange is interpreted as gas. Note the channel deposits on the horizontal slice (Figures 5.4 and 5.5).

One of the goals of this project was to evaluate other seismic attributes other than simple amplitude to that could confirm, support, or delineate the gas hydrate deposit.

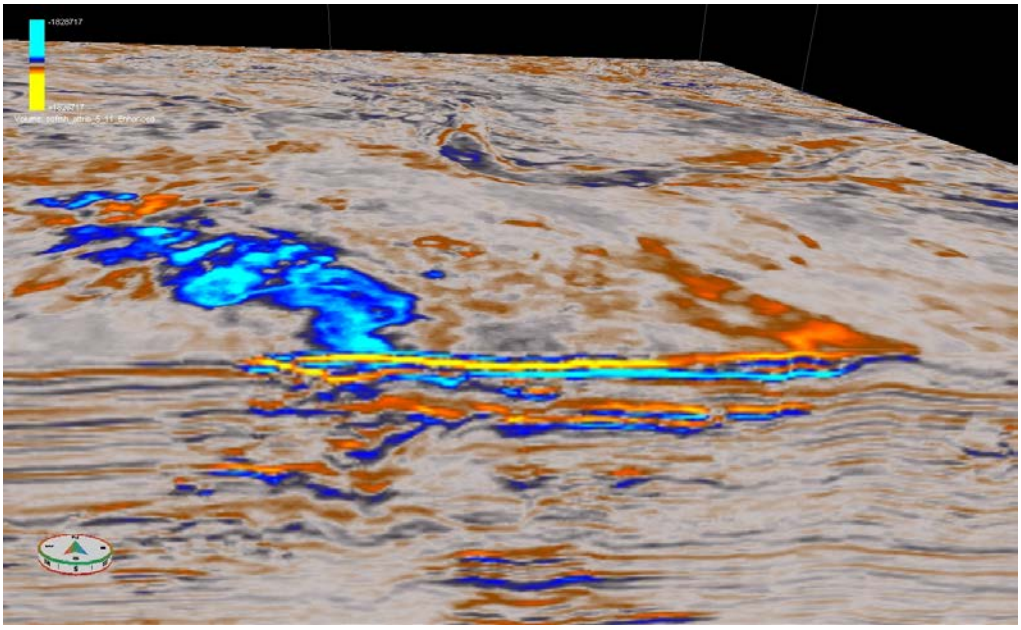

**Figure 5.4 Seismic amplitude cube (full stack). Top surface is a time slice intersecting the top of the gas hydrate deposit (blue-cyan) in west that transitions to gas (bright orange – yellow) in the east at the base of gas hydrate stability.**

## 5.3 Seismic Attributes

As discussed, the purpose of using seismic attributes is to help reveal geologic features or properties that are not as easily seen in the original seismic data (Figure 3.8). In the time category, semblance attributes were

run to help delineate channel morphology and sedimentary architectures. In the amplitude category, various amplitude attributes were used for prospect screening. Envelope attributes and derivations were used to help identify multiple high-energy reflectors. Frequency attributes were used to help identify areas of energy attenuation beneath interpreted gas hydrate and gas deposits.

Several seismic attribute volumes were generated using the Rock Solid Attributes attribute generation module with The Kingdom Suite interpretation software. The attribute generation definitions are not disclosed by Kingdom Suite but are similar and assumed to be based on RSI_ATTRIB3D computational program developed at Seismic Research Corporation. References for the definition and derivation of these attributes are given by Taner (2003). Several attribute volumes were generated. The most useful of the seismic attributes that were generated were similarity variance, second derivative of the envelope, and instantaneous Q.

**Table 5.1 Select Seismic Attributes**

| Attribute and (Type) | Description | Definitions (all from Taner, 2003) | Utility |
|---|---|---|---|
| Similarity Variance<br><br>(Geometric) | Difference between maximum lateral semblance and smoothed maximum lateral semblance. | Semblance:<br>$Semb(t) = \frac{\sum_{\tau=-N/2}^{\tau=N/2} \{\sum_{m=1}^{M} f_m(t+\tau)\}^2 - \sum_{\tau=-N/2}^{\tau=N/2} \sum_{m=1}^{M} f_m^2(t+\tau)}{\sum_{\tau=-N/2}^{\tau=N/2} \sum_{m=1}^{M} f_m^2(t+\tau)}$ | Shows local depositional anomalies and architecture |
| Derivative of the Envelope<br><br>(Amplitude) | Envelope represents total instantaneous energy. The time rate of change is the derivative of the envelope | $d[E(t)]/dt = E(t) * diff(t)$ | Relates directly to impedance contrasts. Bright spots and strong lithology changes. Derivatives of the Envelope can show the reflecting interfaces within the seismic bandwidth. Application for gas hydrate? |
| Instantaneous Q<br><br>(Frequency) | Local variation in transmission of energy | $q(t) = -\pi . freq(t) / decay(t)$<br><br>decay = derivative of the instantaneous envelope/envelope | Can show absorption of energy and can be a DHI for gas. Application for a DHI for gas hydrate? |
| Instantaneous Frequency<br><br>(Frequency) | Time rate of the change in phase | $Freq(x,t) = \frac{\partial arctan[g(x,t)/f(x,t)]}{\partial(t)} = \frac{[f(x,t).dg/dt - g(x,t).df]}{[f^2(x,t) + g^2(x,t)]}$ | Can show thin beds; low frequency anomalies can be a DHI in gas. Application for a DHI for gas hydrate? |

*Similarity Variance.* The attribute computes the maximum lateral continuity of adjacent traces and corresponding dips. Semblance values are computed for the dip values. The semblance value and the dip corresponding to the maximum semblance is computed and compared to the overall maximum semblance. The output uses the summation of traces along the dip of maximum coherency and displays the most laterally continuous events to compute semblance (Taner, 2003). Similarity variance is computed from the difference between the maximum instantaneous lateral semblance and the average lateral semblance within the computation window.

Edges of channels and MTD deposits are shown with high similarity variance shown as red in Figure 5.5. Sediments between the channels have lower similarity variance shown as green in Figure 5.5. The geometrical attribute similarity variance is effective in defining channel boundaries and provided insight into the channel architecture, channel width and channel height, and expected lithology.

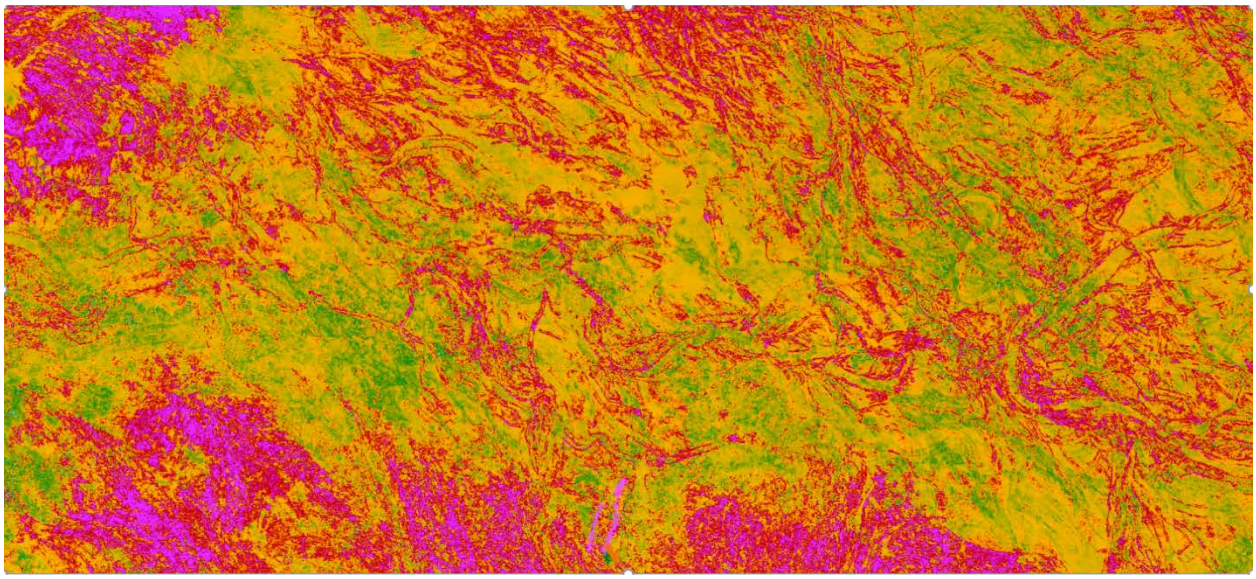

**Figure 5.5 Similarity variance showing channel and MTD deposits. Channels widths range from 0.5 km to 1.5 km for scale. Magenta corresponds to the highest similarity variance. Green corresponds to the low values of similarity variance.**

*Second Derivative of the Envelope.* Envelope attributes are effective at defining bright spots and can be a DHI for gas. The second derivative of the envelope sums these reflecting interfaces and can detect layered high energy anomalies. The attribute is summing multiple positive energy layers consistent with layered gas hydrate deposits within the channel lithology. Anomalous positive second derivative of the envelope attributes within the context of a gas hydrate hydrocarbon system can be a gas hydrate DHI. Note the high positive values colored in blue that correspond with the area of the channel interpreted to have of gas hydrate fill. There are more reflecting interfaces within the channel than outside the channel, so the attribute is, in part, responding to lithology. The positive energy summation (multiple positive high energy reflecting interfaces) is also likely responding to gas hydrate fill within channel layers (Figure 5.6).

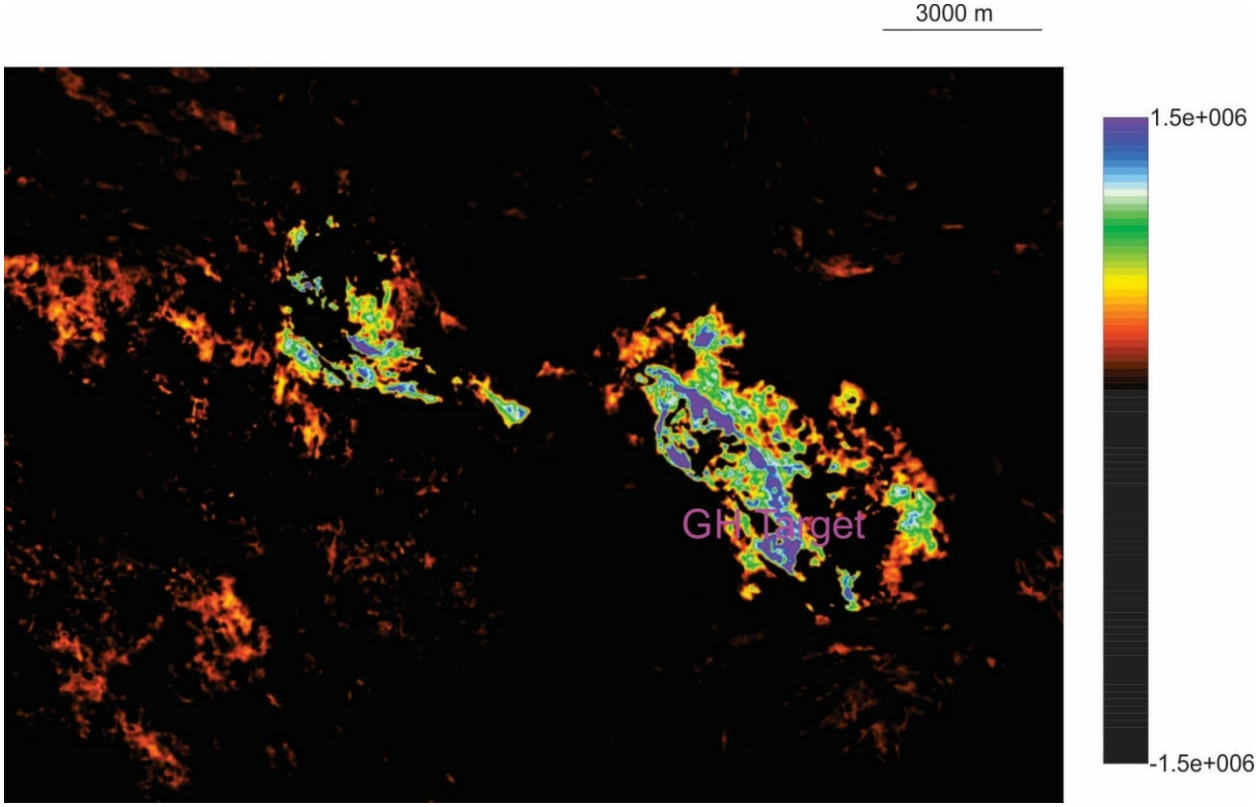


**Figure 5.6 Second derivative of the envelope showing multiple positive high energy thin beds in the gas hydrate.**

*Attenuation Attributes.* Oil and gas reservoirs often cause a loss of higher frequencies and phase shifts. Post-stack attenuation attributes to indicate zones of attenuation include instantaneous frequency, the slope of instantaneous frequency, 1/2/3 peak spectrum frequencies, ratio of adjacent peak amplitude, windowed amplitude and spectrum ratios, (Chen and Sidney, 1997). Attenuation attributes are those that are thought be sensitive to energy absorption or scattering. Absorption refers to the fundamental loss of seismic energy loss through the medium while scattering is the cumulative effect of reflections and scattering through multiple interfaces (Barnes, 2016).

*Instantaneous Q.* The quality factor, or Q, describes the attenuation or loss of seismic energy through the medium. Gas sands attenuate energy and show as low Q. Instantaneous Q is an attribute that can detect attenuation. On first principles, sediments uniformly cemented with gas hydrate would have low attenuation. Analysis of the Mallik well showed strong attenuation with gas hydrate saturation (Guerin and Goldberg, 2001). Laboratory studies by Priest (2006) designed to test this did not show a strong relationship between attenuation and gas hydrate saturation. Lee, 2007, was able to build rock physics models that would attenuate with gas hydrate saturation but were orders of magnitude less than measured at Mallik. Dvorkin and Uden, 2004, suggest that the mechanism for strong attenuation in gas hydrate deposits result from gas hydrate saturation increasing the elastic moduli of the sediment and that attenuation results from increased pore-fluid cross flow. This and scattering are thought to be mechanisms for attenuation associated with gas hydrate saturation.

Gas reservoirs, however, attenuate seismic signal and detection of attenuation is used for hydrocarbon exploration in conjunction with other attributes. Attenuation in gas reservoirs can be related to gas saturation where seismic amplitude is insensitive to gas saturation. The attribute might be useful to discriminate between low saturation gas and higher saturations of gas at the base of gas hydrate stability. Barnes (2016) however argues that the gas amplitude attribute and attenuation attribute at the gas sand are too related- the attenuation attribute will be just as insensitive to gas saturation as the amplitude attribute. Barnes further cautions that the strong influence of reflectivity hinders attenuation analysis and that attributes such as Instantaneous Q should be viewed skeptically.

Nevertheless, Instantaneous Q is one of the few post stack attributes that could be related to attenuation. The attribute is noisy. There is, for instance, a wide range of Instantaneous Q values in the interpreted MTD deposits and within the channelized sediments. However large areas of contiguous low Instantaneous Q are thought represent signal vs noise. A slice through the Instantaneous Q data showed a correlation with interpreted gas hydrate and gas at the target seismic anomaly and contiguous low Instantaneous Q indicating high attenuation (Figure 5.7).

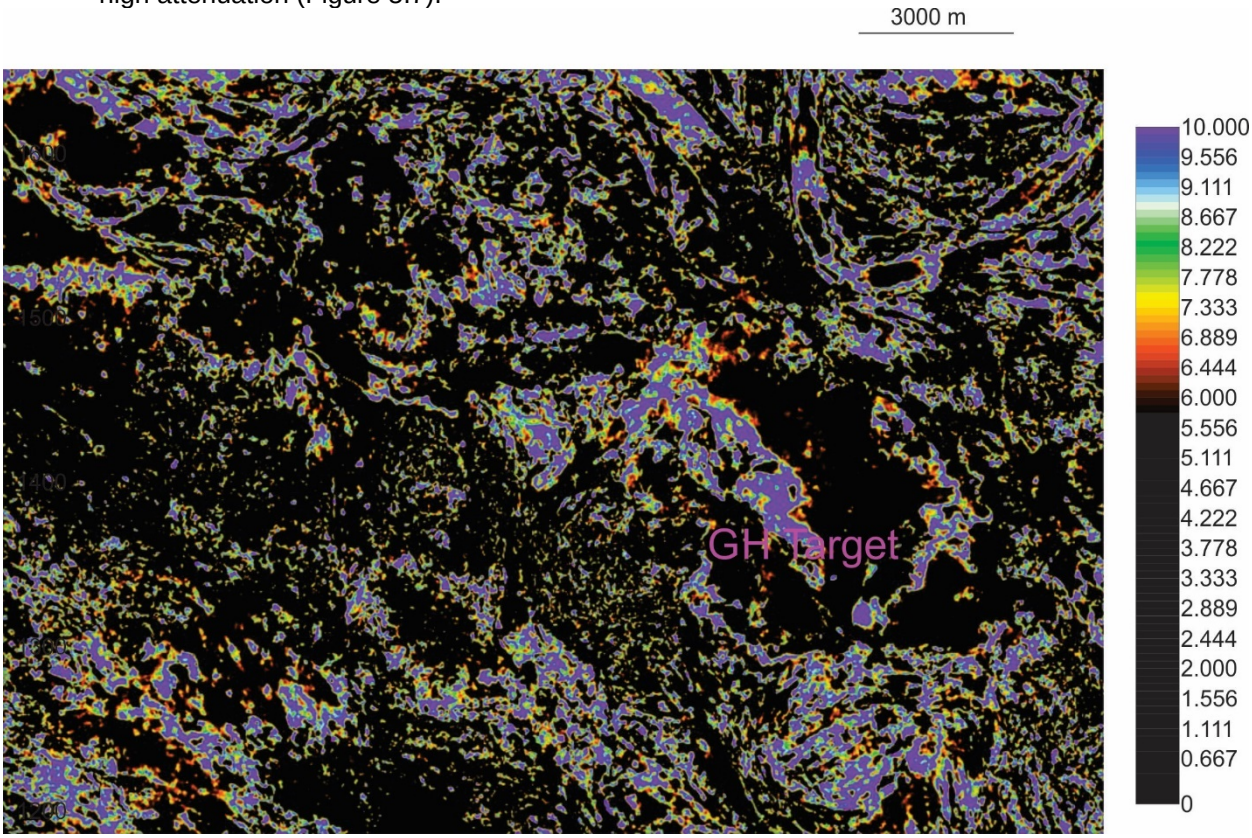


**Figure 5.7 Instantaneous Q. Contiguous areas of low Q correspond with both the gas hydrate and gas area of the impedance anomaly.**

A perspective view of the full stack amplitude over the gas hydrate and gas deposits and Instantaneous Q shows that that both the gas hydrate leg and the gas leg show attenuation (Figure 5.8). Instantaneous Q in Figure 5.8 shows low Inst. Q as blue where in Figure 5.7 low Inst. Q is modified to show as black.

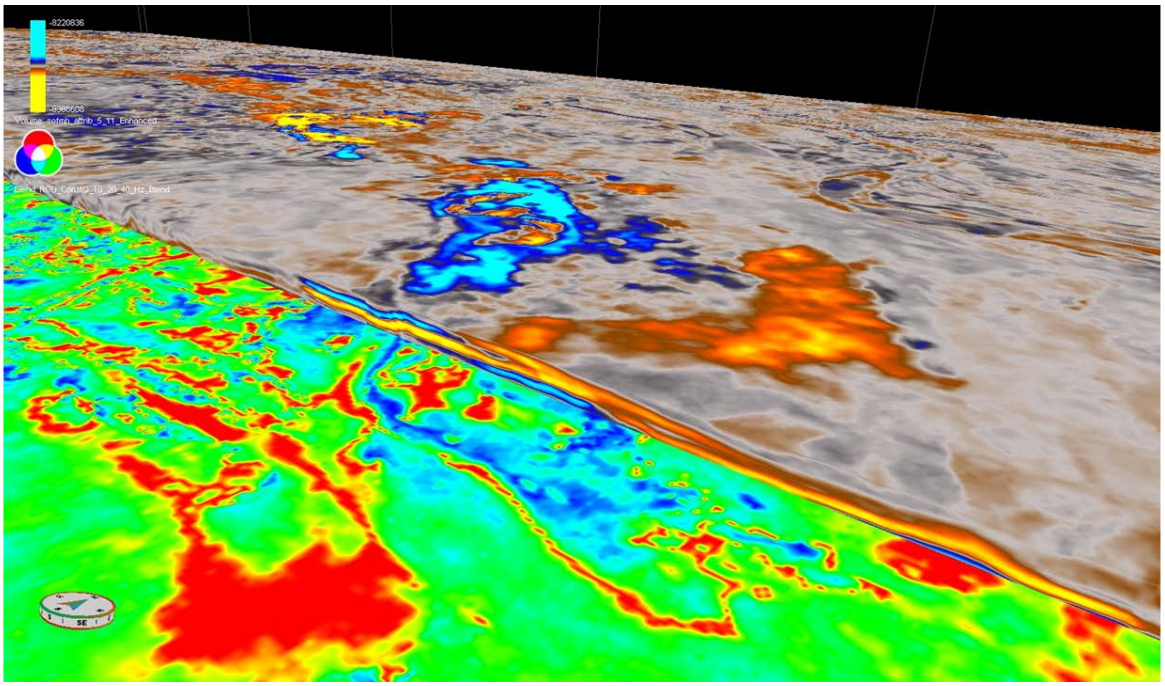

**Figure 5.8 Perspective view of Instantaneous Q in south (low Q values are blue; high Q values are red) and full stack amplitude in north showing "leading peak" blue-cyan gas hydrate and "leading trough" orange-yellow gas corresponding with interpreted attenuation.**

A cross plot for low Instantaneous Q and the second derivative of the envelope was taken from an 80 ms window over an area of 146 sq. km. The cross plot of areas of high attenuation (low Instantaneous Q) and the presence of multiple positive reflectors (second derivative of the envelope, positive) correlate to the seismic anomaly interpreted be gas hydrate (Figure 5.9). This shows that cross plots of attributes to isolate attenuation and high positive impedance thin beds can be used to confirm an interpretation of high saturation gas hydrate sands and discriminate against adjacent gas sands.

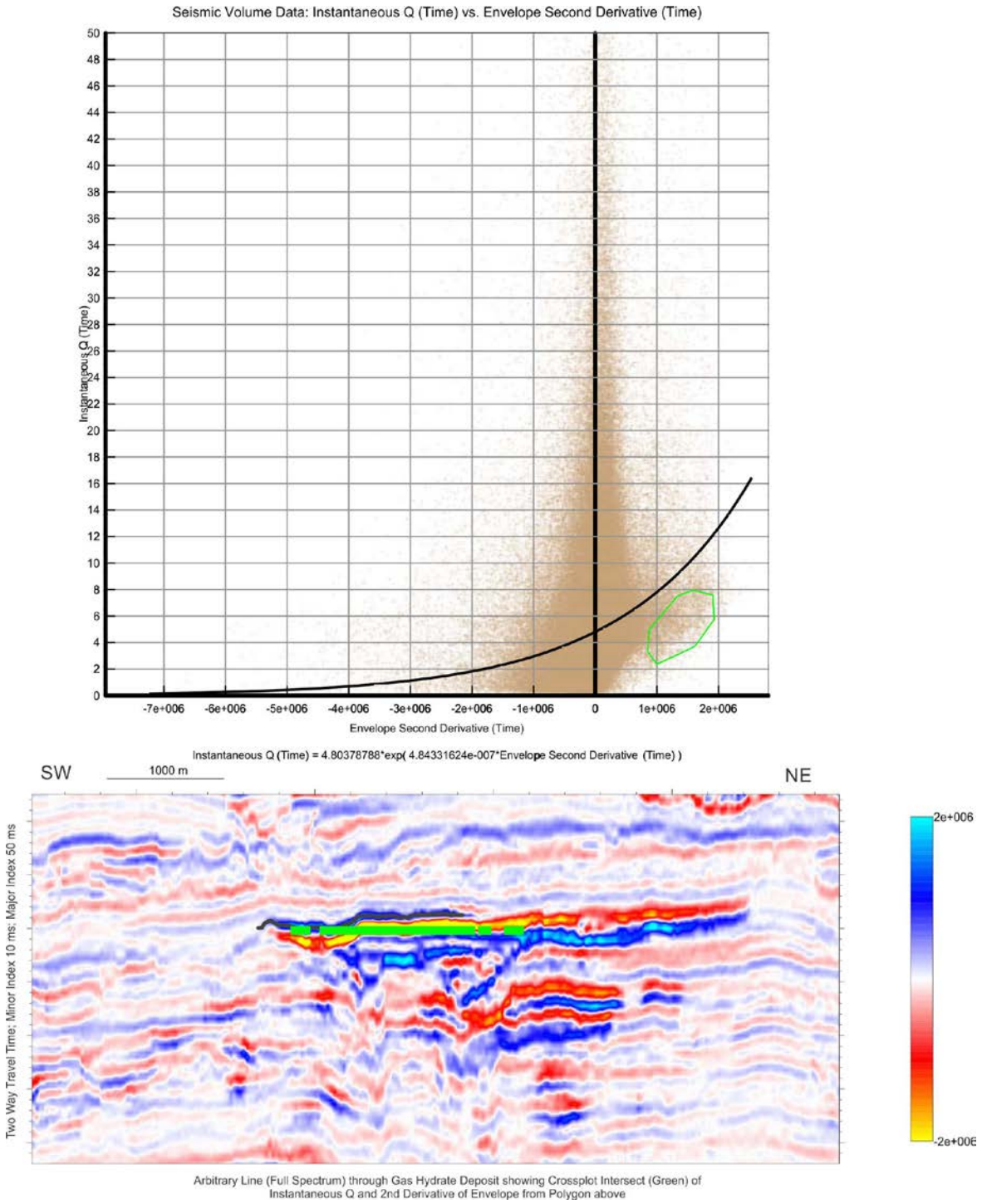


**Figure 5.9 Cross plot of Instantaneous Q and 2nd Derivative of the Envelope showing areas of high attenuation and multiple high energy positive reflectors (above) and corresponding points on full spectrum seismic data at interpreted gas hydrate deposit**

## 5.4 Spectral Decomposition

Bandlimited frequency attributes by means of spectral or frequency decomposition were used to determine channel morphology, but it became clear during this investigation that frequencies separated between the interpreted gas hydrate fill and gas filled sediments.

Spectral decomposition is a way of decomposing the seismic signal into frequency bandlimited volumes. By blending different bandlimited frequency volumes into either a red, green or blue channel different geologic information is imaged. Different frequencies in the data contain different information. Regional structural information is contained in the lower frequencies and smaller detailed information relating to faulting and fractures can be detected with higher frequencies. Additionally, different lithologies tune to different frequencies depending on composition and thickness (Marfurt and Kirlin, 2001). Combining selective bandlimited frequencies into red, green and blue channels allow for these differences to be seen in the seismic data. The blending of the frequencies can enhance interpretation of structure and faults. Spectral decomposition is especially useful in imaging channels and channel morphology. Channel thickness and architectural components such as bars, avulsions, fans have variable thicknesses can be imaged by spectral decomposition because narrow band frequency components are sensitive to reflector thickness tuning effects. An RGB blend, respectively, of 20 Hz (red), 39 Hz (green), and 65 Hz (blue)is shown in the east in Figure 5.10. Channels are apparent in the east in the full stack seismic date, in this case 70 ms deeper than the RGB cube in the west. The channel architecture is enhanced and easily visualized in the RGB blend.

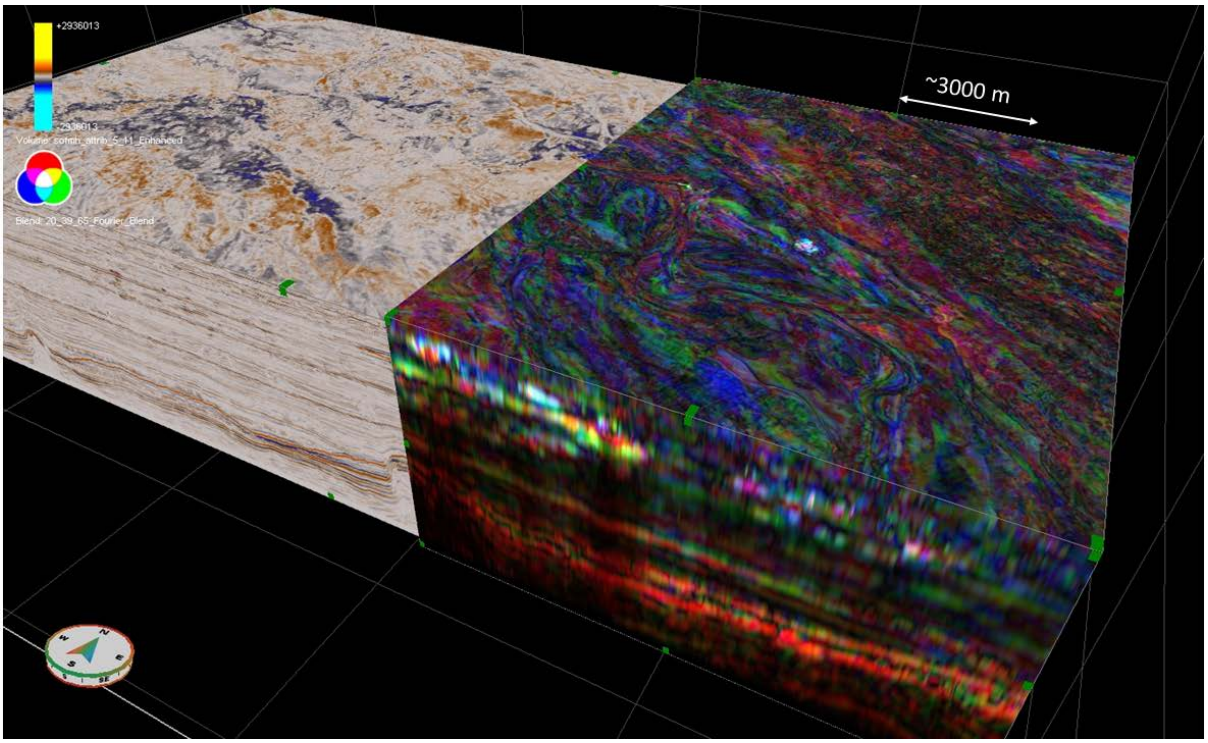


**Figure 5.10 In the west, cube of enhanced full stack 3D seismic. In the east Red Green Blue blend of 20 Hz, 39 Hz and 65 Gz Fourier amplitudes. The top plan view face in the east is 70 ms (56 m) above the gas**

**hydrate target. West: Inline 1055 south face; 4.67 s top face sofmhattribute 5 11 Enhanced East: Inline 1050 south face; 4.60 s top face 20_39_65 Fourier RGB blend**

Moving the slices in the 20-39-65 Hz Fourier RGB blend from the channel deposits from a time slice 70ms above the gas hydrate deposit to a time slice 40 ms above the gas hydrate deposit is shown in Figures 5.10, 5.11 and 5.12. Note that the blue-green channels are continuous and trend east-southeasterly above the gas hydrate target in Figure 5.10 and Figure 5.11 with high amplitude 20 Hz low frequency beginning to appear at the southeast of the gas hydrate-gas deposit.

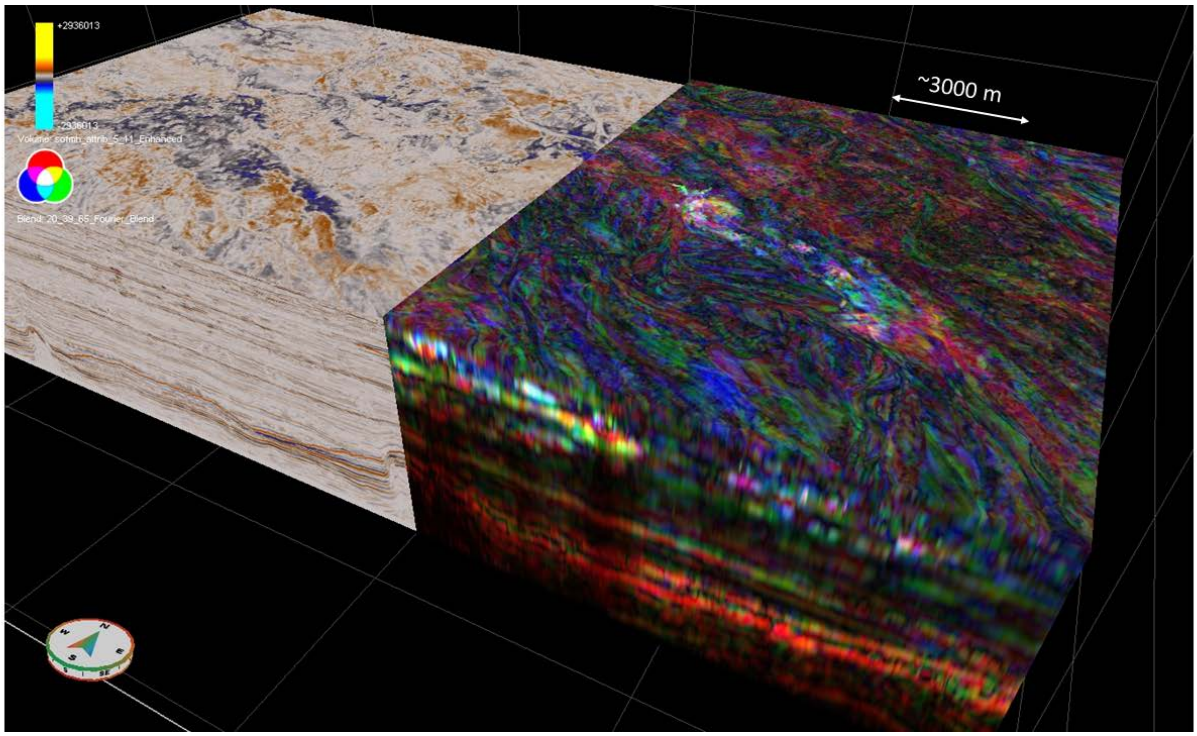


**Figure 5.11 In the west, cube of enhanced full stack 3D seismic. In the east Red Green Blue blend of 20 Hz, 39 Hz and 65 Gz Fourier amplitudes. The top plan view face in the east is 40 ms (32 m) above the gas hydrate target.**

A slice though the 20-39-65 Hz RGB blend that fully illuminates the extents of the gas hydrate-gas deposit is shown in Figure 5.12. The basal fan channel architecture is seen entering the high-amplitude events from the west-northwest with the same architecture exiting the high amplitude events in the east-southeast. As the 20-39-65 Hz RGB blend is fully illuminated by the flat-lying gas hydrate and gas pore fill at the base of gas hydrate stability, the slightly up dip gas hydrate leg is illuminated by the high frequency 65 Hz narrow band. The same channel sediments slightly downdip in the gas leg is illuminated by the low frequency 20 Hz narrow band. An inset of the fully illuminated gas hydrate – gas deposit shows more clearly the separation of the high amplitude high-frequency trend from the high amplitude low-frequency trend (Figure 5.13).

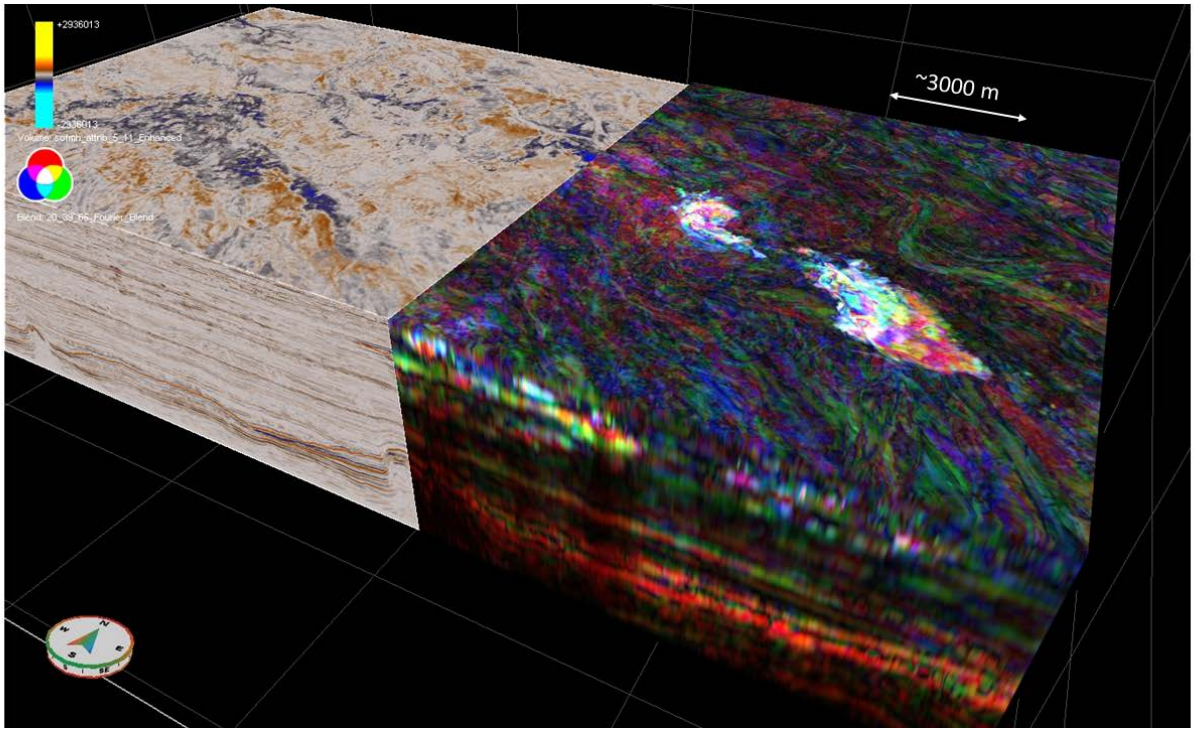


**Figure 5.12 In the west, cube of enhanced full stack 3D seismic. In the east Red Green Blue blend of 20 Hz, 39 Hz and 65 Hz Fourier amplitudes. The top plan view face in the east is at the same time and intersects the gas hydrate target.**

The relationship between the 20-39-65 Hz RGB blend and the full amplitude stack at the gas hydrate target is shown in Figures 5.14 and 5.15. There is a clear correlation between the "leading peak" amplitude anomaly in the full stack amplitude data and the high amplitude high frequency band that corresponds with highest confidence gas hydrate deposit interpreted from the full stack amplitude data. The RGB blend data also shows higher frequency corresponding to the leading peak high amplitude anomaly as it tapers to a high-amplitude trough gas signature. Where the high amplitude trough (high amplitude low impedance) is the top reflector, the RGB blend trends to a high amplitude low frequency response. These relationships are apparent in the non-blended individual narrow band frequencies. The 20 Hz narrow band does show high frequencies at channel edges and generally, where the full stack data is interpreted as gas (Figures 5.15 and 5.16). The mid-frequency 39 Hz narrow band illuminates where the full stack data interpretation suggests gas hydrate over gas (Figures 5.15 and 5.17). The 65 Hz narrow band amplitude maximum correlates to the high confidence gas hydrate deposits interpreted from the full stack amplitude data (Figures 5.15 and 5.18).

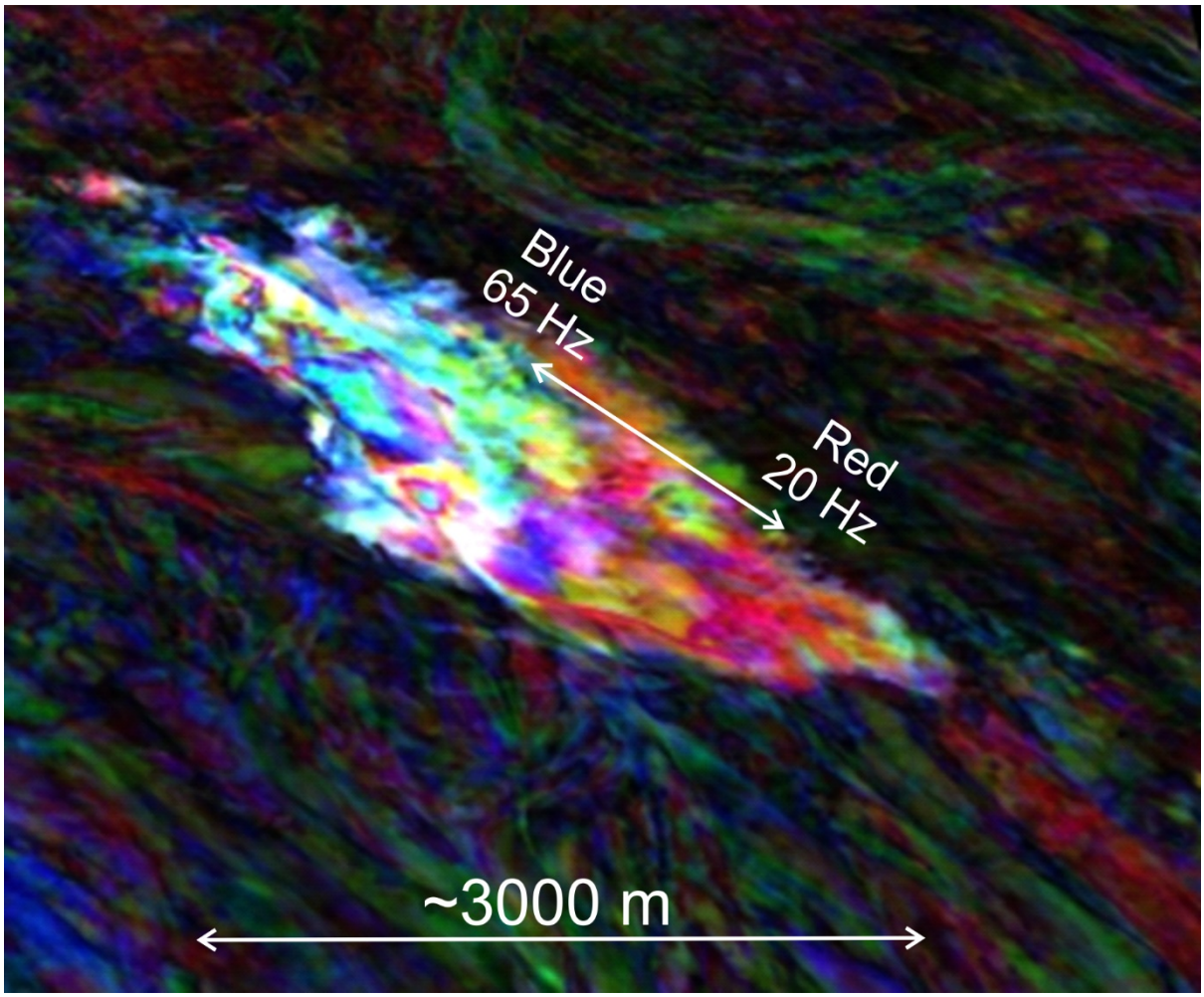


**Figure 5.13 Inset RGB blend of 20 Hz, 39 Hz and 65 Gz Fourier amplitudes time slice from Figure 5.12 at gas hydrate target showing a demarcation from high frequency trend to low frequency trend. High amplitude high frequency relates to gas hydrate pore fill. High amplitude low frequency relates to gas pore fill.**

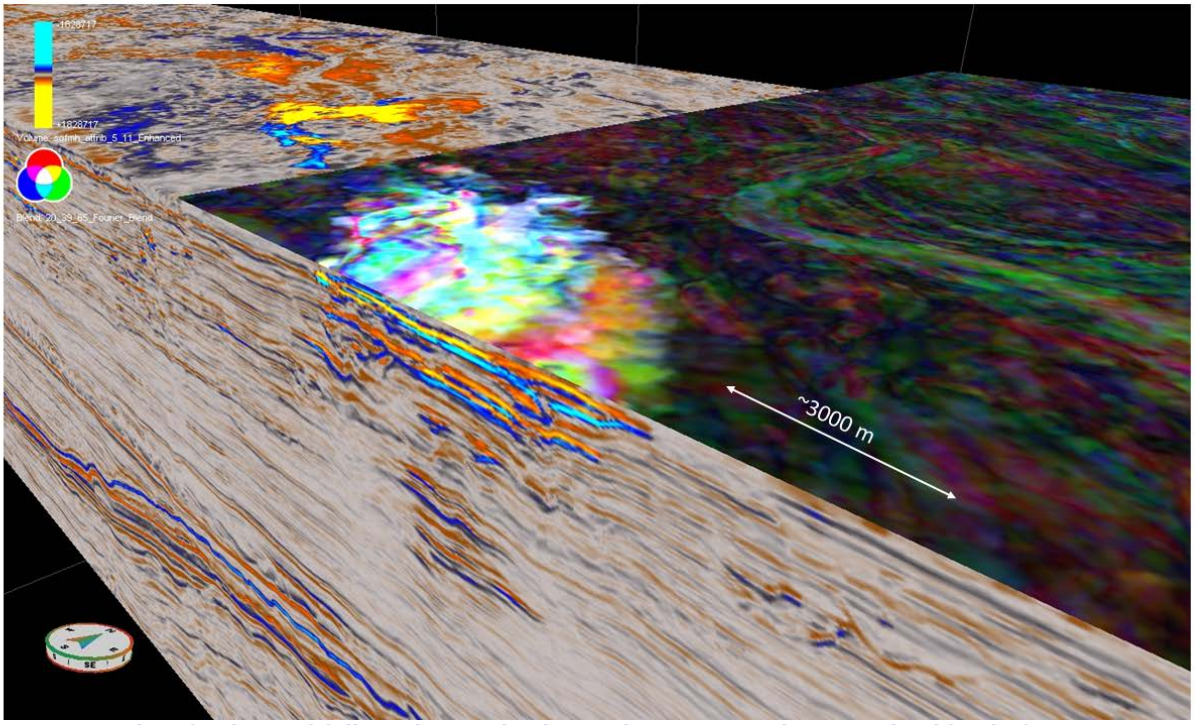


**Figure 5.14 A cube of enhanced full stack 3D seismic. In the east, a Red Green Blue blend of 20 Hz, 39 Hz and 65 Gz Fourier amplitudes. The top plan view face in the east intersects the gas hydrate target and is 10 ms shallower than the surface in the west.**

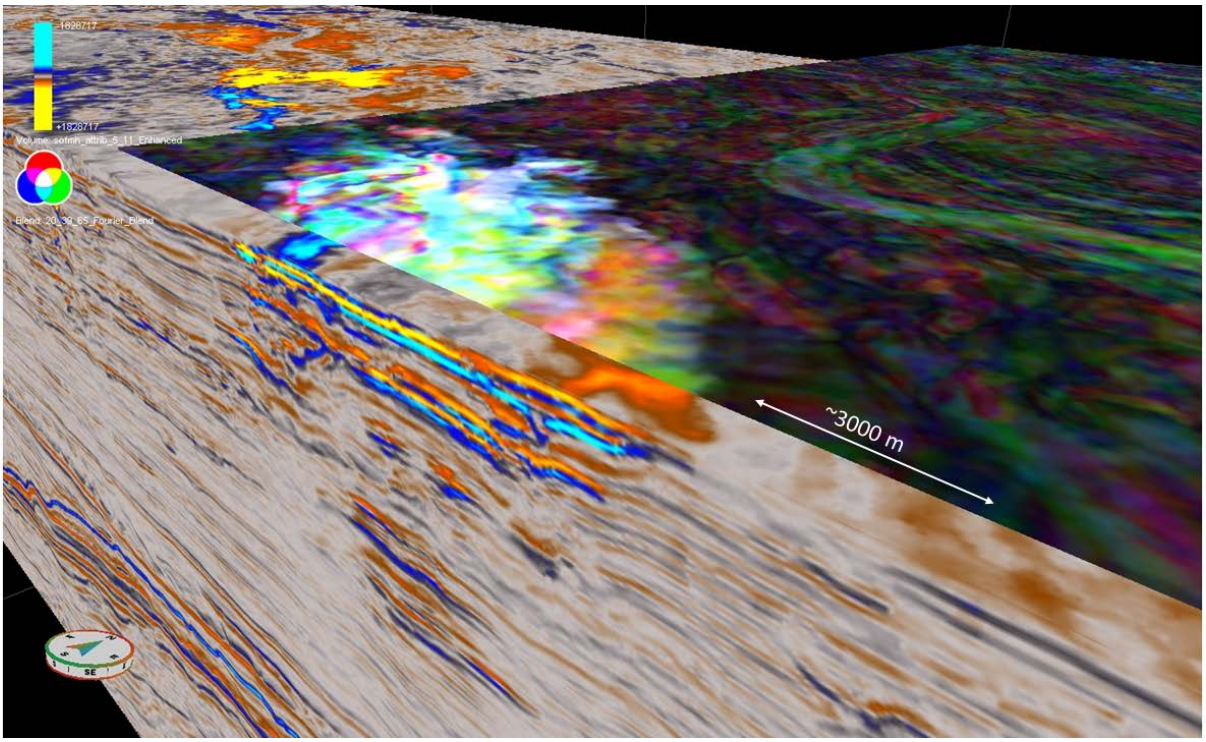


**Figure 5.15 Same as the preceding figure except that the RGB surface is scrolled to the north to reveal relationship to the enhanced full stack 3D seismic. The Red Green Blue blend of 20 Hz, 39 Hz and 65 Gz Fourier amplitudes surface is 10 ms shallower than the surface in the west and below.**

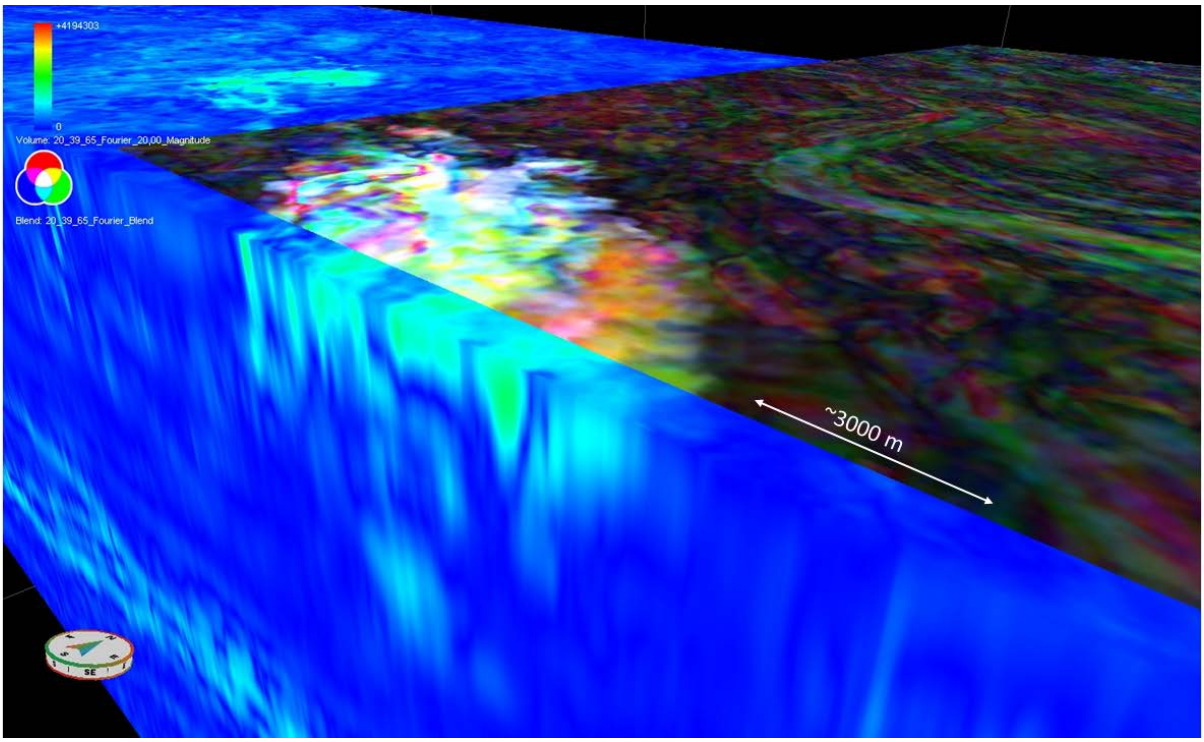


**Figure 5.16 Same as the preceding figure except that the blue-green cube is 20Hz Fourier frequency spectra. The Red Green Blue blend of 20 Hz, 39 Hz and 65 Gz Fourier amplitudes surface is 10 ms shallower than the surface in the west and below.**

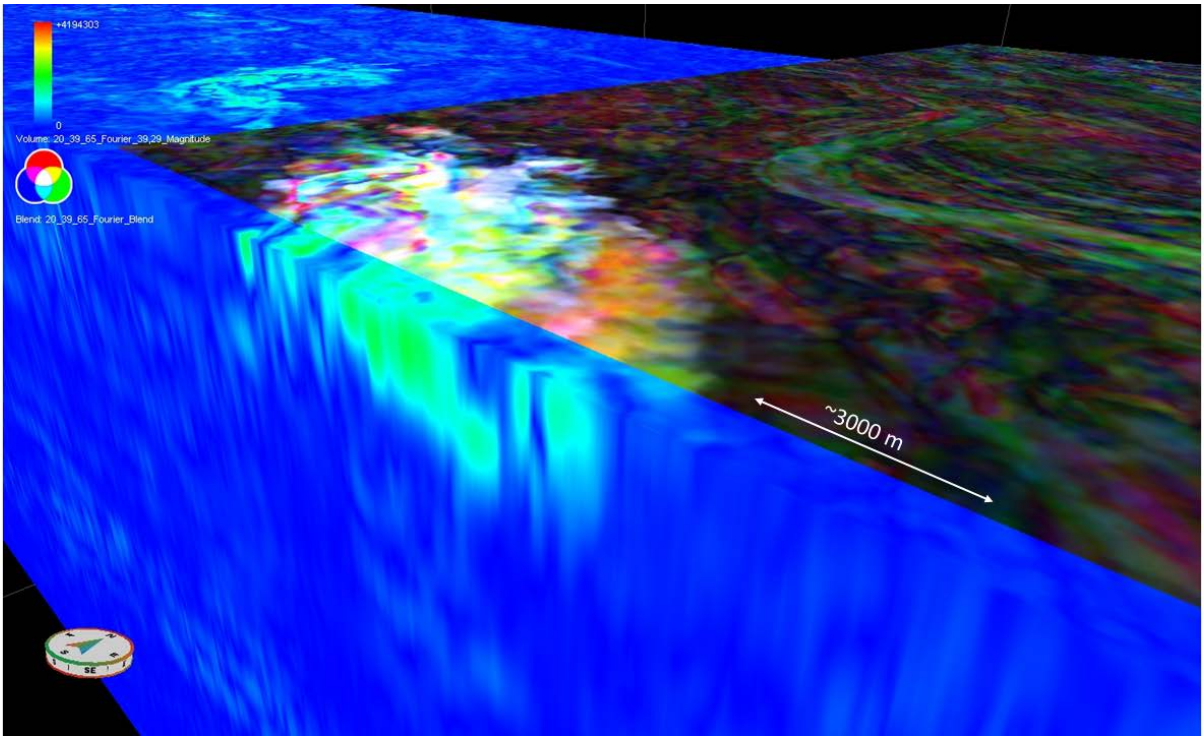


**Figure 5.17 Same as the preceding figure except that the blue-green cube is 39Hz Fourier frequency spectra. The Red Green Blue blend of 20 Hz, 39 Hz and 65 Gz Fourier amplitudes surface is 10 ms shallower than the surface in the west and below.**

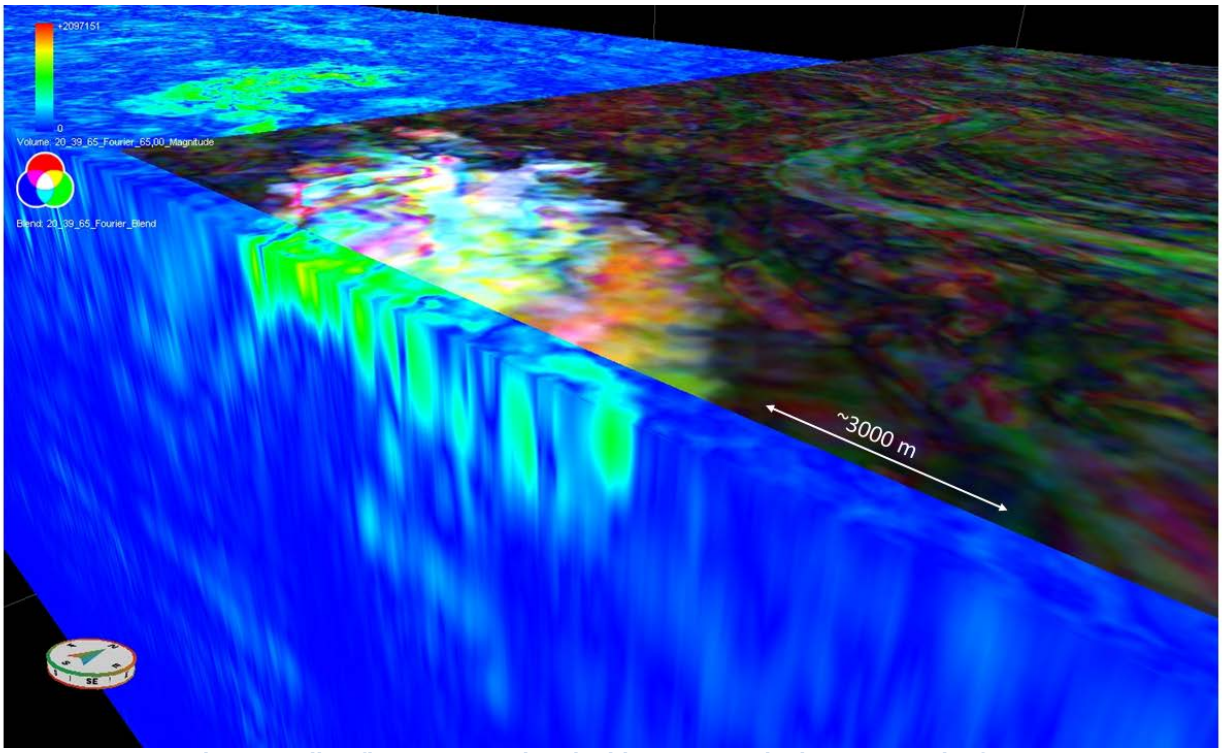


**Figure 5.18 Same as the preceding figure except that the blue-green cube is 65Hz Fourier frequency spectra. The Red Green Blue blend of 20 Hz, 39 Hz and 65 Gz Fourier amplitudes surface is 10 ms shallower than the surface in the west and below.**

### 5.4.1 Thin-bed Imaging

Gas hydrates and shallow gas are typically seismic thin beds. The tops and bases are usually do not correspond to a separate reflector. The velocity-density contrasts between earth layers, are of course, what enable seismic reflection technology to be extremely useful for imaging distinct geologic formations. If these formations are thick enough and there are velocity-density contrasts between the bounding geologic strata, then seismic reflections from both the top and bottom of the formation will be imaged. Within such formation, there will be additional layers with velocity-density characteristics that are below seismic resolution. In deepwater marine exploration seismic data, in many settings, the geologic strata will consist of seismically identifiable units such as normal marine clays, mass transport deposits, and channel deposits. Anomalous low-amplitude noisy geo-bodies that are typical in seismic images in deepwater settings can include extrusive salt, entrained gassy sediments, and the mass transport deposits mentioned previously. Within the upper kilometer of data, many, if not the majority, of coherent reflections are thin bed reflectors, in that the seismically resolvable contrasts will result in composite waveforms. Thick sections of normal marine clays in exploration 3D seismic data, for example, are often imaged as a series of stacked continuous moderate amplitude reflectors. The reflectors do not correspond to geologic beds but are well-behaved composite seismic traces that are produced by thin bed velocity-density contrasts. Turbiditic sands and silts likewise are not usually resolved by tops and bases in exploration 3D seismic data, but instead by amplitude and thickness variations that show channel patterns in map view. Seismic traces through these, too, tend to be composite thin bed responses. The tops of geologically young sands in 3D seismic data within, say, the upper kilometer, however, will tend to resolve (in the North American Polarity Convention)

as a trough reflector. In a standard red-white-blue seismic display color bar, the North American Polarity Convention shows an increase in impedance as positive, “a peak”, a trace excursion to the right, and blue, and a decrease in impedance as negative, “a trough”, a trace excursion to the left, and red. The SEG standard and the European Polarity Convention is the opposite of the scheme just described.

Gas sands in geologically young section, e.g. the Plio-Pleistocene in the Gulf of Mexico are almost invariably, a low impedance, trough, reflector that brightens with some small quantity of gas. The brightening, a high amplitude negative excursion is caused by the low velocity of gas. Only rarely, if ever, will a high impedance, peak, reflector phase reverse to a trough reflector with the addition of gas. The reasons for this are that the sands are less dense than the bounding clays in the upper, unconsolidated, marine sediments. Velocities between the clays and sands in these environments, in the absence of gas fill, are similar. These bright spots are most commonly thin bed responses and usually do not show a top and base. When they do show a top and base it is the top and base of the fluid contacts rather than the top and base of a geologic bed.

Like bright spots caused by gas, gas hydrate deposits in conventional exploration seismic data are most often not thick enough be thick enough to show a top and base and will be imaged as thin beds in conventional exploration seismic data. Furthermore, cores taken from gas hydrate sands show that a common habit for gas hydrates is to be deposited in layers within sandy sediments (Flemings, 2017) owing to the physio-chemical controls of pore water chemistry, pressure, temperature, and subtle lithologic differences. A gas reservoir in the same lithology and similar conditions just below the base of gas hydrate stability not needing additional physio-chemical controls except saturation in excess of solubility and would be expected to have a more homogeneous pore fill.

One of the habits of gas hydrate deposition is that gas hydrate tends to form within layers and are likely guided by the laminar depositional structures. Gas hydrates, then, create high velocity thin beds in sands, but these true gas hydrate layers, in exploration seismic data are not individually resolvable but, taken together, represent a seismic thin bed.

One of the initial applications of spectral decomposition was to image thin beds. Widess (1973) demonstrated the fundamental relationships between seismic amplitude, layer thickness, and layer tuning. When seismic units are thick enough, wavelets recording the top and bottom reflector interfaces are separated. As the seismic geologic beds thin, the wavelets become a composite of the wavelets and increase in relative amplitude. In the general case, the amplitude maximum is reached at $\lambda/4$ in the time domain and has the layer thickens to $\lambda/2$, the amplitude decreases until it reaches the original non-interfering amplitude of the layer reflection coefficient.

Partyka (1999) analyzes the same concept in the frequency domain to estimate bed thickness by means of Fourier transform. A composite seismic trace with a thin bed will contain thin bed wavelet components. Wedge modeling shows that after Fourier transform to the frequency domain, the spectrum amplitude of the composite trace that includes a thin bed reflector will notch with a frequency period that is inversely proportional to thickness in the time domain. The relationship is, $P_f = 1/t$, where $P_f$ is the period of amplitude

spectrum notching with respect to frequency and t is thin bed thickness. For instance, if the period of amplitude notching is 100 Hz, then the temporal thickness is 10 ms. A thicker unit will notch with shorter periods, so that if, for instance, the period of amplitude notching across the frequency spectrum is 20 Hz then the temporal thickness would be 50 ms.

### 5.4.2 Identification of Gas Hydrate in High Amplitude Thin Beds

Thin bed wedge models for gas hydrate saturation response that are applicable to the gas hydrate target in this study are those derived from GC955 (Zhang et al., 2012). In that model, synthetic seismic responses using a 50Hz Ricker wavelet at normal incidence on a wedge model were derived for different saturations of gas hydrate and gas hydrate over gas from the well log data and rock physics model at GC955 H. In the case of the wet sand with 0% saturation of gas hydrate and no gas beneath, the amplitude the reflection coefficient is negative “trough” reflector. The amplitude maximum is reached as the wavelet tunes at lambda/4.6 (Figure 5.19). At 25% saturation of gas hydrate, again with no underlying gas beneath, the models predict a weak amplitude even at the tuning thickness and as the wedge gets thicker a decrease in amplitude- suggesting that amplitude blanking occurs during the transition from water wet to gas hydrate fill (Figures 5.19 and 5.20). At 50% gas hydrate saturation, the sand has phase reversed because of the increase in velocity relative to the surrounding clays with an amplitude maximum at tuning like the water wet sand with 0% gas hydrate saturation but opposite in sign (positive instead of negative) (Figures 5.19 and 5.20). What is significant in the model is that the phase reversed amplitude will increase with increasing gas hydrate saturation. High amplitudes caused by the low velocity of gas sediments, in contrast, are mostly insensitive to gas saturation. These observations and models contributed to the simplified framework for prospecting for high saturation gas hydrate sands discussed earlier (Boswell, et al., 2015).

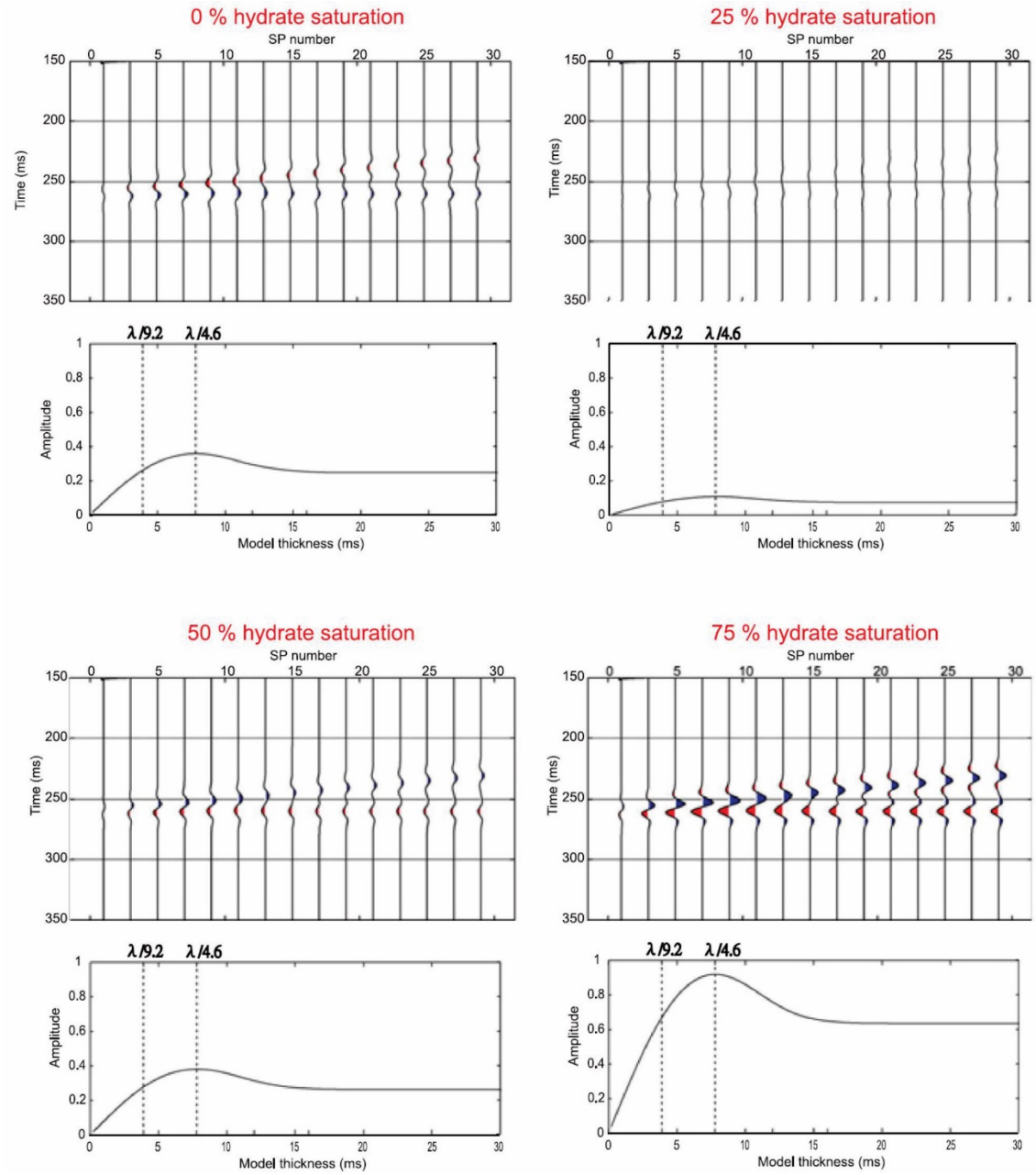


**Figure 5.19 Synthetic seismograms showing gas hydrate saturation wedge encased in water bearing sediments using a 50 Hz Ricker wavelet based on the elastic properties derived from well logs and rock physics model at GC955H and corresponding amplitude vs thickness. From Zhang et al., 2012.**

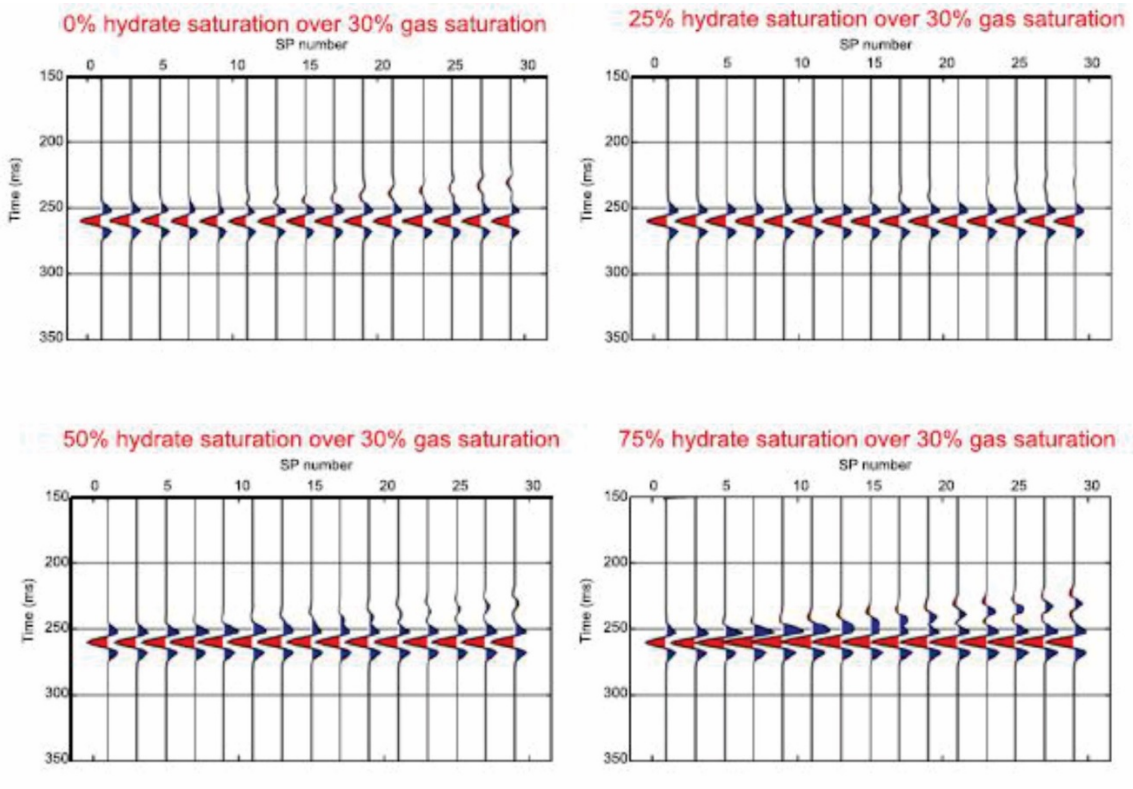


**Figure 5.20 Synthetic seismograms showing gas hydrate saturation wedge over gas sediments using a 50 Hz Ricker wavelet based on the elastic properties derived from well logs and rock physics model at GC955H. From Zhang et al., 2012**

Two methods for determining thickness from spectral amplitudes are the wedge model method (Partyka, 1999) and the observed method, described in Barnes (2016).

The relationship between gas hydrate thickness and band limited amplitude was investigated for the GC955 gas hydrate deposit using the wedge model method. In the 75% gas hydrate saturation wedge model with no underlying gas, the frequency spectra appear to notch at 31 ms at ~31 Hz (Zhang et al., 2013). Given Partyka (1999) that $P_f = 1/t$ in which $P_f$ is the period of frequency notching and t equals thin bed thickness in two-way travel time, then t= 1/0.031 = 32 ms TWT (Figure 5.21). The velocity within gas hydrate saturated sands at GC955 H is approximately 2600 m/s but the velocity of the non-gas hydrate bearing portions of the sand is approximately 1600 m/s. A mean velocity through the entire 350 m sand including both the gas hydrate saturated sand and 0% saturated sand is ~1800 m/s The resulting thin bed thickness from the spectral frequency model wedge is approximately 29 m which is consistent with the 30 m of ~75% saturation gas hydrate sand that was logged at the well (McConnell et al, 2009).

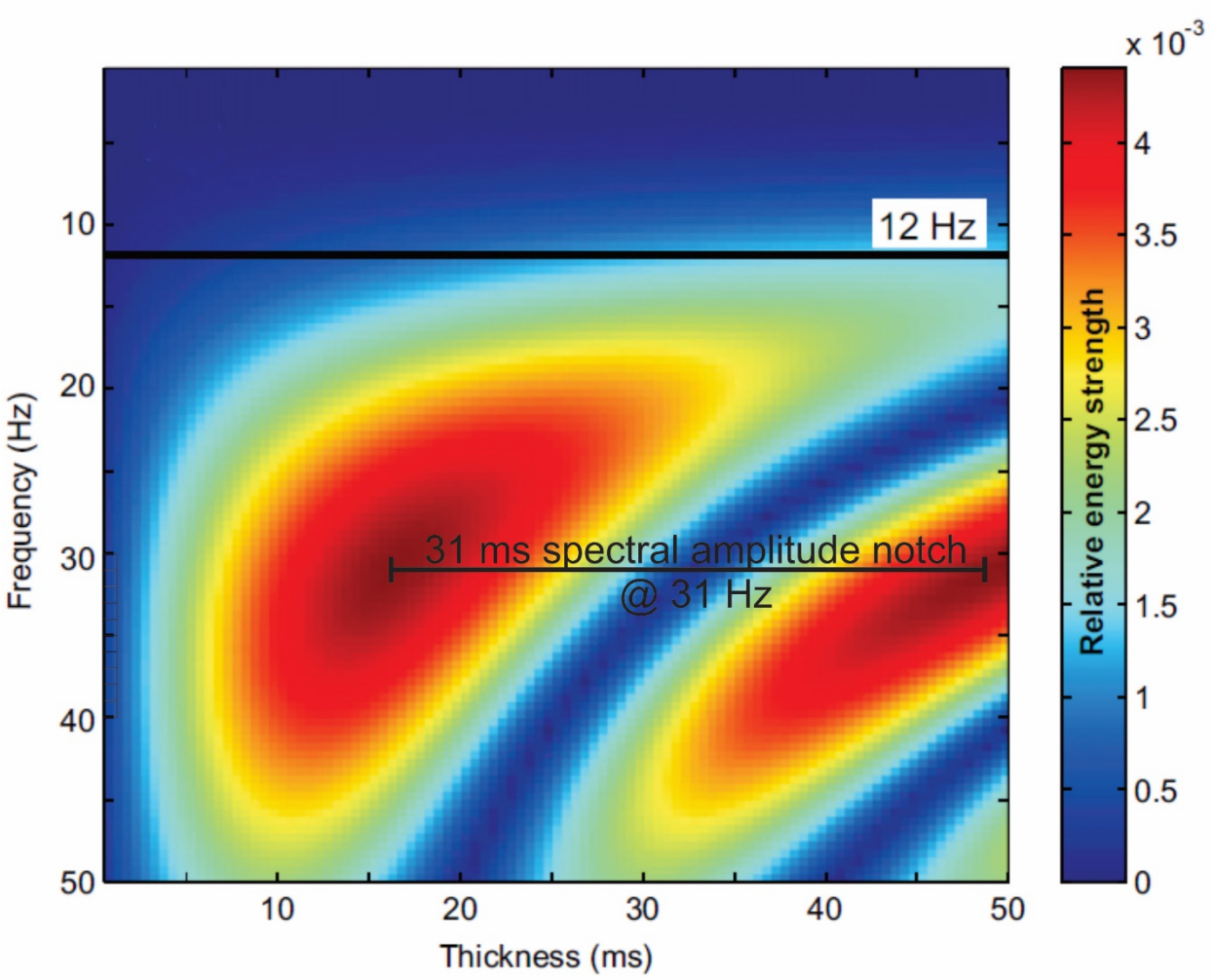


**Figure 5.21 Amplitude spectra for the 75% gas hydrate saturation model derived from the wedge model method at GC 955 H. The spectral shows an amplitude notch of 31 ms at 31 Hz Fourier frequency. The model predicts a 29 m thin bed within the GC 955 sand that corresponds to the logged and cored thickness of high saturation gas hydrate at GC 955 H. The 12 Hz line is not discussed here. Modified from Zhang et al., 2012.**

Spectral amplitude in not in itself meaningful for determining reservoir pore fill. The value of spectral amplitude is for validating the thin bed model (Barnes, 2016). Figures 5.22 through 5.30 shows the same time slice from a series of narrow band frequency volumes were calculated using the Rock Solid Attributes software module. The spectral decomposition of the full stack seismic data into different component frequencies uses Fourier transforms using Gabor-Morlet wavelets (Taner, 2003). The thickness of thin bed channels can be estimated from their first spectral maximum also called the observed method (Barnes, 2016). In the series of figures, channels outside of the areas of hydrocarbon charge are shown. The small channels are shown best at 43 Hz (Figure 5.28). In this depositional environment, the thickness of channel is similar along the length of the same channel. If 43 Hz is the first peak frequency, then by the relationship t=1/2f then the two-way time thickness is 12 ms. By substituting corresponding rock propagation velocities, an estimate of channel thickness can be determined (9.6 m at ~1600 m/s). The first peak frequency is not the same in the gas hydrate filled sand or the gas filled sands.

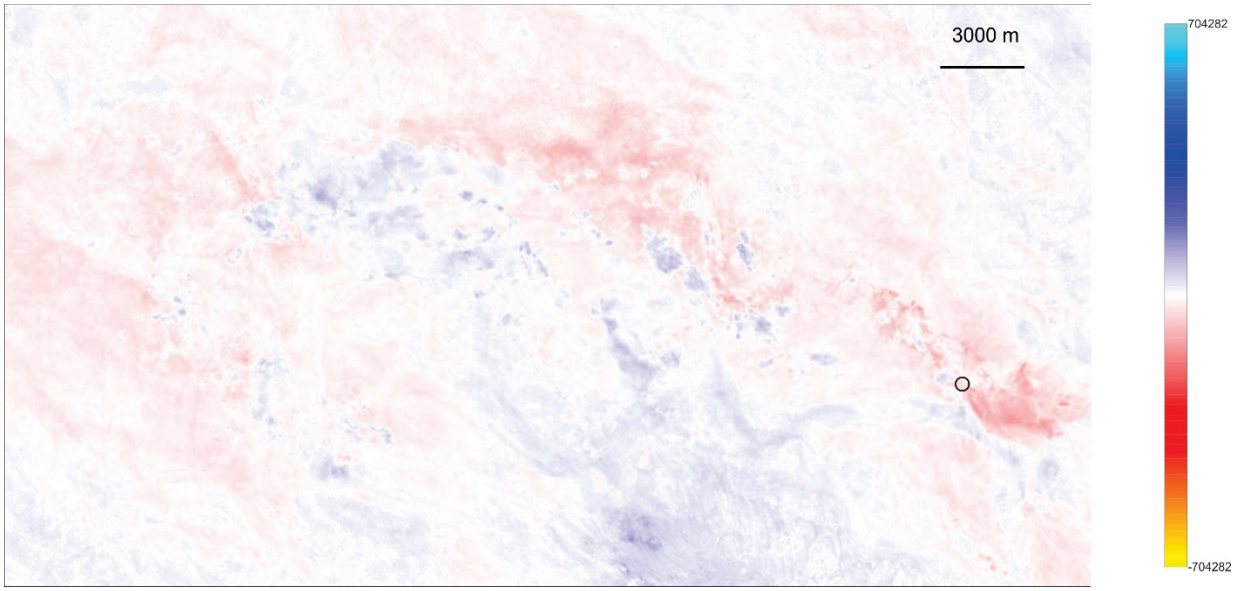


**Figure 5.22 Spectral decomposition at 6 Hz. Circle indicates point on the gas hydrate target.**

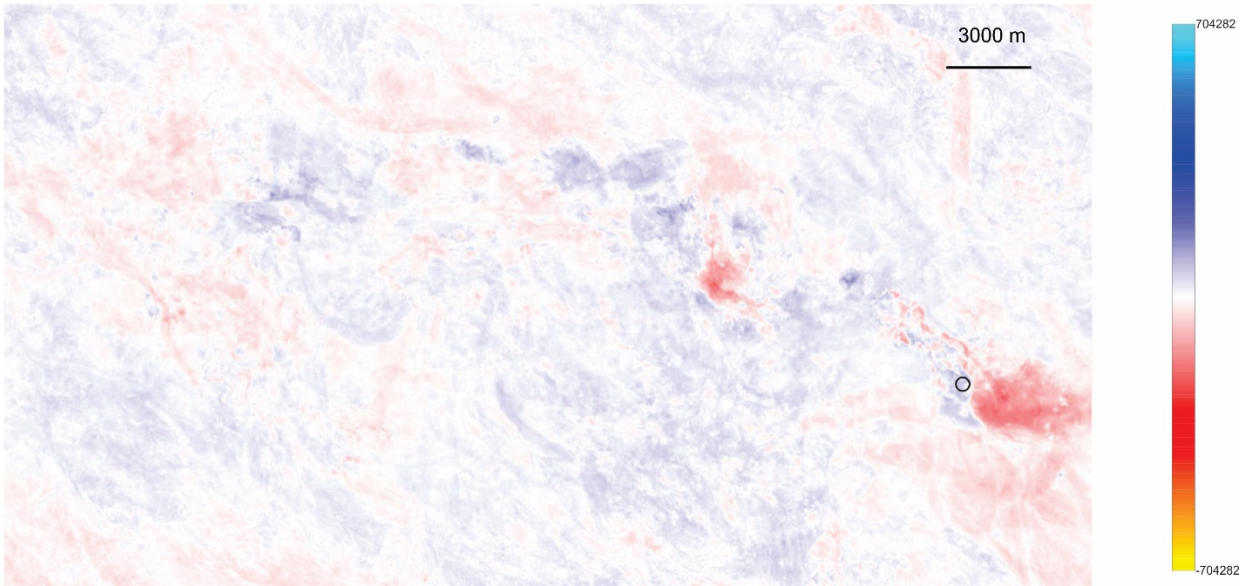


**Figure 5.23 Spectral decomposition at 10 Hz. Circle indicates point on the gas hydrate target.**

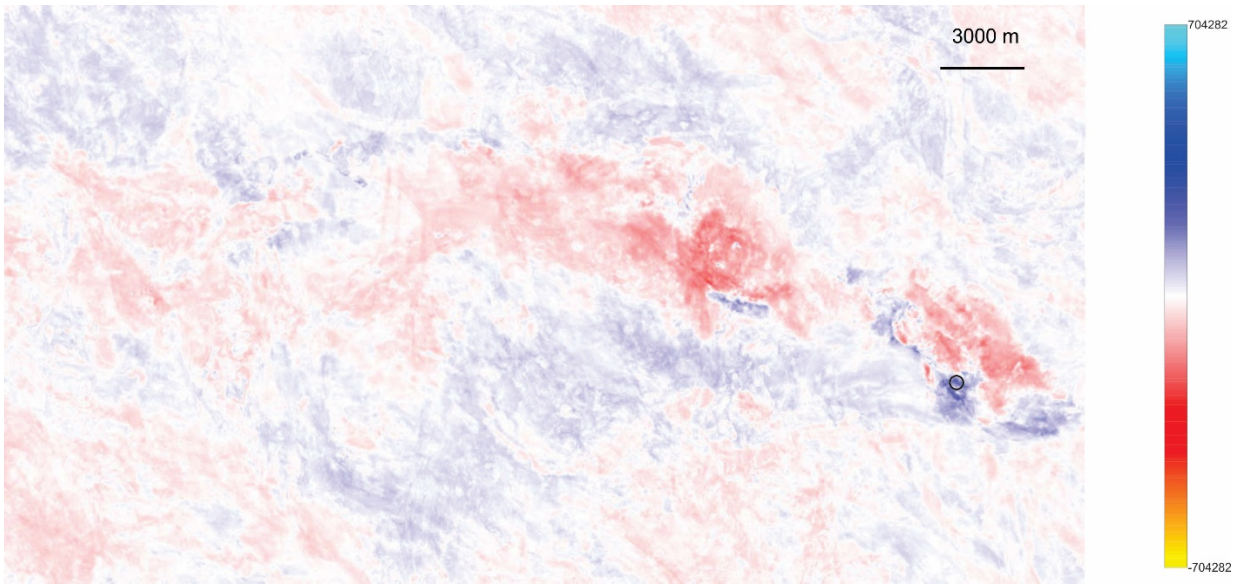


**Figure 5.24 Spectral decomposition at 16 Hz. Circle indicates point on the gas hydrate target.**

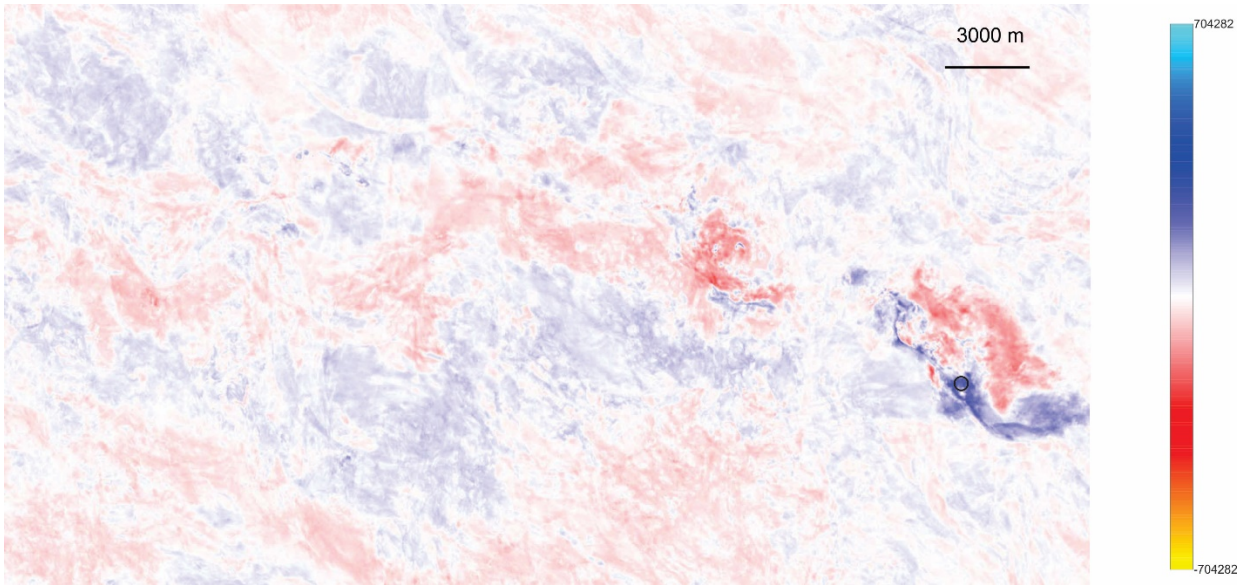


**Figure 5.25 Spectral decomposition at 21 Hz. Circle indicates point on the gas hydrate target.**

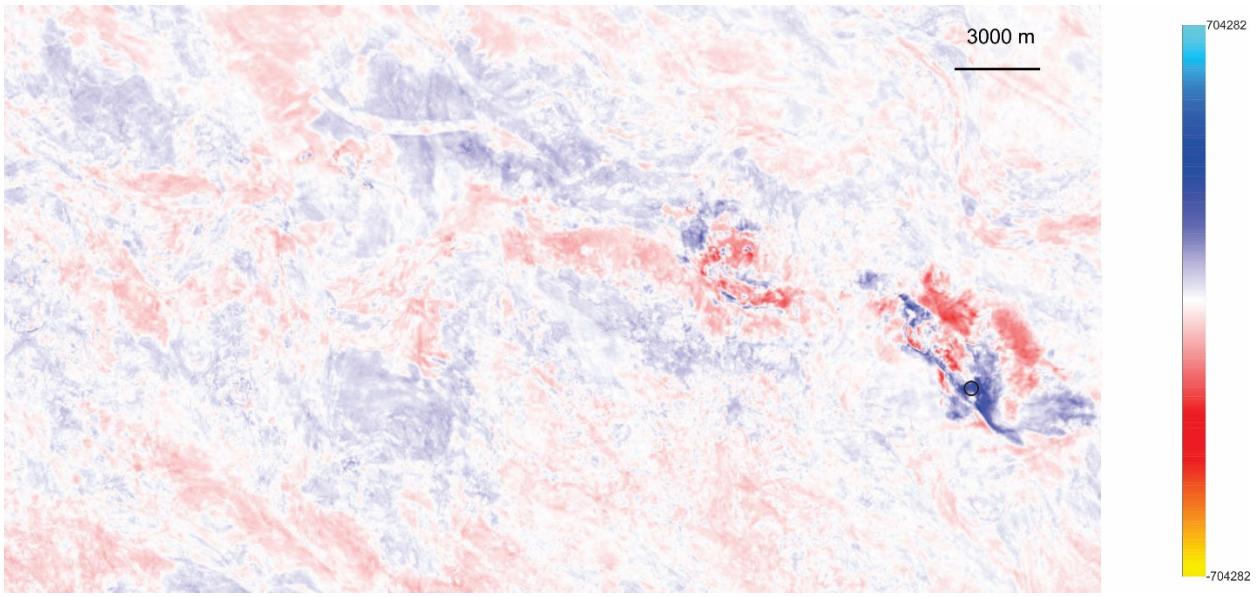


**Figure 5.26 Spectral decomposition at 26 Hz. Circle indicates point on the gas hydrate target.**

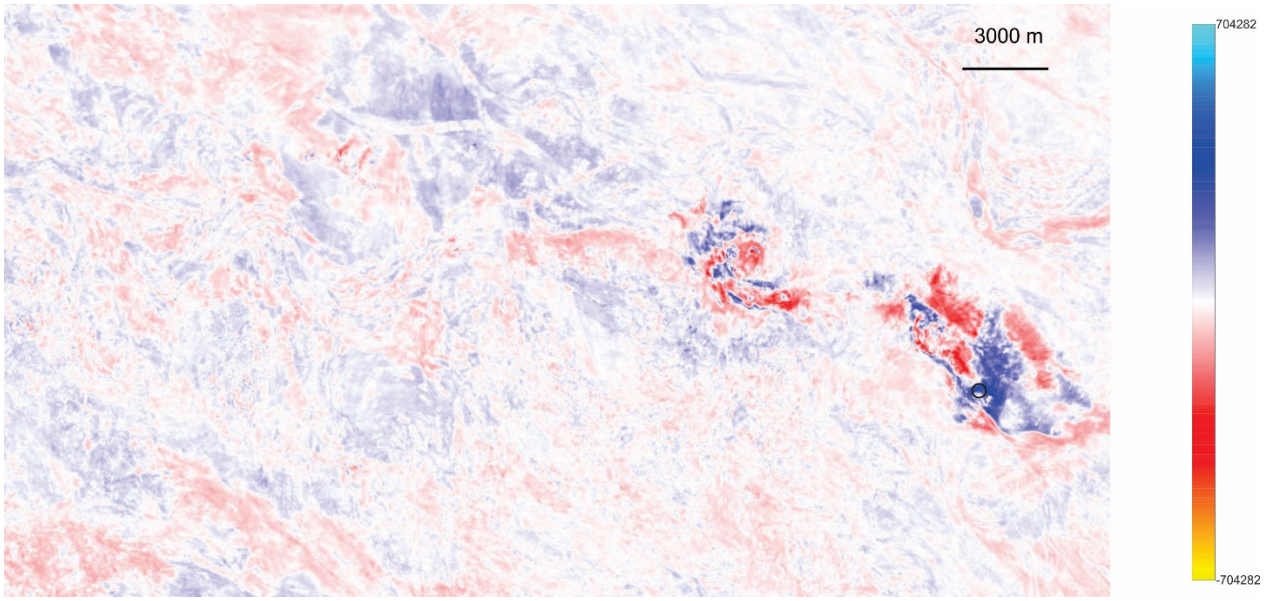


**Figure 5.27 Spectral decomposition at 34 Hz. Circle indicates point on the gas hydrate target.**

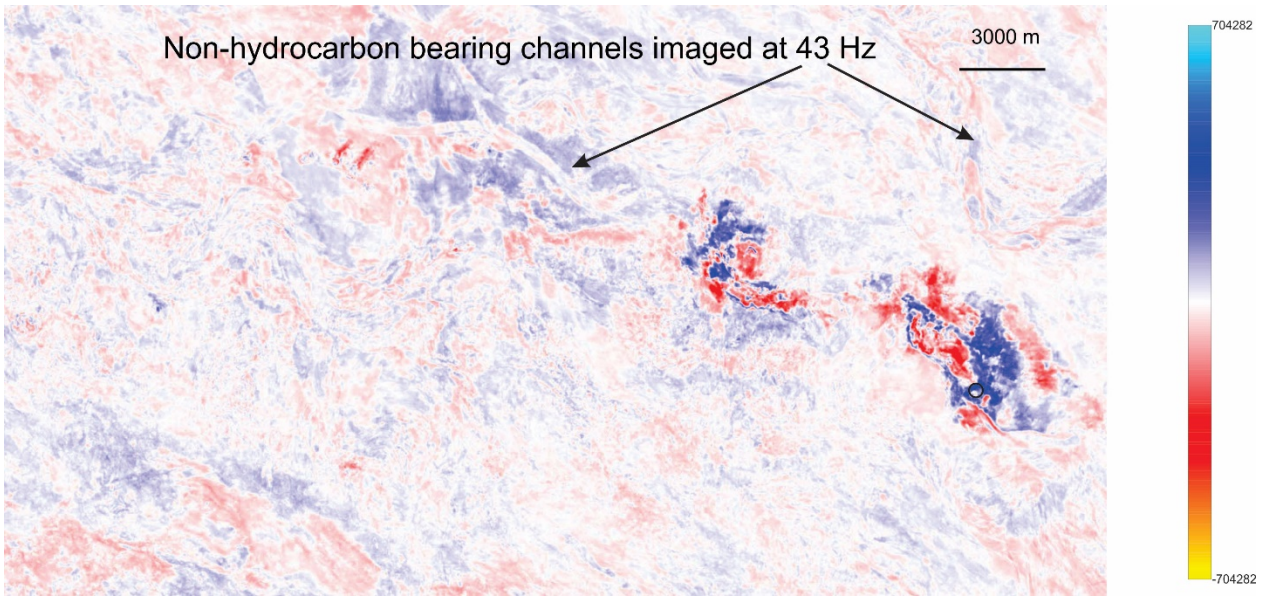


**Figure 5.28 Spectral decomposition at 43 Hz. Circle indicates point on the gas hydrate target.**

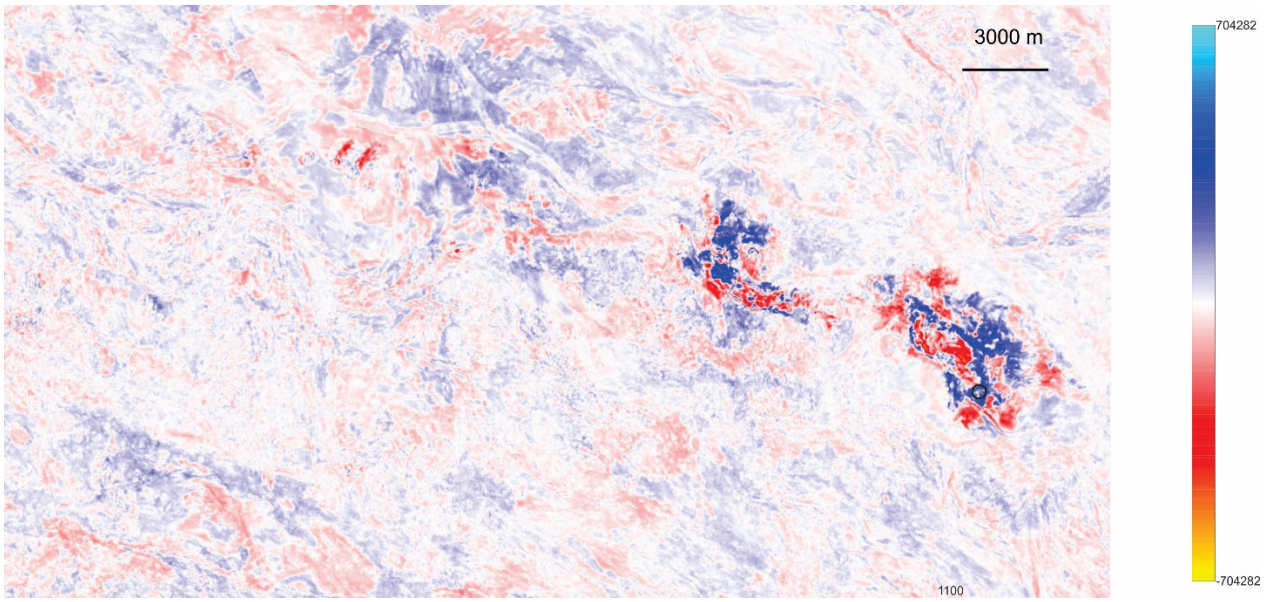


**Figure 5.29 Spectral decomposition at 55 Hz. Circle indicates point on the gas hydrate target.**

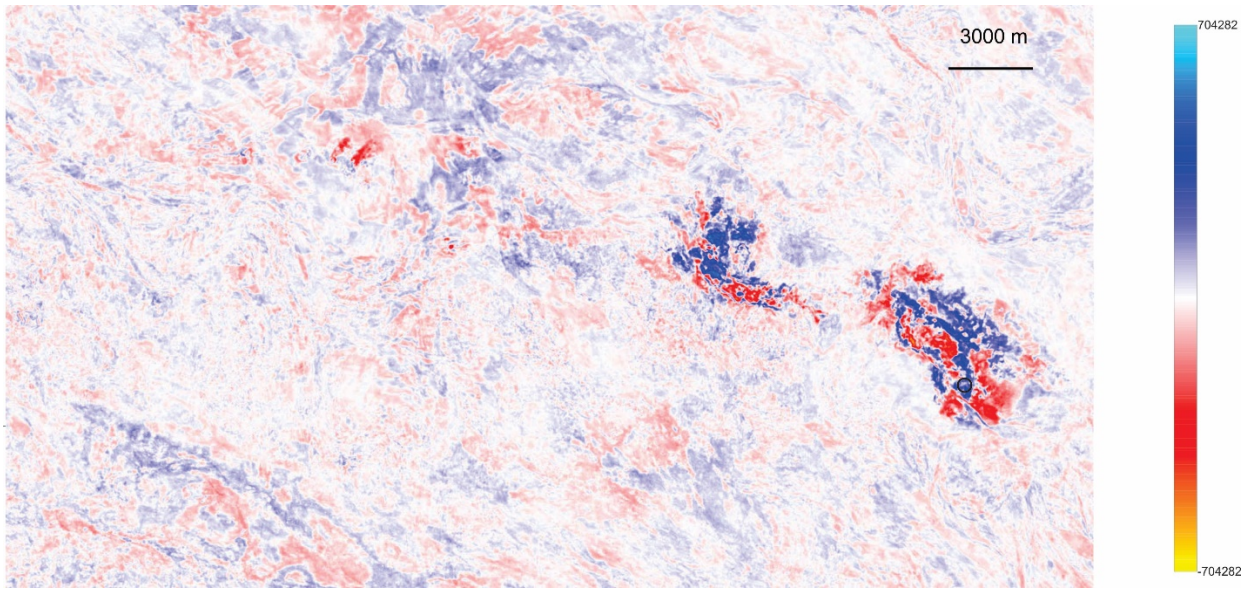


**Figure 5.30 Spectral decomposition at 70 Hz. Circle indicates point on the gas hydrate target.**

In the larger channel that contains the gas hydrate deposit the strongest peak frequency in the water wet leg is 34 Hz (Figure 5.27) corresponding to a time thickness of 14 ms. In the gas hydrate leg, the observed peak frequency is 55 Hz (Figure 5.29) which corresponds to a time thickness of 9 ms. In the gas leg, the observed peak frequency is 26 Hz (Figure 5.26) corresponding to a time thickness of 20 ms. Taken at face value without the interpretation of pore fill, the spectral frequency data indicates that the channel maintains a constant thickness until it crosses the zone of gas charge, at which point the channel abruptly thins 35% and within a few hundred meters further downstream thickens 220%. Such an abrupt change in channel thickness is not geologically reasonable in this setting. If rock propagation velocities of 1600 m/s for wet sand, 2600 m/s for high saturation gas hydrate sand, and 1200 m/s for gas sand, the thickness of the channel is constant at 23 m. Therefore, pseudo-thickness variations in spectral decomposition data can be a gas hydrate (and gas) direct hydrocarbon indicator. This concept is shown on Figure 5.31.

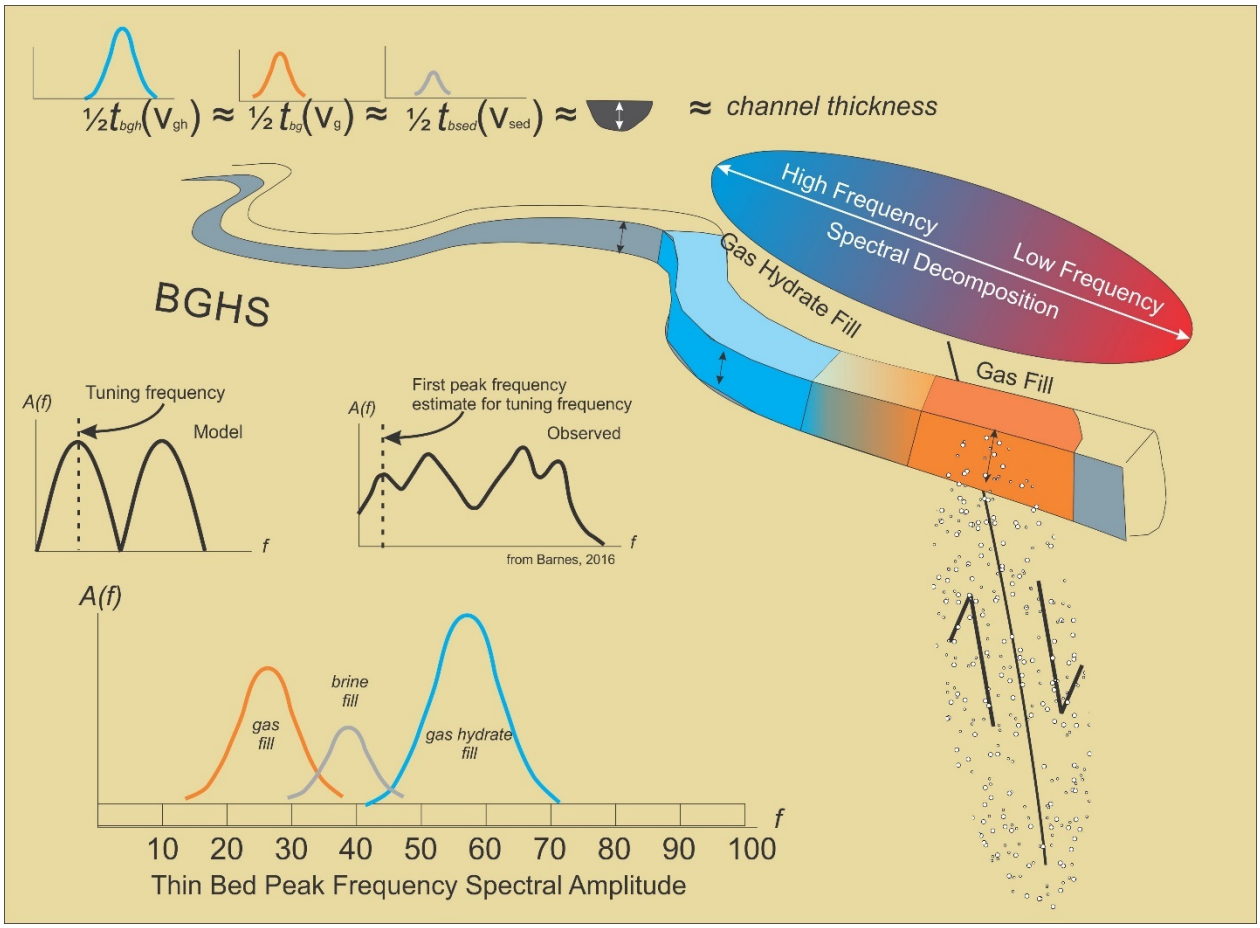


**Figure 5.31 Cartoon showing thin bed peak frequency response to gas hydrate and gas fill in a uniform channel. Compare to Figure 5.13**

Figure 5.32 shows vertical slices through the spectral frequency sections with corresponds with Figures 5.22 through 5.30. In each the gas hydrate leg is on the left (SW) and the gas leg is on the right (NE). A black horizon segment is shown that corresponds with the gas hydrate leg. Note the peak in constructive interference amplitude at 26 Hz in the gas leg and the rapid fall off of spectral amplitude at the high frequencies. In the gas hydrate leg, the constructive interference amplitude peaks at 55 Hz in the gas hydrate leg. In the bottom right the cross sections are shown over Instantaneous Q which indicates continuous low Q (high attenuation) beneath both the gas hydrate deposits and the gas deposits.

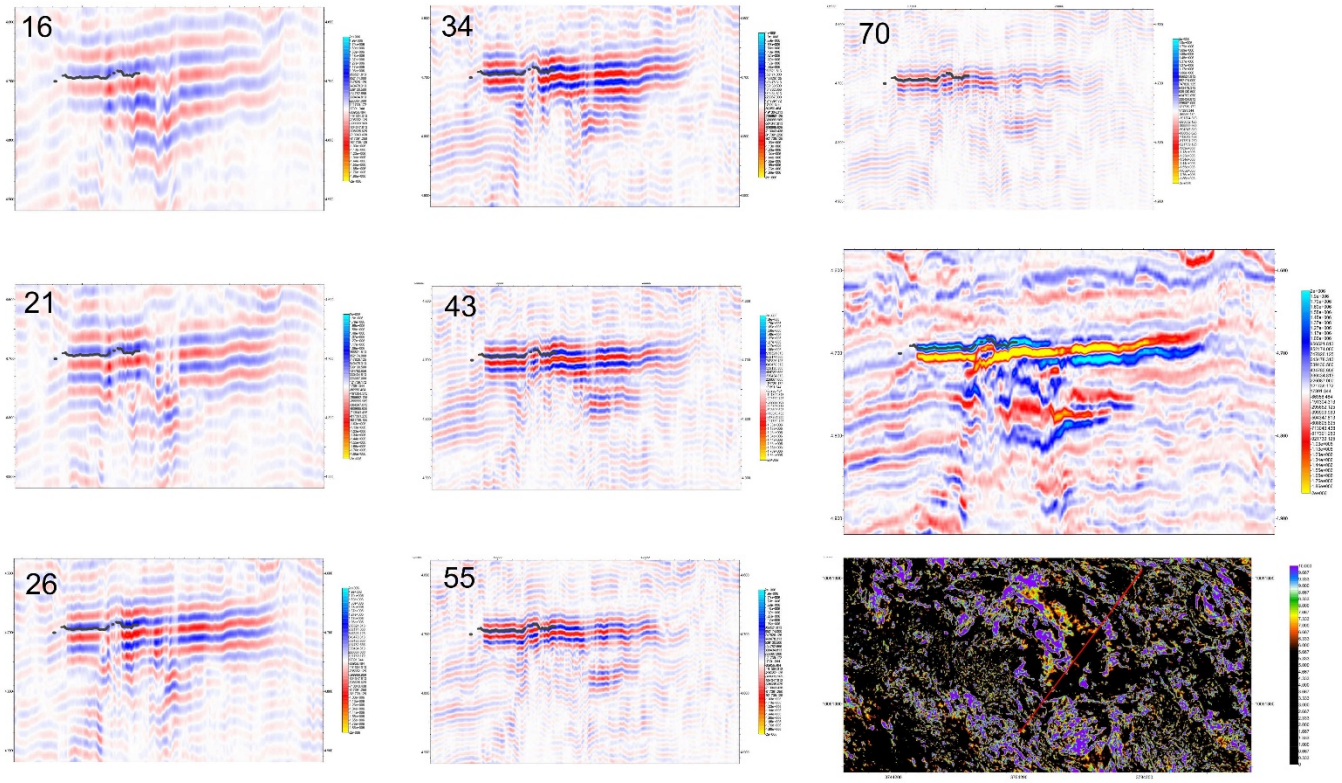


**Figure 5.32 Frequency spectra showing that gas hydrate in the high impedance zone increases at higher frequencies. Gas in the high impedance zone does not. Both gas hydrate and gas attenuate data.**

## 5.5 Gas Hydrate Saturations from Acoustic Inversion

A trace-based inversion for acoustic impedance using Linear Programming Sparse Spike Inversion was performed with Hampson-Russell software. The inversion finds acoustic impedance by minimizing the objective function that is a combination of the reflection coefficient and seismic fit. The function is given as

$$J(m) = \sum_{n=0}^{N-1} |r_n| + |Lm - d|$$

where rn is the reflection coefficient of the model, L is the linear operator, m is the model data, and d is the actual seismic data. Such seismic inversion for gas hydrate characterization in shallow unconsolidated sediments has been used by many places, such as Gulf of Mexico.

The low frequency impedance is not present in the seismic data. It is usually derived from well logs or a seismic velocity model. We estimated the low frequency Vp and density from well log data from Lloyd Ridge 511-1 that was drilled by Murphy Oil Company in 2008. The wavelet was defined by finding the best match

between the real seismic data and the synthetic data computed by convolving well log reflection coefficients with the source wavelet.

Rock physics relationships can transform seismic parameters Vp, density, and P-impedance to the sediment parameters, porosity and gas hydrate saturation. The relationships between porosity and impedance can be derived from a mud-rock compaction equation which is often applicable in deepwater passive margin sediments that have a simple compaction structural history. In a gas hydrate study, pore fill can be divided as belonging to three types: brine, gas, and gas hydrate fill. High impedance layers (given reservoir facies and a gas hydrate system) can indicate gas hydrate fill and anomalously low impedance layers in a reservoir facies may indicate gas fill.

A three-phase model of matrix, fluid, and gas hydrate is used to calculate gas hydrate saturations. For sediments without gas hydrate. The high velocity of gas hydrate replacing brine in the pore space causes high impedance layers and the low velocity of gas replacing brine in the pore space results in low impedance layers. Sediments without gas hydrate can be described by Hertz-Mindlin contact theory and Gassman fluid substitution. The Hertz-Mindlin rock frame moduli can be extended to all porosities by the Hashin-Shtrikman lower bounds and the critical porosity. Above the critical porosity, sediment grains are suspended, below the critical porosity grains are in contact. Gas hydrate in the pore space can be both suspended in the fluids and in contact with the grains. Above a certain saturation, ~40%, gas hydrate becomes load bearing and a Hashin-Shtrikman lower bound can be used as a critical porosity parameter to calibrate a model for gas hydrate saturation as a function of impedance ratios (Zhang et al, 2011).

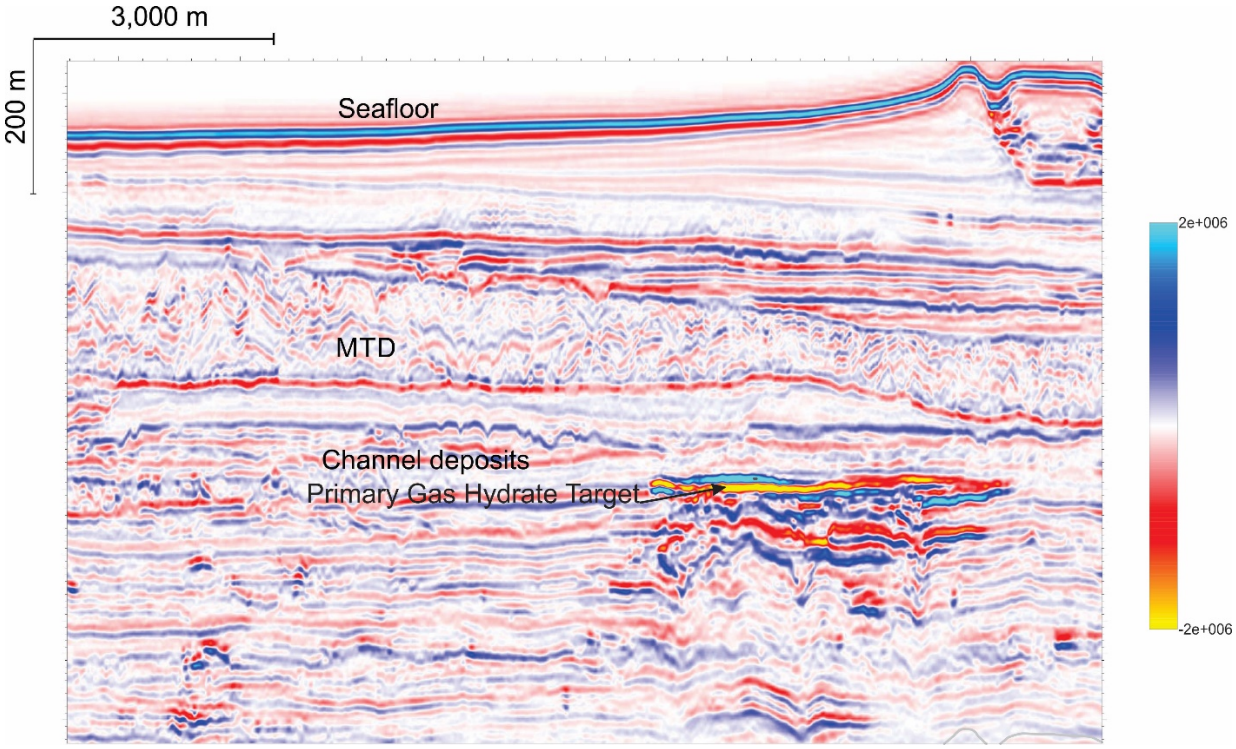


**Figure 5.33 Full stack seismic reflection data showing primary gas hydrate target**

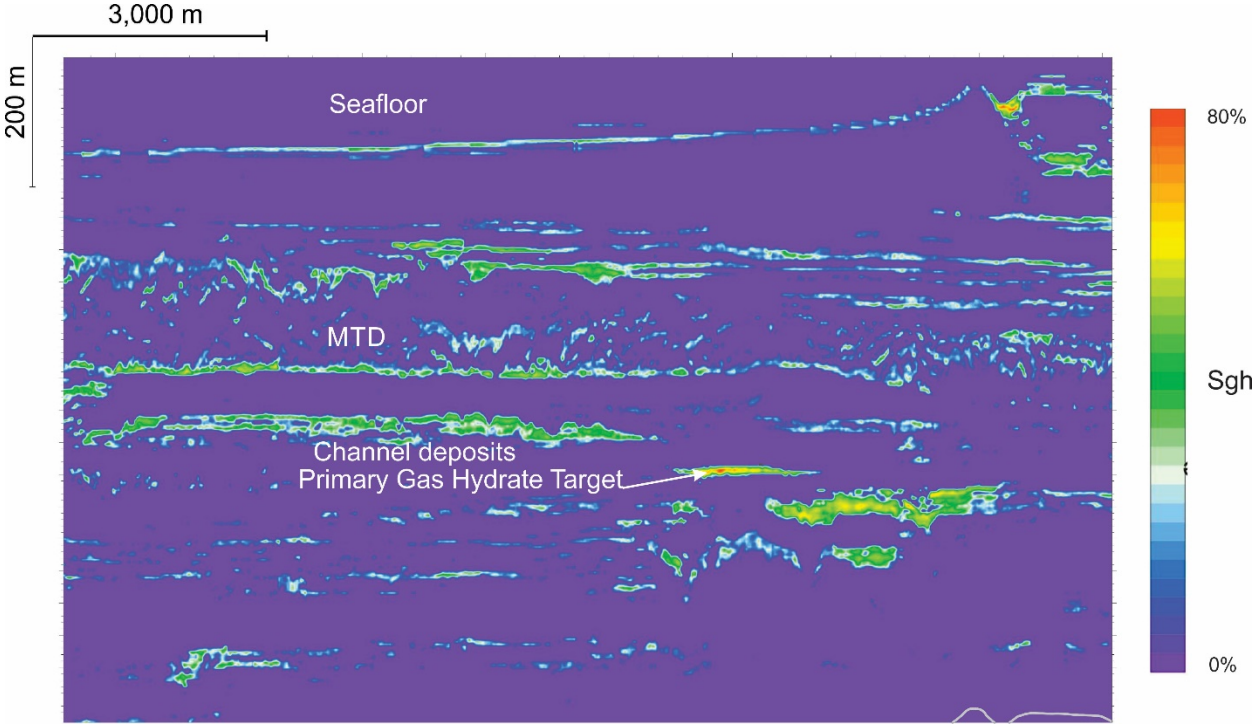


**Figure 5.34 Gas hydrate saturation derived from acoustic inversion. Note the method predicts a much wider distribution of gas hydrate. Some may be false positives.**

High gas hydrate saturation was predicted at the primary target (Figures 5.33 through 5.36). Saturation ranged from ~70 % at the primary gas hydrate target and diminishing to 40% where transitioning towards the free gas leg (Figure 5.36). No gas hydrate saturation was predicted in the interpreted free gas leg of the channel sand (Figure 5.36). Like the gas hydrate saturations predicted in advance of JIP Leg II drilling, inversion, being amplitude driven, will produce likely false positives, e. g. predicting uniform gas hydrate coincident with the seafloor reflector. The gas hydrate saturation volume, here, also produced likely false positives at the seafloor and at the base of thick mass transport deposits (shown as MTD on Figure 5.33) and the top of a channel sequence. While high saturation gas hydrate cannot be ruled out, these are likely false positives. The base of the mass transport deposits is not likely to have a regional semi-continuous gas hydrate layer. Gas hydrate deposits are also predicted below the primary target. These could represent thermogenic gas hydrate deposits. At GC955, the predrill predictions of gas hydrate showed additional deeper gas hydrate deposits under the area of highest flux (Shelander et al., 2012)

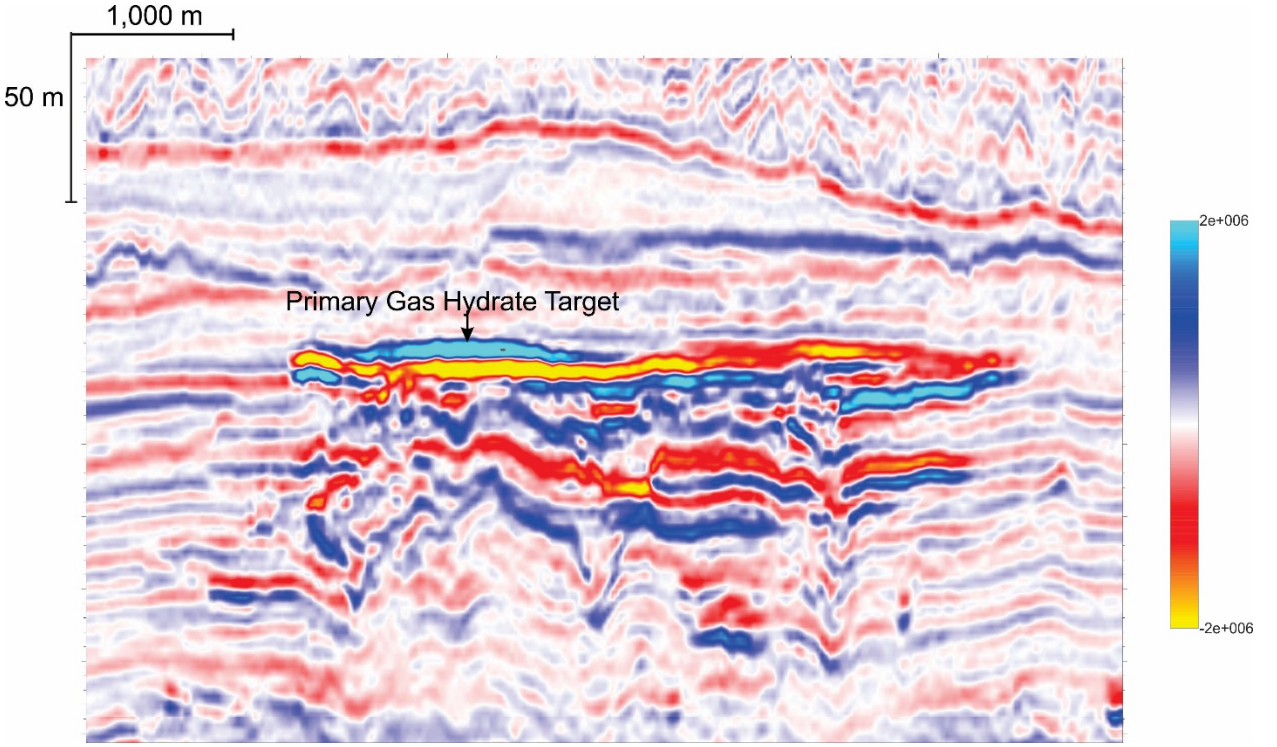


**Figure 5.35 Full stack seismic reflection data showing primary gas hydrate target in detailed view.**

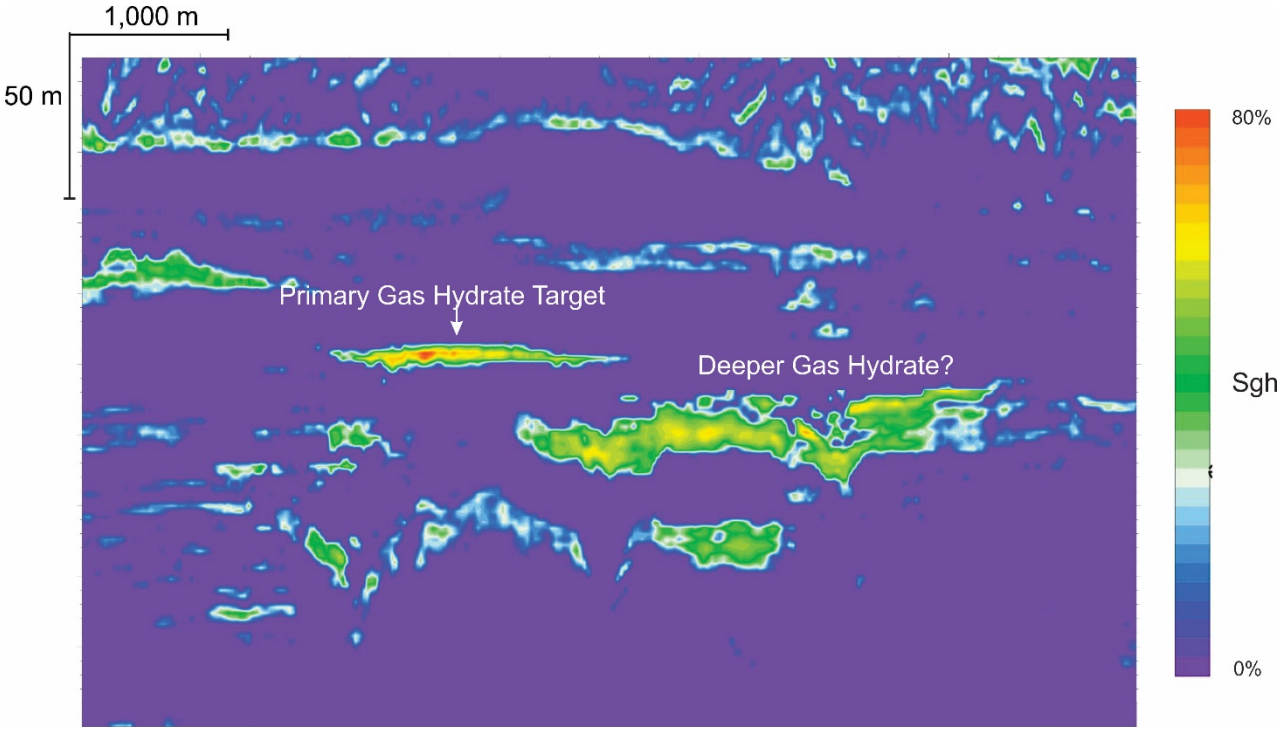


**Figure 5.36 Gas hydrate saturation derived from acoustic inversion. 60 to 80 % saturation gas hydrate is predicted at the primary target. Possible deeper gas hydrate is also indicated.**

# 6. RESULTS AND DISCUSSION

## 6.1 Results

Prospecting for gas hydrates in the Eastern GoM utilized an exploration strategy that included a screening for gas hydrate DHI using a petroleum systems approach. A large, 3 sq km, gas hydrate deposit approximately 23 m thick was identified in a thick section of Pliocene Mississippi Fan abyssal sands. The interpreted gas hydrate deposit is at the base of gas hydrate stability for methane where gas is apparently migrating along one of the few deep seated fault from a Jurassic source that offset the gas hydrate stability zone. The screening for the gas hydrate sand utilized the approach taken by the JIP Leg II gas hydrate program.

Several post stack seismic attributes and frequency attributes that might reveal properties that could be associated with gas hydrates were investigated. Good agreement was found between the seismic amplitude interpretation of gas hydrate, spectral frequency illumination that indicated high velocity pore fill by pseudo-thickness. Two of these attributes, Instantaneous Q that could detect attenuation, and second derivative of the envelope that is a measure of stacked high energy reflectors within thin beds were found to correlate as expected to gas hydrate deposits.

Both high saturation gas hydrate sands and gas sands attenuate seismic energy. Several seismic attributes attempt to indicate Q, the quality factor. The inverse of Q is a measure of attenuation. The seismic attribute instantaneous Q tries to detect attenuation by the frequency change with energy decay.

Frequency analysis shows different illumination frequencies for the gas hydrate leg and the gas filled leg. The gas hydrate leg illuminates at higher spectral frequencies and the gas leg illuminates at lower frequencies. The illumination is not a reservoir property but is instead a measure of thin bed thickness. The brightening in spectral frequency data is interpreted as representing the peak of the first cycle of constructive interference and represents thin bed pseudo-thickness. The channel is thinnest in time-thickness corresponding to the gas hydrate deposit, intermediate in time-thickness entering and exiting the zone of gas migration, and thickest in time-thickness in the interpreted gas leg.

This thin bed response is caused by fast velocity of gas hydrate deposit and is recognized by constructive interference seen in isolated high frequency bands within the seismic bandwidth. Spectral decomposition is a particularly useful attribute to help delineate high saturation gas hydrate deposits in seismic thin beds by identifying anomalously thin pseudo-thicknesses.

Importantly, wedge models can be employed to determine the thickness of gas hydrate deposits even when within a sand body that is thick enough to have seismically discernable top and bottom. The gas hydrate deposit within such a sand body will likely be a seismic thin bed.

## 6.2 Discussion

The gas hydrate deposit, while not a singularity, is an anomaly within a large area of the Eastern GoM. Nevertheless, the large interpreted gas hydrate deposit provides an excellent testing ground for testing other

gas hydrate DHIs, with the important caveat that the interpreted gas hydrate deposit has not been drilled. The gas hydrate deposit was first identified as a leading peak (high positive impedance) anomaly in a sand that would normally be low impedance. The high saturation gas hydrate fill causes a phase reversal in what would, outside of the gas hydrate pressure temperature conditions, be a gas sand (high negative impedance). The path for a wet sand to move from low negative impedance to high positive impedance with increasing gas hydrate fill means that seismic amplitude is more diagnostic than for oil and gas fill and elements of this progression might be captured by other seismic attributes. Certainly, it was hypothesized that there would be seismic attributes that could correspond the high saturation gas hydrate end member and the acoustic properties of a high velocity sand.

The flat-lying nature of channel sediments produced homogenous architectures for each channel sand. Each channel body at this distance from the source on an abyssal plain has consistency of architecture along the channel axis and locally orthogonal. In the absence of wells, this simple geometry where a channel is wet, filled with gas hydrate, gas filled, and then wet in the same body allowed for the testing various attributes to identify gas hydrate and was especially useful in isolating the frequency response across the wet, gas hydrate, and gas channel fill.

### 6.2.1 High Energy Thin Bed and Attenuation Attributes

Analysis of well logs has shown strong attenuation caused by saturation of gas hydrate in sediments. Guerin and Goldberg (2001) showed strong P and S wave amplitude losses at the Mallik 2L-38 well in the Canadian Arctic. Matsushima (2006) used the same approach in gas hydrate sediments Nankai trough in Japan which also showed strong attenuation.

A widely accepted mechanism that causes intrinsic attenuation is wave induced fluid flow in the pore space of rocks. Gas hydrates do not completely occlude the pore space. Therefore, wave compression induces squirt-flow in the pore spaces. The loss of energy associated with squirt flow causes seismic attenuation.

Specifically, with Q attributes, Barnes warns against bold claims and treats Q attributes with much skepticism (Barnes, 2016). The high amplitude low impedance reflectors that can be caused by a range of gas concentrations attenuate and are associated with low Q. This implies that low Q as a measure of attenuation, like amplitude, may not be able to distinguish between low saturation gas and high saturation gas. Frequency attributes that relate to attenuation should also relate to gas hydrate saturation. Q attributes values, like amplitude values, may better relate to gas hydrate concentration.

While attenuation is s fundamental geophysical property in that a wave traveling through the earth “will undergo amplitude decay proportional to the number of wavelengths traveled”, it can be difficult to measure in seismic data. Nonetheless, a low Q gas sand in a high Q, should cause a sharp drop in energy and average frequency beneath the channel (Barnes, 2016).

### 6.2.2 Thin-Bed Seismic Attributes for Detecting Gas Hydrate

An important class of gas hydrate deposits are those in which a sand body crosses the base of gas hydrate stability in an area of gas flux. This scenario can result is a situation in which different portions of the sand body are gas hydrate filled, gas filled, and wet over a short distance.

The first approach for using spectral decomposition at the interpreted gas hydrate deposit was the same empirical approach used in hydrocarbon exploration. In this case, to find frequency characteristics that appear to associate with the gas hydrate deposit. The spectral data show an increase in amplitude at higher frequencies associated with the gas hydrate deposit with the highest Fourier amplitude in the ~70 Hz band. The spectral data over the interpreted gas in the eastern part of the anomaly in contrast show brightest Fourier amplitude in the ~30 Hz range with reducing Fourier amplitude at higher frequencies.

It appears that high saturation gas hydrate Illuminates at higher frequencies in spectrally decomposed data. What became clear when working through this study is that gas hydrate deposits need to be analyzed in the context of seismic thin beds. At the core scale, gas hydrates in sands tend to form in lamina, these laminae taken together a seismic thin bed. For many gas hydrate deposits the top of the gas hydrate section may not be at the top of the sand nor will it always extend to the base. In exploration seismic data gas hydrates will almost always be a seismic thin bed and, in many cases, will be a seismic thin bed within a seismic thin bed. The hind cast example at GC955 shows that the thickness of the GC955H gas hydrate sand could be predicted by thin bed analysis.

### 6.2.3 Thin-Bed DHI for Gas Hydrate using Spectral Decomposition

Spectral decomposition methods may be effective for identifying gas hydrates in sands. Spectral amplitude is responsive to both impedance and thin layers. Pseudo-thickness variations in spectrally decomposed data may be a gas hydrate (and gas) direct hydrocarbon indicator. Gas hydrates in sands, like gas in sands, cause high impedances because of the velocity contrast. Gas hydrate sands are polarity reversed with respect to gas sands in the same setting because gas hydrates are high velocity and gas is low velocity relative to the layer above. In spectral data corresponding to an impedance anomaly caused by gas hydrates, the spectral amplitudes will increase in amplitude at higher frequencies. In a gas sand, the spectral data corresponding to the gas impedance anomaly will increase in some low to mid frequency range, depending on the setting and decrease in amplitude at higher frequencies.

One possible cause for this behavior is that gas in the pore spaces of a typical heterogeneous sand reservoir suppresses the thin bed response. The opposite behavior will tend to be found in gas hydrate deposits. Gas hydrate deposits in sands enhance the thin bed response and will show more layering than the non-gas hydrate filled seismic architecture. Gas hydrates create thin high impedance layers that can be detected with common seismic interpretation tools.

Gas hydrates also tend to deposit in layers because of the processes that favor gas hydrate formation. So, this contrasts with the spectral response of a gas sand in which spectral amplitudes associated with the impedance anomaly decrease at higher frequencies (Figure 5.32).

A thin bed channel of consistent dimensions with gas hydrate fill just above the base of gas hydrate stability that, as it continues beneath the base of gas hydrate stability, is gas filled, will show variations in peak spectral amplitude. The peak spectral amplitude will occur at higher frequencies in the gas hydrate filled channel because the gas hydrate filled channel has higher interval velocities. In contrast, the peak spectral amplitude for the gas filled portion of the channel will occur at lower peak spectral frequencies because of the lower interval velocities. If the gas hydrate and the gas fully fill the thin bed channel, then the thin bed time thicknesses, the shorter time thickness in the gas hydrate and the longer time thickness in the gas portion, should, upon substitution of respective velocities should compute approximately the same channel thickness. The spectral amplitude, however, is expected to be more sensitive to the gas hydrate fill than to the thin bed channel architecture, because of the high velocity contrast in the gas hydrate bearing sediments. If the gas hydrate does not completely fill the channel, then the channel thickness calculated from peak spectral amplitude could be thinner than the geologic thickness of the channel. In the case of gas fill, it is geologically reasonable for the gas to tend to fill the channel or even cross bedding planes, so the thin bed thickness calculated from peak spectral amplitude could be thicker than the geologic thickness of the thin bed channel.

### 6.2.4 Correlation of Attributes with Acoustic Inversion and Gas Hydrate Saturation

There is a strong correlation between seismic amplitude and acoustic inversion. inversion is a layer property whereas the amplitude data shows interfaces between layers. The inversion improves the interpretation of thin bed by the removal of side lobes but does not resolve thin beds as well as bandlimited frequency methods. Gas hydrate saturations derived from critical porosity were populated through a large subset of the seismic cube. Comparisons between gas hydrate saturation and other seismic attributes were only made at the primary target. While there were small differences in areal extents, there was good agreement between gas hydrate saturation, high spectral frequencies, and stacked positive impedance high energy layer attributes.

## 7. RECOMMENDATIONS FOR FUTURE WORK

The gas hydrate deposit in this report has not been drilled. Confirmation of the interpretation of the gas hydrate deposit would need to come from drilling, such as a LWD, wireline logging, or pressure coring. Post stack seismic attributes such as envelope attributes, spectral decomposition, and attenuation attributes appear to be useful in identifying gas hydrate deposits. Even though the close analog to gas hydrate behavior in GC 955 is referred to, these techniques have not been applied over known gas hydrate deposits in this report. It would be useful to use these techniques and findings of additional seismic attributes and spectral decomposition over known gas hydrate deposits, ideally the close analog GC955. It would also be useful to compare some of the findings against pre-stack methods. Finally, it would be useful if workers tried these or other attributes in gas hydrate reservoir characterization. This could help validate or refute the approach and concepts presented here.

# 8. SUMMARY AND CONCLUSIONS

## 8.1 Summary

A large seismic high amplitude anomaly with impedance characteristics consistent with gas hydrate deposit was found in the Eastern Gulf of Mexico at a depth consistent with the predicted base of gas hydrate stability for the area. The amplitude anomaly encompasses NW-SE oriented channel sediments, interpreted to be sandy, within abyssal fan deposits. The amplitude anomaly shows a polarity reversal- a high amplitude "leading peak" on the western side that transitions to high amplitude "leading trough" on the eastern side. The deposit was ideal for the for the testing of other seismic attributes that can indicate gas hydrate presence, saturation, and thickness. The combined gas hydrate-gas amplitude anomaly covers an area of 19 sq. km.

Post stack seismic attributes from the seismic volume were generated including geometric, amplitude, and frequency attributes. Geometric attributes can help define the sediment architecture and lithologies. Amplitude attributes can indicate impedance, fluid content, lithology contrasts, cementation, among others. Frequency attributes can show energy loss, absorption, attenuation, among others. Time-frequency attributes using spectral decomposition were used to identify channel geometries and for gas hydrate imaging. Instantaneous Q attributes indicated attenuation from both the gas hydrate and gas deposits. Derivatives of the amplitude envelope corroborated the time-frequency attributes associated with interpreted gas hydrate deposits.

Spectral decomposition, a process of transposing the seismic bandwidth in the seismic data in time (or depth) into separate frequency domain components is widely used for visualizing seismic architectural components within seismic facies such as channel systems. Spectral decomposition is also used to identify hydrocarbon reservoirs in a manner below the resolution limit of other direct hydrocarbon indication methods. Using the principles of tuning interference between layers, spectral decomposition methods allowed the thickness of impedance events below the resolution of the seismic data to be estimated.

In addition to frequency attributes to determine gas hydrate fill, seismic attributes related to attenuation, thin-bed stacked high energy layer that are associated with gas hydrates were tested on the gas hydrate deposits. All provided multiple lines of evidence of being useful for direct hydrocarbon indicators for gas hydrate and were consistent with saturation model derived from acoustic impedance.

## 8.2 Conclusions

This study reviews gas hydrate interpretation techniques for identifying gas hydrate bearing sands, expands on direct hydrocarbon indicators for high saturation gas hydrate sands. As the famous geologist Wallace Pratt said, "oil is found in the minds…" (Halbouty, 1972) so too, with gas hydrates. With this in mind, a case is made for the presence of a large gas hydrate deposit in the deepwater Eastern Gulf of Mexico. Prospecting for high saturation gas hydrate deposits can be greatly aided with improved approaches to seismic interpretation and especially if sets of seismic attributes can be shown as diagnostic or direct hydrocarbon indicators for high saturation gas hydrates in sands that would be of most interest for gas hydrate production.

Spectral decomposition methods may be effective for identifying gas hydrates in sands as are other seismic attributes that detect attenuation and layered high energy in thin beds. Spectral amplitude is responsive to both impedance and thin layers. In spectral data corresponding to an impedance anomaly caused by gas hydrates, the spectral amplitudes will increase in amplitude at higher frequencies. In a gas sand, the spectral data corresponding to the gas impedance anomaly will increase in some low to mid frequency range, depending on the setting and decrease in amplitude at higher frequencies. Frequency attributes derived from spectral decomposition proved to be direct hydrocarbon indicators by pseudo-thickness that could be only be reconciled by substituting gas hydrate in the pore space. The study emphasizes that gas hydrate exploration and reservoir characterization benefits from a seismic thin bed approach.

## 9. ACKNOWLEDGEMENTS

The P. I. thanks Fugro and Spectrum for permission to the use of the Florida 3D for this research. This study would not have been possible without this generous contribution. The P. I. thanks Gitta Zaalberg for making this possible including the retrieval of the data from CGG when Fugro owned the data and for approaching Spectrum for permission to use the data after the data were sold to Spectrum. A debt of gratitude is owed to Mark Walker of Geoteric and the local team Rachael Moore, and Tom Wooltorton for providing the use of their excellent frequency decomposition software for this project. Thanks are given to Fausto Mosca of Murphy Oil Corporation for securing permission and providing us with digital copies of Manhattan prospect well logs. Fugro scientists that contributed to the search for gas hydrates in the data included Greg Nash, Mike Kucera, Brendan Gao, and William C. Haneberg, Steve Wardlaw patiently assisted with administration issues. The P. I. thanks Fugro management for allowing us to continue to put research funds into this project beyond the federal support. Finally, the P. I. thanks long term collaborator Zijian Zhang for his contribution to the geophysics behind these gas hydrate discoveries.

.

## 10. REFERENCES


Bangs, N. L., D. S. Sawyer, and X. Golovchenko, 1993, Free gas at the base of the gas hydrate zone in the vicinity of the Chile triple junction: Geology, v. 21, p. 905-908.

Barnes, A. E., 2016, Handbook of poststack seismic attributes. Geophysical References Series No. 21, Harvey, E. L., and R, Latimer eds., Society of Exploration Geophysicists, Tulsa, OK, 254 p.

Boswell, R., C. Shipp, T. Reichel, T. Saeki, M. Frye, W. Shedd, T. Collett and D. McConnell, 2015, Prospecting for marine gas hydrate resources, Interpretation, v. 4, i. 1, p. 25-37.

Brooks, J. M., Cox, H. B., Bryant, W. R., Kennicutt II, M. C., Mann, R. G., and McDonald, T. J., 1985. Association of gas hydrates and oil seepage in the Gulf of Mexico., Advances in Organic Geochemistry, v. 10, p. 221-234.

Brown, A. R., 1996 (fourth edition), Interpretation of three-dimensional seismic data. AAPG Memoir 42, American Association of Petroleum Geologists, Tulsa, OK, USA. 424 p.

Castagna, J. P., and R. W. Siegfried, 2003. Instantaneous spectral analysis: Detection of low-frequency shadows associated with hydrocarbons, The Leading Edge, February 3003, p 120-127.

CGG, 2014, Florida 3D seismic data processing report. CGG, Calgary, Canada 40 p.

Chowdhury, A., 2009, Salt geology and hydrocarbon plays in the northeastern Gulf of Mexico: American Association of Petroleum Geologists Search and Discovery Article 10215, 9 p., www.searchanddiscovery.net/documents/2009/10215chowdhury/images/chowdhury.pdf.

Collett T. S., M. Riedel, J. R. Cochran, R. Boswell, P. Kumar, A. V. Sathe, and the NGHP Expedition 01 Scientific Party, 2008, Indian contentintal margin gas hydrate prospects: results of the Indian National Gas Hydrate Program (NGHP) Expedition 01, Proceedings of the 6th International Conference on Gas Hydrates (ICGH 2008), Vancouver, British Columbia, CANADA, July 6-10, 2008.

Combellas-Bigott, R. I., and W. E. Galloway, 2002, Origin and evolution of the Middle Miocene submarine-fan system, East-Central Gulf of Mexico: Gulf Coast Association of Geological Societies Transactions, v 52, p 151-163.

Cook, A. and U. Majumdar, 2016. A new approach to understanding the occurrence and volume of natural gas hydrate in the northern Gulf of Mexico using petroleum industry well logs, Final Report, DOE Award No.: DE-FE0009949, prepared for United States Department of Energy and National Energy Research Laboratory, 24 p.

Dillon, W. P., and C. K. Paull, 1983, Marine gas hydrates—II: Geophysical evidence, in Cox, J .L., ed., Natural gas hydrates: Properties, occurrence and recovery: Boston, Butterworth, p. 73-90.

Fahmy, W. A., G. Matteucci, J. Parks, M. Matheney, and J. Zhang, 2008. Extending the limits of technology to explore below the DHI floor; successful application of spectral decomposition to delineate DHI's previously unseen on seismic data, Proceedings of the Annual Meeting of the Society for Exploration Geophysicists, Las Vegas, NV, USA.

Flemings, P., 2017. GOM^2: Prospecting, Drilling and Sampling Coarse-Grained Hydrate Reservoirs in the Deepwater Gulf of Mexico. Proceedings of the 9th International Conference on Gas Hydrates (ICGH 2017), Denver, Colorado, USA, June 25-30, 2017

Forrest, F., E. Marcucci, and P. Scott, 2005, Geothermal gradients and subsurface temperatures in the Northern Gulf of Mexico, GCAGS Transactions v. 55, p. 233-248.

Fugro, 2013, Florida 3D- Processing report for 3D PSTM, Project Nos. 2011-4502 and 2012-4571, Fugro Seismic Imaging Inc., Houston, USA, 59 p.

Galloway, W. E., P. E. Ganey-Curry, X. Li, and R. T. Buffler, 2000, Cenozoic depositional history of the Gulf of Mexico basin: AAPG Bulletin, v. 84, no. 11, p. 1743-1774

Guerin G and D. Goldberg, 2001, Sonic waveform attenuation in gas hydrate-bearing sediments from the JAPEX/JNOC/GSC Mallik 2L-38 research well, Mackenzie Delta, Canada. Journal of Geophysical Research, 2001; 107(B5):2088.

Hood, K. C., L. M. Wenger, O. P. Gross, and S. C. Harrison, 2002, Hydrocarbon systems analysis of the Northern Gulf of Mexico: delineation of hydrocarbon migration seepage pathways using seeps and seismic imaging, in Surface exploration case histories: applications of geochemistry, magnetics, and remote sensing, D. Schumacher and L. A. LeShack, eds., AAPG Studies in Geology No. 48 and SEG Geophysical References 11, p. 25-40.

Hyndman, R. D., and E. E. Davis, 1992, A mechanism for the formation of methane hydrate and sea floor bottom-simulating reflectors by vertical fluid expulsion: Journal of Geophysical Research, v. 97, p. 7025-7041.

Jones, M.L., 2003, The regional geothermal heat flow regime of the North-Central Gulf of Mexico continental slope, Thesis for Master of Science, Texas Tech University, 150 p.

Kojima, S., 2002. Deep-Sea Chemoautosynthesis-Based Communities in the Northwestern Pacific, Journal of Oceanography, v. 58, p. 343- 363.

Lee, M. W., 1995. Application of the heat flow equation to analyses of bottom simulating reflectors, U.S. Geological Survey Open-File report 95-262.

MacKay, M. E., R. D. Jarrard, G. K. Westbrook, R. D. Hyndman, and Shipboard Scientific Party of Ocean Drilling Program Leg 146,1994. Origin of bottom-simulating reflectors: Geophysical evidence from the Cascadia accretionary prism, Geology, v. 22, p. 459-462

Marfurt, K. J., and R. L. Kirlin, 2001, Narrow-band spectral analysis and thin-bed tuning. Geophysics, v. 66, n. 4, p. 1274- 1283.

Martin, A., 2004, Hydrate bearing sediments- thermal conductivity. Thesis, Master of Science in Civil and Environmental Engineering, Georgia Institute of Technology, December 28, 2004, 133 p.

Matsumoto and Sato, 2011, Fluid flow and evolution of gas hydrate mounds of Joetsu basin, Eastern Margin of Japan Sea: Constraints from high-resolution geophysical survey by AUV, Proceedings of the 7th International Conference on Gas Hydrates (ICGH 2011), Edinburgh, Scotland, United Kingdom, July 17-21, 2011.

Matsushima J., 2006, Seismic wave attenuation in methane hydrate-bearing sediments: Vertical seismic profiling data from the Nankai Trough exploratory well, offshore Tokai, central Japan, Journal of Geophysical Research 111:B10101.

McBride, B. C., P. Weimer, and M. G. Rowan, 1998, The effect of allochthonous salt on the petroleum systems of Northern Green Canyon and Ewing Bank (offshore Louisiana), Northern Gulf of Mexico, AAPG Bulletin, v 82/5B p. 1083-1112

McConnell, D. R. and Kendall, B. A., 2002. Images of the base of gas hydrate stability, northwest Walker Ridge, Gulf of Mexico: Proceedings, Offshore Technology Conference, Houston, Texas, 6-9 May 2002, OTC 14103

McConnell, D. and Zhang, Z., 2005. Using acoustic inversion to image buried gas hydrate distribution: Fire in the Ice newsletter, Fall, 2005, p. 3-5, National Energy Research Laboratory, US Department of Energy.

McConnell, D. R., J. Gharib, D. L. Orange, J. Henderson, H. Danque, and A. Digby, 2008. Seep-Hunting in Deepwater for Frontier Basin Prospectivity Assessment, World Oil, May 2008

McConnell, D., R. Boswell, T. Collett, M. Frye, W. Shedd, G. Guerin, A. Cook, S. Mrozewski, R. Dufrene, and P. Godfriaux, 2009 a, Proceedings of the Drilling and Scientific Results of the Gulf of Mexico Gas Hydrate Joint Industry Project Leg II: Walker Ridge 313 Site Summary: https://www.netl.doe.gov/File%20Library/Research/Oil-Gas/Methane%20Hydrates/JIPLegII_WR313SiteSum.pdf

McConnell, D., R. Boswell, T. Collett, M. Frye, W. Shedd, G. Guerin, A. Cook, S. Mrozewski, R. Dufrene, and P. Godfriaux, 2009 b, Proceedings of the Drilling and Scientific Results of the Gulf of Mexico Gas Hydrate Joint Industry Project Leg II: Green Canyon 955 Site Summary: https://www.netl.doe.gov/File%20Library/Research/Oil-Gas/Methane%20Hydrates/JIPLegII_GC955SiteSum.pdf

Nur, A. and J. Dvorkin, 2008. Seismic-scale rock physics of methane hydrate – Final report, prepared by Stanford University for the National Energy Technology Laboratory.

Park, Keun-Pil, Bahk, Jang Jun, Kwon, Youngin, Kim, Gil Young, Riedel, M., Holland, M., Schultheiss, P., Rose, K., and the UBGH---1 Scientific Party, 2008. Korean national program expedition confirms rich gas hydrate deposits in the Ulleung Basin, East Sea, in DOE---NETL Fire In the Ice Methane Hydrate Newsletter, Spring, 2008, p. 6---9

Partyka, G., J. Gridley, and J. Lopez, 1999, Interpretational implications of spectral decomposition for reservoir characterization, The Leading Edge, v. 18, i. 3, p. 353-360

Pashin, J. C., J. Meng, D. J. Hills, G. Jin, M. R. McIntyre, and R. A. Esposito, 2017, Geologic framework and CO2 storage potential of the Eastern Gulf of Mexico continental shelf, GCCC, poster, http://www.beg.utexas.edu/gccc/IWOGCO2S/EGOM%20SOSRA%20poster-1.pdf

Paull, C.K., R. Matsumoto, P. J. Wallace, and W. P. Dillon, (Eds.), 2000 a. Proc. ODP, Sci. Results, 164: College Station, TX (Ocean Drilling Program)

Priest, J. A., A. I. Best, and C. R. I. Clayton, 2006, Attenuation of methane hydrate bearing sands, Geophysical Journal International, 164, 149-159.

Rastogi, A. A., and B. Deka, 2001, Estimates of geothermal gradients and heat flow from BSRs along the western continental margin of India: Geophysical Research Letters, v. 28, n. 2, p. 355-358.

Roberts, Glyn, and Kjell Finstad, 2006, Eastern GoM indicates numerous petroleum plays: Offshore Magazine, v. 66, i. 6, 8 p.

Salvador, A., 1991, Triassic and Jurassic, in A. Salvador, ed., The Gulf of Mexico Basin: Geological Society of America, The geology of North America, v. J, 568 p.

Shelander, D., J. Dai, G. Bunge, D. McConnell, and N. Banik, 2010. Predicting Gas Hydrates Using Pre-stack Seismic Data in Deepwater Gulf of Mexico, AAPG Geoscience Technology Workshop, March 16, 2010

Shelander, D., J. Dai, G. Bunge, S. Singh, M. Eissa, and K. Fisher, 2012. Estimating saturation of gas hydrates using conventional 3D seismic data, Gulf of Mexico Joint Industry Project Leg II, J. Marine Petroleum Geology, 34 (1)

Smith, T., Puzzling Salt Structures, 2015, Geo ExPro, v. 12, n. 2, p. 20-24

Taner, T., 2003, Attributes revisited, http://www.rocksolidimages.com/attributes-revisited/

Thematic set on resource and hazards implications of gas hydrate in the Northern Gulf of Mexico: Results of the 2009 Joint Industry Project Leg II drilling expedition, Journal of Marine and Petroleum Geology, v. 34, i. 1, June 2012.

Toth, Z., V. Spiess, and H. Keil, 2015. Frequency dependence in seismoacoustic imaging of shallow free gas due to gas bubble resonance, J. Geophys. Res. Solid Earth, v. 120, p. 8056-8072

Uyeda, M.Y.S., Y. Aoki, and T. H. Shipley, 1982, Estimates of heat flow derived from gas hydrates: Geology, v. 10., p. 339-343.

Vanneste, M., S. Guidard, and J. Mienert, 2005, Bottom-simulating reflections and geothermal gradients across the western Svalbard margin: Terra Nova, v. 17, p. 510-516.

Widess, M. B., 1973. How thin is a thin bed?, Geophysics, v. 38, n. 6, p. 1176-1180.

Zhang, Z., 2010, Personal communication. Rock physics-derived seismic modeling analysis and characterization of a gas hydrate and free gas mixed system in Green Canyon, Gulf of Mexico., in AOA Geophysics company technical presentation materials.

Zhang, Z., D. Han, and Q. Yao, 2011, Quantitative interpretation for gas hydrate accumulation in the eastern Green Canyon area, Gulf of Mexico using seismic inversion and rock physics transform. Geophysics, v. 76, n. 4, p. B139-B150.

Zhang, Z., D. McConnell, and D. Han, 2012 a. AVO crossplot analysis in unconsolidated sediments containing gas hydrate and free gas: Green Canyon 955, Gulf of Mexico, Proceedings of Annual Meeting of the Society of Exploration Geophysicists 2012, Las Vegas.

Zhang, Z., D. McConnell, and D. Han, 2012 b. Rock physics based seismic trace analysis of unconsolidated sediments containing gas hydrate and free gas in Green Canyon 955, Gulf of Mexico. J. Marine and Petroleum Geology 34 (1), p.119-133

**National Energy Technology Laboratory**

626 Cochrans Mill Road
P.O. Box 10940
Pittsburgh, PA 15236-0940

3610 Collins Ferry Road
P.O. Box 880
Morgantown, WV 26507-0880

1450 Queen Avenue SW
Albany, OR 97321-2198

Arctic Energy Office
420 L Street, Suite 305
Anchorage, AK 99501

Visit the NETL website at:
www.netl.doe.gov

Customer Service Line:
1-800-553-7681